ABSTRACT

Title of Dissertation:	MRP5 AND MRP9 PLAY A CONCERTED ROLE IN MALE REPRODUCTION AND MITOCHONDRIAL FUNCTION
	Ian George Chambers, Doctor of Philosophy, 2021
Dissertation directed by:	Professor Iqbal Hamza, Department of Animal and Avian Sciences

Heme is an essential iron-containing cofactor in proteins that perform diverse functions in biology. Free heme is not only hydrophobic but also generates cytotoxic peroxide radicals. In eukaryotes, heme synthesis occurs in the mitochondria but must be transported to different intracellular organelles to be utilized by hemoproteins, a process that remains poorly understood. In *Caenorhabditis elegans*, MRP5/ABCC5 is an essential heme exporter as *mrp-5* knockout worms are unviable due to their inability to export nutritional heme from the intestine to extra-intestinal tissues. Heme supplementation restores viability of these mutants but fails to restore male reproductive deficits. By contrast, MRP5 in mammals regulates heme levels in the secretory pathway but shows no reproductive phenotypes. Phylogenetically, the closest homolog of MRP5 in vertebrates is MRP9/ABCC12, which is absent in *C. elegans* raising the possibility that MRP9 may genetically compensate for MRP5 loss in vertebrates. Here, we show that MRP5 and MRP9 double knockout (DKO) mice are

viable but reveal significant male reproductive deficits, reminiscent of *mrp-5* worms. Although MRP9 is highly expressed in sperm, MRP9 knockout mice show reproductive phenotypes only when MRP5 is absent. Unlike other ABCC transporters, these proteins localize to mitochondrial-associated membranes (MAMs), dynamic scaffolds that associate the mitochondria and endoplasmic reticulum. Consequently, combined loss of both transporters results in abnormal sperm mitochondria and reduced fertilization rates in DKO mice. Untargeted metabolomics show striking differences in metabolite profiles in the DKO testes, consistent with the localization of these transporters to MAMs where inter-organellar metabolite exchange occurs. RNA-seq results show significant alterations in genes related to mitochondria function and energy production, EIF2 signaling, and retinoic acid metabolism. Targeted functional metabolomics reveal retinoic acid levels are significantly lower in the DKO testes. These findings establish a model in which MRP5 and MRP9 play a concerted role in regulating normal male reproductive functions and mitochondrial sufficiency.

MRP5 AND MRP9 PLAY A CONCERTED ROLE IN MALE REPRODUCTION AND MITOCHONDRIAL FUNCTION

by

Ian George Chambers

Dissertation submitted to the Faculty of the Graduate School of the
University of Maryland, College Park, in partial fulfillment
of the requirements for the degree of
Doctor of Philosophy
2021

Advisory Committee:
Professor Iqbal Hamza, Chair
Dr. David M. Bodine
Professor Lisa Taneyhill
Assistant Professor Nishanth Sunny
Professor Caren Chang

Dedication

The following body of work represents the culmination of the past eight years of my life spent in graduate school here at the University of Maryland. The road has been long, arduous and undoubtedly challenging. I would like to dedicate this dissertation to all the people who have helped me to persevere through the hardest of times, and for those that will come after me who also face seemingly insurmountable obstacles. There is always a light at the end of the tunnel… anything is possible.

Acknowledgements

There are a countless number of individuals who require my immeasurable thanks for this achievement. Without their selfless efforts, this dissertation would have not been possible. I am in debt both academically and professionally to my mentor, committee members, collaborators, scientific colleagues and friends both in the ANSC department and abroad for all of their assistance in this project and graduate school in general. I also must thank all of those outside of academia, in particular my friends and family for their unwavering support over the last eight years. The combined efforts of these groups helped me to achieve something that for a stretch of time felt impossible, and for that I am eternally grateful.

To my advisor and mentor, Dr. Iqbal Hamza, thank you for being a role model for the scholar that I aim to become and for molding me into the scientist that I am today. I can unequivocally say you are both my harshest critic and my biggest champion in the scientific arena, and I hope that my development over the last six plus years has made you proud. Coming from the Orlando lab you have effectively taught me everything that I know and will be able to take forward as I pursue my career. Thank you for giving me this opportunity that was both incredibly challenging and rewarding at the same time.

Thank you to all of my past and present committee members, Dr. David Bodine, Dr. Lisa Taneyhill, Dr. Caren Chang, Dr. Bhanu Telugu and Dr. Nishanth Sunny for your critical feedback, constructive support and guidance throughout this project. Your patience and support through these difficult and challenging times faced this past year

with the COVID19 pandemic did not go unnoticed and for that I am very thankful. Drs. Taneyhill and Telugu, having been on my original PhD committee in the Orlando lab and also my professors in the first Animal Sciences courses taken at the University of Maryland, I thank you for your teachings and friendship, which helped shape me as scientist. Dr. Dave Bodine, without your expertise, advice and friendship this project would not have succeeded. Thank you for always being an exceptional collaborator and most importantly, your entire lab for all their endeavors in the generation and analysis of the MRP9 KO mouse. In particular, thank you to Dr. Jens Lichtenburg and Dr. Elisabeth Heuston for everything you have taught me over the years and to Ms. Lisa Garrett for helping us make the mice.

Thank you to all of the other collaborators on this project for spending your valuable time, energy and resources on this work. Dr. Maureen Kane, Dr. Praveen Kumar and the entire Kane Lab at UMB School of Pharmacy, thank you for all of your assistance with metabolomics; Dr. John Phillips and Ms. Nancy Chandler at the University of Utah and the Health Sciences Center Core, thank you for all of your assistance with electron microscopy; Dr. Michael Eckhaus and the Mouse Pathology Core at the NIH, thank you for your tutelage and assistance with a phenotype outside of my wheel house; and Dr. Ji-Xin Cheng and Mr. Yifan Zhu at Boston University, for your assistance with transient absorption microscopy.

Thank you to all of the Hamza Lab members, both past and present who I fondly will always refer to as family. Current members in the lab: Andrew, Sohini, Maria, Xuedi, Melissa, Sandeepan, and Indira - I leave knowing that the Hamza lab is in good hands. I would be remiss to not give a special shout out to a past Hamza lab member

and one of my first friends in graduate school, Mr. Simon Beardsley. Simon and I TA'd together my very first semester and he was the one who wisely told me before I ever joined the Hamza lab that the rigors of science are far more than just taking classes - warning that if I decided to join it would not be easy, but it would make me into a "real" scientist. He was of course correct and thinking of it now still makes me chuckle to this day. Though Simon and nearly everyone else I started with are long gone, one who still remains in Dr. Xiaojing Yuan. Xiaojing, thank you for being a selfless lab mentor and a true friend. Words cannot do you justice and I look forward to our reunion when you finally return from China. Since starting at the University of Maryland, a number of people not directly involved in my dissertation have always been supportive of me in the department who I would also like to acknowledge: Dr. Keefer, Dr. Xiao, Dr. Porter, Dr. Kim and Dr. Peters, thank you for always opening your doors. Especially Dr. Carol Keefer, as the graduate student coordinator I thank you for always supporting me and being a staunch student advocate.

Thank you to all of my friends and family who have been on this journey with me and shared in both my triumphs and heartbreaks. To all new friends made along the way: my classmates, my teammates, on clubs and extracurricular activities, my past students, sporting events, the Greek Heritage Society, St. Sophia Greek Orthodox Cathedral and everything in between, thank you for making this experience what it was. To the old guard, my past friends, who I could always turn to through thick and thin to pick me up, you know who you are, I thank you. And finally, and most importantly of all, my family. I would not have made it to this point without you, and I am eternally grateful. To my cousins, the George family, thank you for always being there for me,

for practically taking me in as a second son when I moved up here all those many years ago. To my sister and now her entire young beautiful family, thank you, from the bottom of my heart, you have always been my best friend and biggest cheerleader. To my parents, who have given me the world and raised me into the man I am today, I love you more that you will ever know. Your unfaltering support kept me going when it seemed everything was lost, and I strive to make you proud every single day. And last but not least, to my wife Vaso, thank you for being my everything. Thank you for all of your innumerable sacrifices, the facetimes, the night shifts, the meals, and the seemingly infinite late nights. Your love and support have been unbreakable, and this dissertation is as much mine as it is yours.

Table of Contents

List of Figures and Tables

Figures:

Tables:

List of Abbreviations

ABC	ATP binding cassette
ATP	adenosine triphosphate
BSA	bovine serum albumin
CE	caudal epididymides
cGMP	guanosine 3',5'-cyclic monophosphate
CRISPR	clustered regularly interspaced short palindromic repeats
cryo-EM	cryogenic electron microscopy
DAPI	4',6-diamidino-2-phenylindole
DI-MS	direct infusion mass spectrometry
DKO	double knockout
DMEM	Dulbecco's modified Eagle's medium
DNA	deoxyribonucleic acid
DPBS	Dulbecco's phosphate-buffered saline
DTT	dithiothreitol
EDTA	ethylenediaminetetraacetic acid
EGTA	ethylene glycol tetraacetic acid
ER	endoplasmic reticulum
FDR	false discovery rate
GaPP	gallium protoporphyrin
GO	gene ontology
GTP	guanosine-5'-triphosphate
HEPES	4-(2-hydroxyethyl)-1-piperazineethanesulfonic acid
HPC	high performance cluster
HRG	heme responsive gene
HRP	horseradish peroxidase
IHC	immunohistochemistry
IPA	ingenuity pathway analysis
IVF	*in vitro* fertilization
KEGG	Kyoto encyclopedia of genes and genomes
KO	knockout
LHP	labile heme pool
MAM	mitochondrial-associated membrane
MEF	mouse embryonic fibroblasts
mRNA	messenger RNA
MRP	multidrug resistance-associated protein
MS	mass spectrometry
MSD	membrane spanning domain
MTBE	methyl-tert-butyl ether
NaB	sodium butyrate
NBD	nucleotide binding domain
NT	non-targeted
ORF	open reading frame

PBS	phosphate buffered saline
PCR	polymerase chain reaction
PDI	protein disulfide isomerase
PFA	paraformaldehyde
RA	retinoic acid
RAR	retinoic acid receptor
RBC	red blood cell
RE	retinyl ester
RFLP	restriction fragment length polymorphism
RIN	RNA integrity number
RNA	ribonucleic acid
ROL	retinol
SDS-PAGE	sodium dodecyl sulfate polyacrylamide gel electrophoresis
SIM	standard immunoblotting method
siRNA	small interfering RNA
SNP	single nucleotide polymorphism
STAR	spliced transcripts alignment to a reference
T-SNE	t-distributed stochastic neighbor embedding
TA	transient absorption
TEER	transepithelial electrical resistance
TEM	transmission electron microscopy
TMD	transmembrane domain
TPM	transcripts per million
UHPLC	ultra high-performance liquid chromatography
UPR	unfolded protein response
UV	ultra violet
VIP	variable importance in projection
WT	wildtype
ZnMP	zinc mesoporphyrin

1 Chapter 1: Introduction

1.1 Heme homeostasis

1.1.1 Diverse and essential role of heme in biology

Heme, a porphyrin ring containing iron, performs diverse biological functions as a cofactor, signaling molecule, and nutrient [1-10]. As a prosthetic group in a myriad of proteins, heme primarily endows the ability to mediate electron transfer and subsequently, has critical roles in catalysis, binding synthesis and sensing of gases, xenobiotic detoxification, signal transduction, microRNA processing, and circadian clock control [2,5,7,11-14]. Specifically as a signaling molecule, heme binding to or dissociating from target proteins can further alter their expression and/or activity [4,15-21]. This heme regulation of transcription factors, translational activators, ion channels, kinases, and microRNA processing factors has been shown to collectively control a multitude of pathways, including the antioxidant stress response, apoptosis, cell proliferation, mitochondrial homeostasis and respiration, mitophagy, and translation [5,13,22-37].

1.1.2 Necessity for heme trafficking

Due to the nearly ubiquitous and essential role for heme in all forms of life, its synthesis and degradation are well understood processes that have been reviewed extensively [4,5,38-42]. In eukaryotes, enzymes for heme biosynthesis and degradation have been structurally characterized to atomic resolution with deep insights into their molecular mechanisms [39,43-45]. This conserved synthesis pathway for heme occurs

in and around the mitochondria across metazoans, the final step being the incorporation of iron into the porphyrin ring in the mitochondrial matrix via ferrochelatase [5,46]. Once formed in the mitochondria, this heme then needs to be incorporated into hemoproteins, the majority of which are not present in the mitochondria but found rather in extramitochondrial compartments [4,5,8,42,47-49]. This poses a major problem for the cell as free heme itself is cytotoxic, catalyzing the production of reactive oxygen species, and being hydrophobic, can easily intercalate into lipid bilayers [50,51]. Unsurprisingly, defects in heme homeostasis manifest these deleterious properties and are associated with numerous diseases [6]. Therefore to mitigate the potential for this heme toxicity, it stands to reason that a number of proteins are essential for binding and buffering heme, chaperoning its insertion into hemoproteins, storing it into a chemically inert form until it is needed, and transporting it into and out of various cellular and subcellular compartments [4,5,8,11,17,42,52]. Very little was known about these transport and trafficking pathways prior to the last 15 years and many questions still remain unanswered.

1.1.3 Traditional understanding of heme mobilization

For many years the concepts for heme transport and trafficking were limited to the canonical underpinnings of iron metabolism/homeostasis. This meant effectively simplifying the movement of heme to either intestinal heme absorption as a means of iron acquisition, or recycling/scavenging of circulating heme and hemoglobin released by hemolysis via hemopexin and haptoglobin, respectively [50,51,53-58]. Likewise, the recycling of red blood cells themselves by reticuloendothelial system macrophages is a final important traditional mechanism for heme trafficking into cells from

circulation and has been studied extensively [59-62]. Erythrophagocytosis aids in the clearance of heme-laden red cells as they reach the end of their life span (either through damage or senescence), and acts as the primary method for systemic iron recycling in the body [63-66]. Internalized red blood cells are broken down in the endophagolysosome and result in a bolus of cytotoxic heme which is subsequently catabolized by heme oxygenases, releasing free iron that can then be recycled for new heme synthesis, stored, or distributed to other cells and tissues [67-69]. Despite the numerous studies on the significance of heme degradation by erythrophagocytosis on iron regulation, how heme was trafficked out of the phagolysosomal lumen to reach heme oxygenase in the cytosol was still poorly understood, as *bona fide* heme transporters had not yet been discovered [4,11,60,70].

1.1.4 Exploiting a heme auxotroph that requires heme

Despite this obvious physical necessity for heme transporters, calls for their existence were largely dismissed by the argument that all mammalian cells are capable of synthesizing, utilizing and degrading their own heme, a viewpoint that is still maintained even to this day [71]. This naïve notion was finally challenged however, in part by the seminal discovery by the Hamza lab that the microscopic nematode, *Caenorhabditis elegans*, actually lacks all eight enzymes for heme biosynthesis [72]. Like all other free-living metazoans *C. elegans* still requires heme for hemoproteins and acquires heme through its diet via the intestine and subsequently disseminates it to other cells throughout its body for survival [4,72,73]. Though clearly this mechanism is an outlier amongst eukaryotes, *C. elegans'* unique heme auxotrophy allowed for the study of heme transport and trafficking without the confounding contributions from

endogenous heme synthesis [8,72,74]. It also laid the foundation for the possibility that the pathways which enable the distribution of heme to different tissues and subcellular compartments in *C. elegans* may also be conserved in the vast majority of animals that can synthesize heme. Strikingly *Heme-Responsive Gene-1* (HRG-1), the first of those proteins to be characterized, turned out to be the long-sought after heme transporter responsible for import into the cytosol from the phagolysosome in mammals discussed earlier [70,72,75].

1.1.5 Transporters of heme

As has been described and reviewed elsewhere, genetic screens and subsequent characterization of additional HRGs by our lab and others have now identified several novel and conserved importers, exporters, chaperones and signaling molecules of heme [4-6,8,9,17,42,74,76,77]. A summary of all the known factors associated with heme transport and trafficking in metazoans can be seen below in **Figure 1.1** [78].

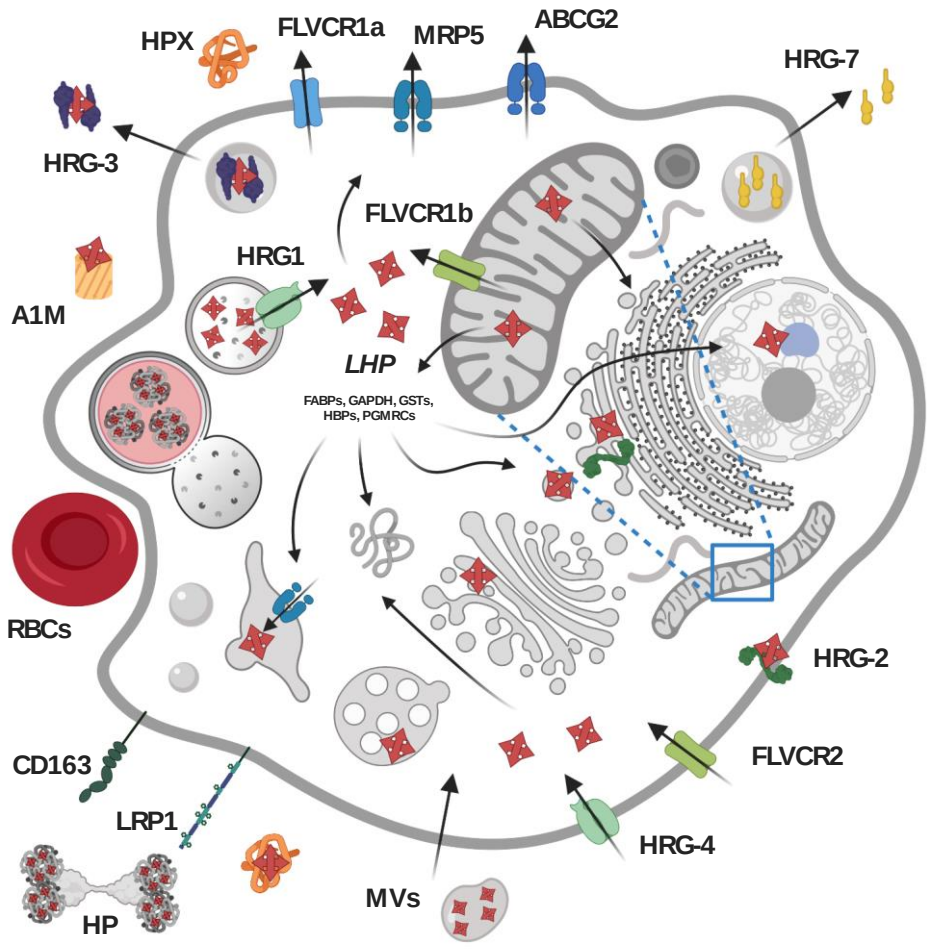

Figure 1.1 Proteins involved in metazoan heme trafficking/homeostasis

Intracellular heme is either produced via de novo synthesis in the mitochondria or imported via transporters or endocytosis (green components). The efflux of heme to exoplasmic spaces is mediated by transporters or exocytosis (blue components). The labile heme pool (LHP) consists of heme that is buffered by a network of proteins which facilitate its trafficking to other organelles throughout the cell. Figure taken directly from Chambers et al [78].

As mentioned above, HRG-1 and its homologs HRG-4, -5, -6 were the first *bona fide* eukaryotic heme transporters to be discovered in *C. elegans*, whose critical function of heme import into the cytosol is evolutionarily conserved [70,75,79-81]. Likewise, we subsequently discovered MRP-5, an essential heme exporter, and regulator of systemic heme homeostasis [82]. Genetic studies in *C. elegans* showed that intestinal heme acquired from the importers HRG-1/4 is transported by MRP-5 from the basolateral surface of the gut intestinal epithelium for utilization by extra-intestinal tissues [82]. Key lines of evidence for this model include functional heme transport assays in yeast, accumulation of fluorescent ZnMP in the intestine, survival in the presence of the toxic heme analog GaPP, high labile heme accumulation in the intestine with a concomitant reduction in extra-intestinal tissues, and embryonic lethality due to *mrp-5* deficiency that is rescued by heme supplementation [82,83]. In vertebrates, knockdown of *mrp5* by anti-sense morpholinos resulted in severe anemia in zebrafish, indicating a critical role in erythropoiesis for this transporter, which incidentally is also highly expressed in human RBCs [82,84]. Furthermore in mammalian cell culture experiments, MRP5 knockout mouse embryonic fibroblasts demonstrated reduced heme export into the secretory pathway, as measured by heme incorporation into a Golgi-targeted horseradish peroxidase reporter [82]. The working model is that heme trafficked into the secretory pathway by MRP5 can be incorporated into hemoproteins or effluxed from the cell via the plasma membrane to extracellular spaces [52,78,82].

1.2 Multidrug resistance transporters

1.2.1 Multidrug Resistance Proteins - the ABCC family of transporters

MRP5/ABCC5 belongs to the family of Multidrug Resistance-associated Proteins (MRPs) within the type C subfamily of the ATP Binding Cassette (ABC) transporters, which are highly conserved evolutionarily in all phyla [85-87]. MRPs have been investigated extensively over the past three decades for their role in cancer drug resistance [88-91]. Initially discovered for their ability to efflux a wide range of chemotherapeutic agents out of cells, MRPs are significantly upregulated in cancer cells, effectively hijacking their endogenous functions in order to confer "resistance" [90,92,93]. Though this class of transporter was first characterized in humans via anticancer drugs, several of these conserved ABCC homologs (see **Figure 1.2** below) will likely have different endogenous physiological substrates from the drugs they efflux in human cancers.

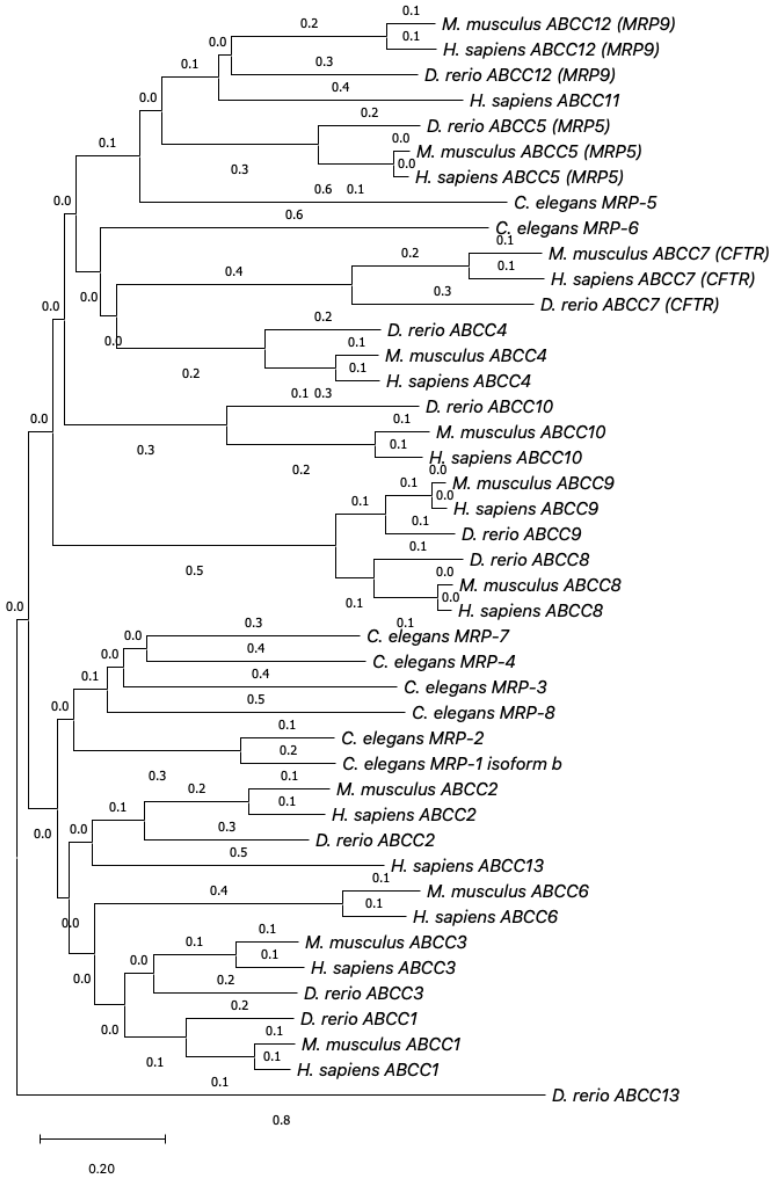

Figure 1.2 Phylogenic analysis of ABCC transporters conserved across metazoans

The type C family of ATP Binding Cassette Transporters, also known as MRPs, are evolutionarily conserved across metazoans from worms to humans. Amino acid FASTA sequences for all known MRPs in humans, mice, zebrafish and worms were aligned and used to generate the optimal phylogenetic tree shown. The evolutionary history was inferred using the Neighbor-Joining method [94]. The tree is drawn to

scale, with branch lengths in the same units as those of the evolutionary distances used to infer the phylogenetic tree. The evolutionary distances were computed using the Poisson correction method and are in the units of the number of amino acid substitutions per site [95]. All ambiguous positions were removed for each sequence pair (pairwise deletion option) with a total of 2012 positions in the final dataset. All alignment and evolutionary analyses were conducted using MEGA X software version 10.2.4 [96,97].

Due to the critical importance in human health and clinical outcomes in cancer, a myriad of MRP substrates have now been identified including organic anions, conjugated drug metabolites, cysteinyl leukotrienes, prostaglandins and signaling molecules [90,91,98,99]. The promiscuity of MRPs for such structurally disparate substrates had been a question in the field for decades until recent breakthrough studies using the model ABCC transporter MRP1 provided a deeper understanding of both transporter substrate and kinetics [100,101]. Indeed, cryo-EM structures of bovine MRP1 show a unique bipartite nature to MRP1's substrate-binding pocket that enables it to recognize large, amphipathic moieties, such as methotrexate, possessing both negatively charged and hydrophobic functional groups, and still transport small organic acids [100,101]. It is likely the case that due to the structural similarities within this entire class of transporters, the wide range of effluxed substrates in a cancer cell context can be attributed to similar mechanisms as all but two MRPs (MRP6 and MRP9) have been shown to have at least some activity in transporting drugs [91]. Nevertheless, our expectation is that the cellular export of many of these substrates should be attributed

to commandeering of said promiscuity of the transporter rather than that being its true evolutionary function.

1.2.2 Phenotypes of Multidrug Resistance Protein 5 or ABCC5

The implication for MRP5's role in heme homeostasis first came from early microarray analysis and quantitative RT-PCR studies in *C. elegans [79,102]*. *mrp-5* was determined to be a heme-responsive gene, with *in silico* promoter analysis revealing a canonical 23-bp heme response element and growth under low heme conditions resulting in three-fold upregulation of its mRNA [102,103]. Prior to this discovery, the role of MRP5 appeared to be that of cyclic nucleotide export from cells as demonstrated by transport of guanosine 3',5'-cyclic monophosphate (cGMP) in membrane vesicles expressing human MRP5 *in vitro* [98,104]. However, the generation of MRP5 null mice demonstrated little to no contribution in cGMP efflux and no observable overt phenotypes, leaving the physiological relevance of this transporter unclear outside its *in vitro* or cancer cell context [105,106]. This is not the case in *C. elegans*, where MRP-5 is absolutely essential for embryonic development and knockout of *mrp*-5 results in heme deficiency and embryonic lethality [82]. Taken together with zebrafish and mammalian cell findings, it would appear that MRP5's regulation of systemic heme homeostasis is likely conserved from worms to vertebrates and is important for efflux of heme from the cytosol [78]. Interestingly, MRP-5 null worms have another striking phenotype related to male fecundity and reproductive fitness. Male *mrp-5(ok2067)* knockout worms rescued via exogenous heme supplementation have previously been demonstrated in our lab by Simon Beardsley to be sterile and unable to sire progeny [107]. Critically, these worms exhibit defective

mating apparatus with stunted male tail fan formation, reduced number of rays, and spicules which fail to retract despite normal mating behaviors (**Figure 1.3**) [107-109]. Given that hermaphrodite *mrp-5* knockout worms mate normally with wildtype males it would appear the defect is in fact paternal. Furthermore, genetic bypass suppressors of *mrp-5(ok2067)* remain deficient in mating; exogenous heme supplementation fails to rescue the mating phenotype **(Figure 1.4)** [107].

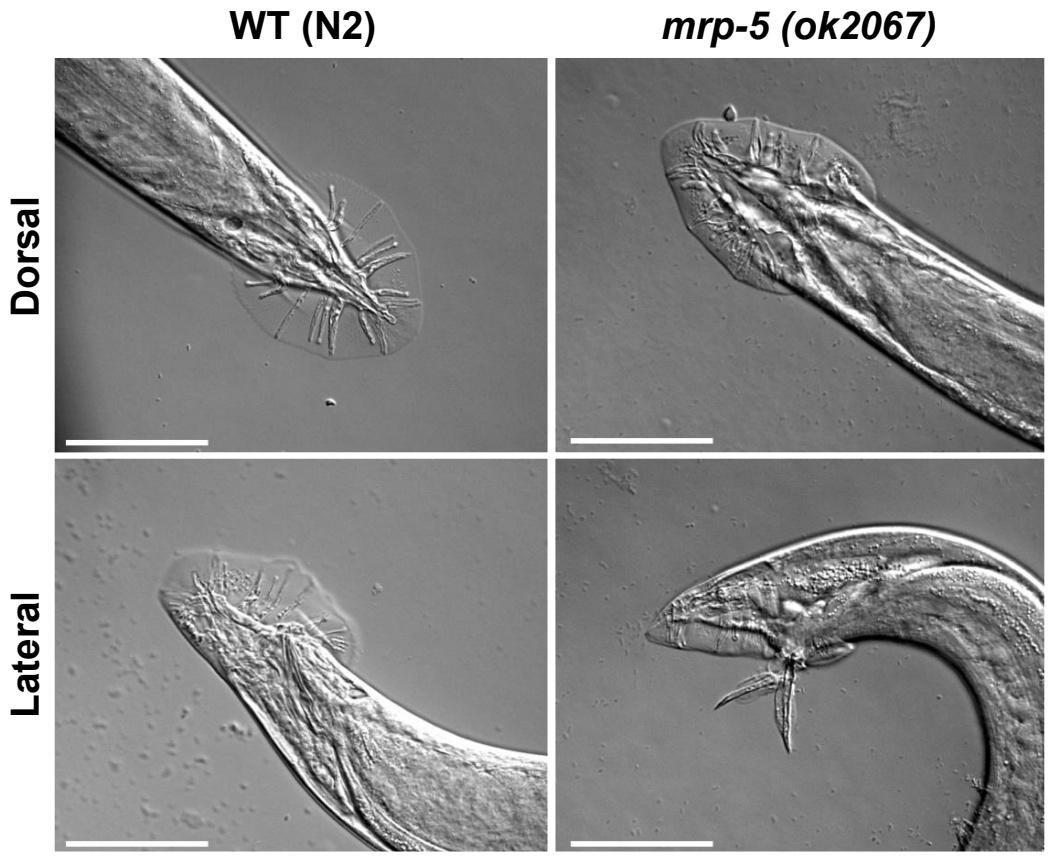

Figure 1.3 Male *mrp-5*(ok2067) worms exhibit tail defects

MRP-5 null worms (right) display reproduction related defects in the male tail with a reduced number of rays (top) and potentially defective spicule retraction after mating attempts (bottom) compared to WT (left) (experiment performed by Simon Beardsley). Scale bar equals 50 μm.

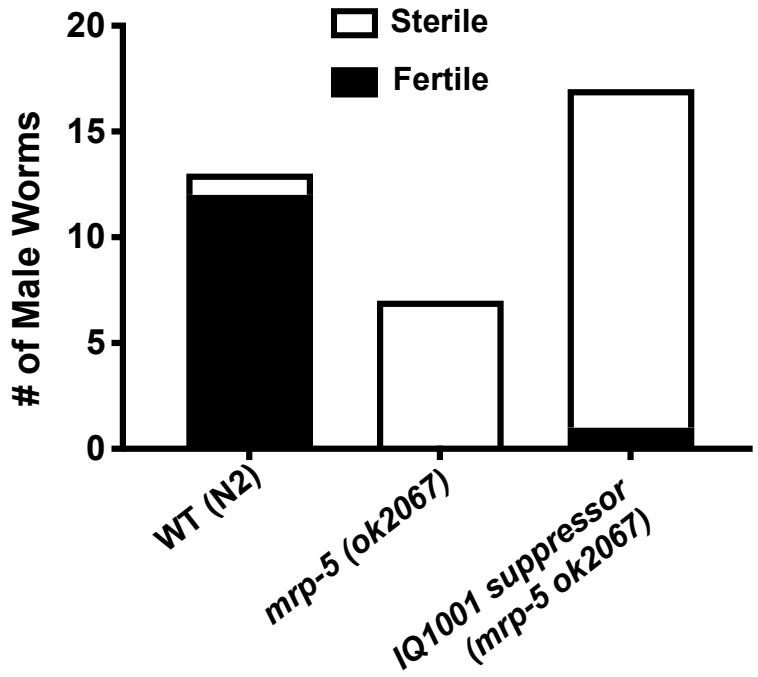

Figure 1.4 Male *mrp-5*(ok2067) worms are sterile and unable to sire progeny

Males of each strain were picked onto a plate with one sperm exhausted WT hermaphrodite per replicate. Presence of progeny was used as a measure of male mating success due to the fact that hermaphrodites were sperm exhausted (experiment performed by Simon Beardsley).

For these reasons, we previously had concluded that MRP-5 may have additional functions outside of its traditional role as a heme transporter [107]. Why then, do MRP5 knockouts in higher order vertebrates such as zebrafish and mice lack overt reproductive and heme homeostasis phenotypes that we observed in the worm? One postulated explanation for this is *in vivo* genetic compensation by other closely related transporters which are phylogenetically conserved in higher order eukaryotes but absent in the *C. elegans* genome [8,82]. It is noteworthy that MRPs are promiscuous in their substrate specificity, therefore other MRPs may be able to moonlight for MRP5 in its absence [110,111].

1.2.3 ABCC transporters "short clade" subclass

The type C subfamily of ABC proteins can be further separated into two distinct clades based on protein topology and size, coined short versus long. The short MRPs all contain two sets of membrane spanning domains (MSDs) and nucleotide binding domains (NBDs) while the long MRPs also have an extra N-terminal membrane spanning domain called MSD0 [91]. MRP5 is closely related to MRPs 4, 8 and 9, falling in the short MRP clade (see **Figure 1.5** below taken from Deeley et al 2006), with twelve transmembrane domains (TMDs) and is typically localized to the plasma membrane and endosomal compartments [82,91,99].

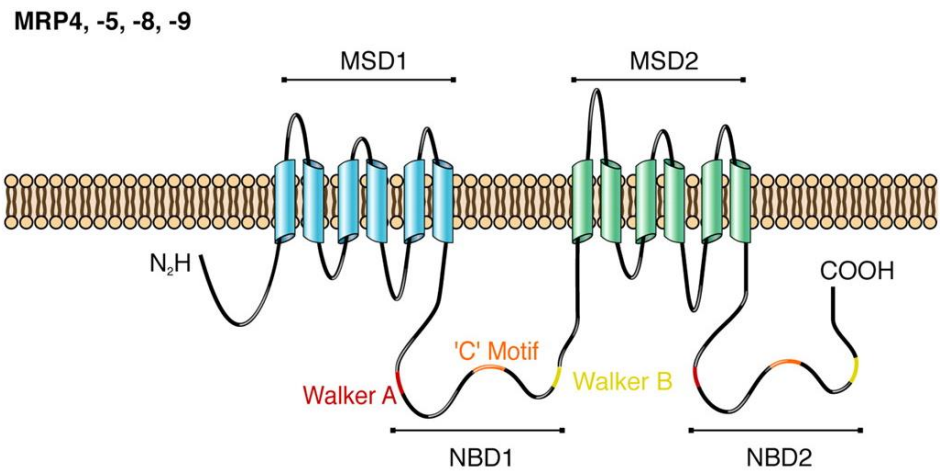

Figure 1.5 ABCC short clade protein topology

MRPs 4, 5, 8 and 9 are all closely related 12-pass membrane proteins divided into two 6 TMD segments (or MSDs) and two ATP binding cassettes motifs (NBDs) that drive active transport across membranes. Taken directly from Deeley et al 2006 [99].

Upon closer inspection of the phylogenetic analysis of ABCC transporters in **Figure 1.2**, we see that members of this short clade cluster together tightly across species indicating that they are evolutionarily related. *C. elegans* has only *mrp-5*, whereas most vertebrates have an additional paralogous gene due to a duplication event, highlighted by the red box in **Figure 1.6** below. This protein, termed MRP9, is the closest related MRP to MRP5 and is conserved in higher-order vertebrates including zebrafish and mice, highlighted by the red branches and nodes in **Figure 1.6**.

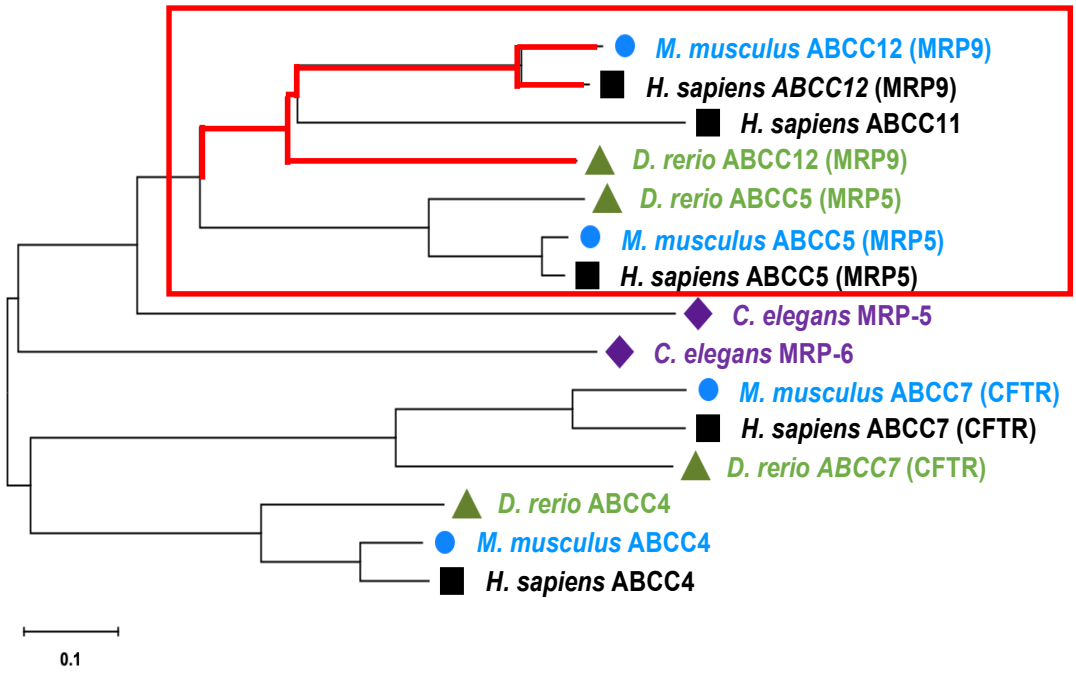

Figure 1.6 The "short" MRP subclass and closest paralogs of MRP5 across metazoans

MRP9 is the closest related and evolutionarily linked ABCC transporter to MRP5 that is conserved across higher order vertebrates (highlighted in red). Short clade ABCC amino acids sequences were used with identical parameters from **Figure 1.2** to generate the phylogenetic tree in MEGA X [96,97]. Output image files were then exported and manually annotated.

Humans also have a third closely related short MRP paralog, ABCC11, which is not found in rodents or fish but is found in other eutherians and has already been characterized extensively as it is the protein specifically responsible for earwax wetness [112,113]. MRP9, on the other hand, is an intriguing candidate for further functional delineation as it was one of the last of the ABCC proteins to have been discovered and the least understood.

Due to the naming conventions and the independent discovery of these ABCC transporter proteins from their respective protein coding genes, there are multiple aliases for a number of these transporters. For the sake of clarity, hereon the ABCC designation (i.e. *ABCC5* and *ABCC12*) will be used when referencing the gene and the MRP designation (i.e. MRP5 and MRP9) for referring to protein.

1.2.4 Multidrug Resistance Protein 9

Published studies show that human MRP9 is widely distributed at low levels in tissues such as the testes, brain, liver, lung and kidney, while in mice MRP9 is only detected in the testes where it is expressed at high levels [114,115]. As mentioned previously, MRP9 is one of the few MRPs that has not been characterized extensively and has not been shown to effectively transport drugs *in vitro* [91]. MRP9 also lacks any detectable N-linked glycosylation and it has multiple RNA splicing variants, all unusual features for traditional MRPs [114]. The Borst group, who published the first initial characterization of mouse MRP9 were unable to generate a knockout mouse and attributed this failure partly to the unique nature of MRP9's multiple downstream start codons [114]. Although Ono et al. successfully targeted the first exon of *ABCC12* as described in their supplementary materials, the first 120 amino acids of the MRP9 open

reading frame (ORF) contain three putative alternate start-site methionines (**Figure 1.7**), which allowed for a near full-length transcript and protein to be produced [114].

Mouse *ABCC12*/MRP9 WT ORF (120/1366 AAs)

```
  34 atggtgggtgaaggcccgtaccttatctcagacctggatcgcaga
     M  V  G  E  G  P  Y  L  I  S  D  L  D  R  R
  79 ggccatcggagatcctttgccgagagatatgaccccagcctgaaa
     G  H  R  R  S  F  A  E  R  Y  D  P  S  L  K
 124 accatgatcccagtgcgaccccgtgcaaggttggcacccaatcct
     T  M  I  P  V  R  P  R  A  R  L  A  P  N  P
 169 gtggatgatgctgggctgctgtccttcgccacgttttcctggctc
     V  D  D  A  G  L  L  S  F  A  T  F  S  W  L
 214 acaccggtgatgattcgaagttacaagcacacgctgactgtggac
     T  P  V  M  I  R  S  Y  K  H  T  L  T  V  D
 259 accctgcccccactgtctccttatgactcatcggacatcaacgcc
     T  L  P  P  L  S  P  Y  D  S  S  D  I  N  A
 304 aagagattccagatcctttgggaagaagaaataaagagggtaggg
     K  R  F  Q  I  L  W  E  E  E  I  K  R  V  G
 349 cctgagaaggcctccctgggccgcgtggtctggaaattccagaga
     P  E  K  A  S  L  G  R  V  V  W  K  F  Q  R
```

Figure 1.7 *ABCC12*/MRP9 partial open reading frame and amino acid sequence

The first 120 amino acids of the mouse MRP9 sequence showing alternative downstream ATG start sites in the *ABCC12* sequence.

Ono et al. showed that MRP9 in mice and boar is expressed in the testes and further demonstrated that MRP9 was highly enriched in the sperm [114]. Puzzlingly, MRP9 did not seem to be plasma membrane or endo-secretory localized, as observed for other MRPs, but instead seemed closest to the ER markers PDI and Calnexin in transfected HEK293 cells [114]. These combined findings resulted in the following conclusions: "*MRP9 is specifically localized in sperm midpiece, yet it does not reside in the mitochondria based on immunolocalization microscopy and cell fractionation studies"* [114]. All of this information taken together is rather perplexing as the sperm midpiece itself is nearly ubiquitously mitochondria. These mitochondria are densely-packed gyres, with the cristae spiraling around the filamentous axoneme core of the sperm, primarily functioning to provide massive amounts of energy for the free swimming sperm [116,117]. It is possible that MRP9 may be present at mitochondrial-associated membranes that are typically characterized as the interface of ER and mitochondria raising the possibility that MRP9 substrates could be a mitochondrial metabolite. The genetic and cell biological characterization of MRP9 is a major outstanding piece in the ABCC transporter field. Coincidentally, additional research into MRP9 and its endogenous substrates may also shed light on the previously discussed genetic compensation hypothesis by this close relative of MRP5 especially since *mrp-5* mutant worms reveal a male reproductive phenotype.

1.3 Heme/Iron and male reproduction

1.3.1 The important role of sperm mitochondria

The primary role of the mitochondria in sperm is largely no different than that of all cell types, providing ATP production to fuel biological activities [118]. Because male germ cells have evolved to be extremely motile and highly specialized however, the importance of sperm mitochondria cannot be understated. The primary components of mammalian spermatozoa can be visualized below in **Figure 1.8** which include the head, midpiece and principal piece.

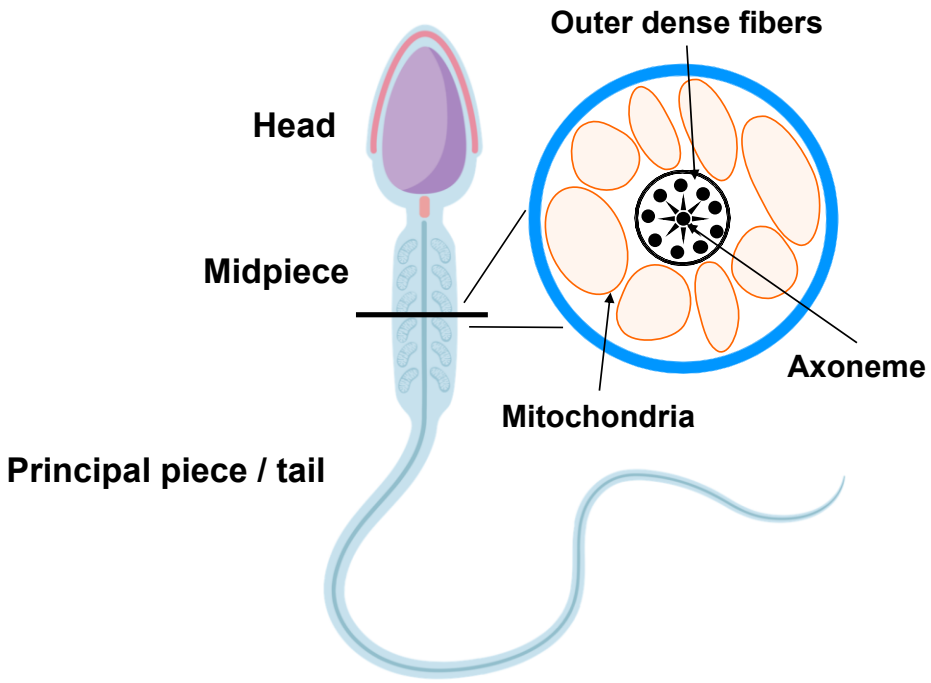

Figure 1.8 The mitochondrial sheath of the sperm midpiece

Schematic of a general mammalian sperm with an inset of a cross section of the midpiece highlighting the mitochondria wrapped around the axoneme and fibers (created with biorender.com).

As mentioned previously, the midpiece of the sperm is made up of the mitochondrial sheath, or a cylinder of mitochondria that envelops the axoneme and fibers that is critical for reproductive fitness [116,119-121]. Within the sheath, adjacent mitochondria associate end to end and along their lateral surfaces forming a tight concentrated gyre, which theoretically allows for maximum efficiency of energy delivery to the structural fibers for motility [122]. The size and total volume of the mitochondrial sheath has also been shown to be directly correlated with sperm ATP production and swimming velocity across species [117]. However, this immense output also comes with a price - because spermatozoa are so densely packed with mitochondria, they are also epicenters for the production of detrimental free radicals/reactive oxygen species [116,119,121,123]. If not balanced and mitigated, this can cause myriads of problems including lipid peroxidation, which has been shown to damage the membranes of sperm and decrease their mitochondrial membrane potential [116,119,121,124]. The relationship between mitochondrial membrane potential and sperm motility has been well documented in the literature and even recently shown to be an excellent indicator for sperm function for up to four hours, directly correlating mitochondrial health with sperm motility observations [125,126]. This is not necessarily surprising given changes in mitochondrial sperm membrane composition have already been shown to modulate activity of the respiratory chain and oxidative phosphorylation pathways, leading to reduction in energy production and a decrease in sperm motility [116,120,125,127]. Spermatozoa mitochondrial dysfunction therefore is of particular importance clinically, as asthenozoospermia is one of the leading causes of male infertility, typically resulting in a reduction in sperm motility and a subsequent

loss of biological function [120,121]. Concordantly, male fecundity relies heavily on this organelle being fully intact and functional for the overall health of the spermatozoa and additional mitochondrial parameters beyond membrane potential have now been shown to directly impact male fertility *in vivo* [116,119].

1.3.2 Mitochondrial dynamics and male fitness

A significant factor for reproductive fitness and spermatogenesis is mitochondrial fusion, which has been demonstrated to play an essential role both in control of steroidogenesis and mitochondrial capacity [119,128]. Mitochondrial plasticity, or the dynamics of fusion and fission events for altering mitochondria morphology, is essential for replicating, maintaining, and repairing integrity as well as reversibly modifying productive capacity of these organelles [129-131]. In the last 10 years, these mitochondrial dynamics have been demonstrated to be critical in male reproduction in particular due to the link of steroid synthesis enzymes shared between the mitochondria and endoplasmic reticulum, indicating the necessity of interorganellar contact and substrate transport [119]. Indeed, the mitochondria are the site of cholesterol side-chain cleavage enzyme (P450scc), a hemoenzyme that converts cholesterol to pregnenolone a precursor to various steroid hormones [132,133]. Naturally, the sex steroid hormones produced by these organelles in the cells of the gonad can feedback and regulate mitochondrial function itself [119,133]. Strikingly however, Duarte et al showed that stimulation of hormone synthesis immediately upregulated Mitofusin 2 expression, a critical GTPase protein for mitochondrial fusion, and promoted the association between the mitochondria and the mitochondria-associated membranes (MAMs) [128]. Furthermore, this induction of mitochondrial

fusion is essential as they and others have now shown that mice conditionally depleted of mitofusins are unable to elongate and increase their mitochondria, resulting in not only reduced steroid production, but also diminished oxidative phosphorylation and arrest of germ cell maturation [128,134]. This dynamic regulation is likely not limited to spermatogenesis and development in the gonad as Mitofusin 2 protein expression was recently shown to be positively correlated with human sperm motility and cryopreservation in mature free-swimming spermatozoa, further confirming the essential role for mitochondrial fusion in male reproductive fitness [134,135].

1.3.3 Iron status and male fitness

Another critical and interrelated parameter of mitochondrial health in reproduction that is often forgotten is iron status [136]. Iron is a trace mineral essential for biology and one of nature's most abundant nutrients, yet its deficiency still affects billions of people every day [137,138]. Iron-deficiency anemia is the most common pathology manifesting in a reduction of circulating red blood cells, and amongst many other dysfunctions, has been shown to have significant impact on male reproduction and spermatogenesis [136,137,139]. Iron metabolism has been well studied for decades as it plays key roles in numerous metabolic processes throughout the cell but notably it must be transported into the mitochondria for its most important functions: heme synthesis and iron-sulfur cluster biogenesis [138,140]. Once generated, these cofactors are essential for synthesis of nucleic acids, proteins, and numerous enzymes involved in redox reactions, electron transport and cellular respiration - all of which are also critical in spermatogenesis due to the high rates of cellular proliferation and differentiation [141,142]. This is not surprising in part because hundreds of billions of

spermatozoa are produced continuously throughout adult male life, each with 50-75 mitochondria requiring substantial nutritional and energetic demands predicated on functional levels of iron [118,137,143]. In anticipation of this, Sertoli and Leydig cells responsible for nursing the developing spermatogonia in the seminiferous tubules of the testes are able to uptake circulating iron and store it in the form of ferritin, to ensure a readily available supply for this critical nutrient as spermatids differentiate [142,144,145]. Iron-deficiency anemia, however, poses a problem on two fronts as not only is iron itself now limiting, but additionally reduced oxygenation of circulating blood causes a significantly hypoxic environment in the testes, where spermatogenesis relies on considerable oxygen via diffusion for mitochondrial oxidative phosphorylation [118,136]. Taken together, these conditions pose a challenge to the reproductive niche and result in poor semen parameters and infertility, which are frequently recapitulated in similar disease states such as sickle cell anemia [137,139,146-148]. Interestingly, despite this baseline understanding for the importance of iron and studies indicating reproductive dysfunction in iron perturbation, it was not until the seminal findings of Metzendorf and Lind in *Drosophila melanogaster* that a direct link between mitochondrial iron status and spermatogenesis had been demonstrated [149,150]. They showed that the mitochondrial iron importer Mitoferrin is required for both male fertility and mitochondrial morphogenesis in sperm, and that the genes related to mitochondrial iron metabolism and homeostasis such as mitochondrial ferritin are present and conserved in the testes of both vertebrates and invertebrates [150,151]. In summary, we appreciate the importance of mitochondrial health in male reproductive fecundity, and dysfunctions that cause

infertility including iron deficiency, oxidative stress, lipid peroxidation, and defective mitochondrial plasticity and membrane potential (see **Figure 1.9** below).

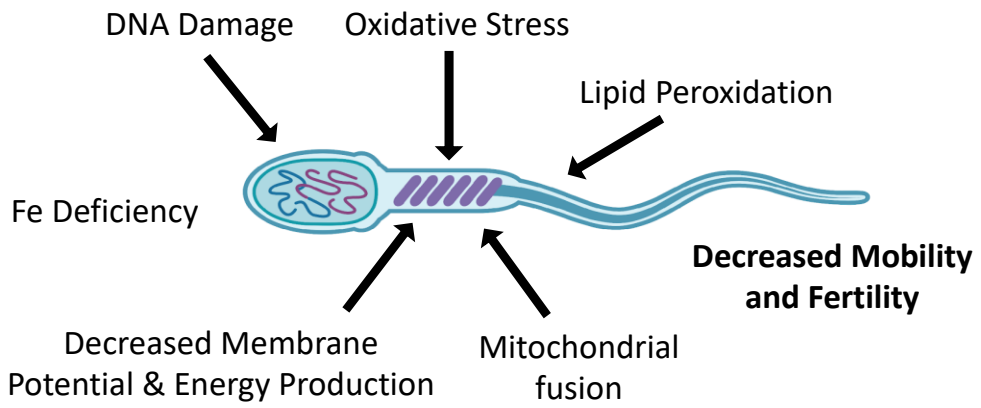

Figure 1.9 Key factors for spermatogenic mitochondria and male fecundity

Factors which negatively impact spermatozoa effectivity and viability in reproduction are highlighted (Created with biorender.com).

1.4 Problem Statement

As described herein, iron and heme trafficking are essential for male reproductive biology and mitochondrial homeostasis. MRP5 is a highly conserved ABC transporter across metazoans that is essential for heme homeostasis and male fecundity in *C. elegans*. A critical role for MRP5 function *in vivo* in mammals, however, has not yet been elucidated and MRP5 knockout mice show no overt reproductive phenotypes. Interestingly MRP5 is found in low abundance in the testes in mammals; gene expression and limited protein localization possibly identifies early spermatogonia, nursing cell types as well as Leydig cells as putative expression sites [152,153]. Additionally, recent papers have implicated a role for MRP5 in prostate cancers and prostate/urethral inflammation and dysfunction, so it is possible that there are as of yet to be discerned role(s) for MRP5 in male reproduction [154-156]. Is there any validity to the hypothesis for genetic compensation by closely related transporters in this distinct tissue niche? MRP9 is phylogenetically related to MRP5 and is highly expressed in the testes. MRP9 has only been the subject of interest for an extremely limited number of studies, with no knockout model system or reported endogenous function. MRP9 was recently reported to be induced in cancer cells by the histone deacetylase inhibitor sodium butyrate [157], a result that we have been unable to reproduce ourselves (unpublished results, Chambers and Hamza). What is the functional significance of MRP9 in the sperm mid-piece? In this work, we show that MRP5 and MRP9 regulate male reproductive fitness in a concerted manner and are essential for mitochondrial health. Single knockout mice are reproductively viable but double knockout mice have reduced fecundity due to dysfunctional mitochondria and

reduced fertilization rates. Together, our results imply that the ancestral role of MRP5 in *C. elegans* reproduction was co-opted in the vertebrate ancestor by the concerted roles of MRP5 and MRP9.

2 Chapter 2: Materials and Methods

2.1 General methods

2.1.1 Animals

All mice used were housed in Animal Sciences Departmental facilities at the University of Maryland and kept in standard 12-hour light-dark cycles. Both sexes were used for all experiments unless stipulated otherwise, such as the analysis of male sex organs and requisite male reproduction phenotypes. *ABCC12*/MRP9 mutant mice were generated via CRISPR/Cas9 RNA injections at the National Human Genome Research Institute (NHGRI). Guide RNAs (**Appendix I**) were purchased from Sage Laboratories, St Louis, MO and Cas9 RNA was purchased from Trilink Biotechnologies, San Diego, CA. The guide RNA and Cas9 RNA were combined at a concentration of 5 ng/µl each in 10 mM Tris, 0.25 mM EDTA pH 7.5 for pronuclear injection. Performed using standard procedures, fertilized eggs were collected from super-ovulated C57BL/6J females approximately nine hours after mating with C57BL/6J male mice. Pronuclei were injected with a capillary needle with a 1-2 µm opening pulled with a Sutter P-1000 micropipette puller. The RNAs were injected using a FemtoJet 4i (Eppendorf) with continuous flow estimated to deposit approximately 2 pl of solution. Injected eggs were surgically transferred to pseudo-pregnant CB6 F1 recipient females (the pronuclear injections were conducted by Ms. Lisa Garrett, NHGRI). DNA was then obtained from founder (F0) animals by tail biopsy and sequenced to determine mutations. F0 animals carrying mutations were crossed to C57BL/6 animals and the resulting heterozygous F1 animals were either intercrossed

to generate homozygous mutant animals or back crossed to C57BL/6 mice for propagation. MRP5 mutant mice, a gift from Dr. Piet Borst (Netherlands Cancer Institute), had previously been outcrossed into full C57BL/6 background and were bred to MRP9 mutant mice to generate double knockouts (DKOs). MRP5 and MRP9 mice were genotyped from tail genomic DNA via PCR and RFLP methods (see **Appendix II** for complete primer sequences). In brief, tail snips were taken from weaned 21-day old (P21) pups and digested. The MRP5 allele was determined as described previously via amplification of specific MRP5 and hygromycin cassette primers [82]. MRP9 mutants having a +17bp insertion were PCR amplified and subsequently restriction enzyme digested with AvaII (specific to the mutation). All subsequent protocols described below involving these animals were approved by the Institutional Animal Care and Use Committee (IACUC) at the University of Maryland, College Park.

2.1.2 Standard Immunoblotting Method (SIM)

For specific detection of MRP5 and MRP9 protein lysates, as well all other general proteins unless otherwise specified, the following protocol was used: Lysis in lysis buffer (0.75% NP40, 0.5% Triton X-100, 0.1% SDS, 1.75 mM EDTA, 1.25 mM EGTA, 0.25% DOC, 150 mM NaCl, 50 mM HEPES, 25 mM Tris-Cl pH 7.5) with 3x protease inhibitors (cOmplete Protease Inhibitor Cocktail EDTA-free - 1 mM phenylmethylsulfonyl fluoride, 4 mM benzamidine, 2 μg/ml leupeptin, and 1 μg/ml pepstatin, Roche Diagnostics, cat. number 1187358001) and 3x phosphatase inhibitors (Millipore Inhibitor Cocktail Set, cat. number 524627) and sonicated twice. Protein homogenates were then clarified via centrifugation at 15,000 *x g* for 15 min at 4°C and insoluble pellets discarded. Total protein concentration of the supernatant was

measured using the Bradford assay (Bradford Reagent Protein Assay Dye Reagent, Bio-Rad, cat. number 5000006). Unboiled protein samples were then mixed with 4x Laemmli sample buffer and 100 mM dithiothreitol (DTT), and 100 μg of protein/lane was loaded and separated in an SDS-PAGE gel and transferred to a nitrocellulose membrane. Proteins were then cross-linked to membranes by UV treatment and stained with ponceau S solution for 3 minutes for protein loading control before incubation in blocking buffer (5% nonfat dry milk in 0.05% PBS-Tween 20 [PBS-T]) for 1-hour rocking at room temperature. Blots were then incubated overnight at 4°C in blocking buffer containing primary antibody of interest; anti-MRP5 and anti-MRP9 rat monoclonal antibodies are always used at a concentration of 1:200 unless specified otherwise. The following day blots are rinsed once quickly (2 min) and then washed three times (15 min) in PBS-T and subsequently incubated for one hour with horseradish peroxidase (HRP)-conjugated goat anti-rat IgG secondary antibody at 1:20,000 (Invitrogen cat. number 31470). Blots were then rinsed again once quickly, followed by three washes (20 min) with PBS-T and then developed using enhanced chemiluminescence (SuperSignal West Pico PLUS Reagent, Pierce, cat. number 34580) and detected using ChemiDocTM Imaging Systems (Bio-Rad). If subsequent re-probing was necessary, blots were then stripped with 500 mM NaOH for 10min and rinsed quickly with DI H_2O twice, and then PBS-T three times (5min) before blocking again for one hour to repeat the process with subsequent antibodies. The MRP5 (M5I-10, M5-NC3) and MRP9 (M9I-27, M9I-38, M9II-3) antibodies used throughout were a generous gift from Piet Borst (Netherlands Cancer Institute).

2.1.3 Subcellular fractionation and MAM isolation

Mitochondrial Associated Membranes (MAMs) isolation and subcellular fractionizations were based off of Wieckowski et al 2009 Nature Methods Protocol with minor modifications for optimization of testes tissue. Age matched wildtype and double knock out male mice were anesthetized with intraperitoneal injection of ketamine/xylene and then systemic perfusion was performed via standard cardiac puncture method. Perfusion was performed with IB-1 buffer (225 mM mannitol, 75 mM sucrose, 0.5% BSA, 0.5 mM EGTA and 30 mM Tris–HCl pH 7.4) using 25 ml total pushed through a 30 ml syringe with a 26G needle (BD Precision Glide, cat. number 305111) into the left ventricle of the beating heart, which upon completion resulted in completely cleared liver and kidneys. Livers and testes were then immediately harvested and placed in IB-3 buffer (225 mM mannitol, 75 mM sucrose and 30 mM Tris–HCl pH 7.4) on ice at 4°C and the remaining isolation was performed entirely at 4°C in a cold room. A single liver or four pooled testes were necessary to achieve sufficient yield of purified MAMs, which were minced and combined and then lysed in IB-1 buffer via 10 strokes in a 22 gauge 5ml glass duall dounce homogenizer. The homogenate was then spun down twice at 740 *x g* to remove nuclei and cellular debris. The remaining supernatant was spun at 9,000 *x g* for the isolation of crude mitochondria, which was subsequently washed and spun down twice at 10,000 *x g*. The first 10,000 *x g* spin was in IB-2 buffer (225 mM mannitol, 75 mM sucrose, 0.16% BSA and 30 mM Tris–HCl pH 7.4) and then the second in IB-3 for further purification prior to a 100,000 *x g* spin through a Percoll (Sigma, cat. number P1644) gradient to separate MAMs from mitochondria. The original supernatant from the 9,000 *x g* spin

was also spun down at 100,000 *x g* to concentrate the remaining smaller organelles, plasma membranes and cytosolic proteins labeled “Membrane Prep.” Each of the isolated fractions “740 *x g*”, “Membrane Prep”, “Mitochondria” and “MAMs” as well as total initial homogenate were subsequently lysed in lysis buffer and following SIM, ran side by side in a Criterion Precast Gradient 4-15% SDS-PAGE gel for western blotting probing of key intracellular organellar markers and proteins of interest: HSP60 (Abcam, cat. number ab46798), Calnexin (Abcam, cat. number ab22595), Mitofusin 2 (Invitrogen 7H42L13, cat. number 702768), MRP5 and MRP9.

2.1.4 Histology and immunohistochemistry

Paraffin-embedded tissues were sectioned at 4 μm and processed for immunohistochemistry (IHC) as previously described in Pek et al with minor modifications [75]. Slides were first rehydrated in descending gradient from pure xylene through EtOH series (100%, 95%, 80%, 70%) and followed by endogenous HRP quenching before heat-induced epitope retrieval in citrate buffer pH 6 (Target Retrieval Solution, DAKO, cat. number S1700). After epitope retrieval, sections were then rinsed and blocked with avidin, biotin and protein blocking following Vector labs ABC elite staining kit (Vector labs, cat. number PK-6104) prior to incubation with monoclonal rat anti-MRP9 antibodies at 1:50 overnight at 4°C. The next day sections were then incubated with secondary biotinylated anti-rat antibody for 30 minutes at room temperature. ABC tertiary reagent was added and then signals were detected by DAB substrate incubation per manufacturer recommendations (DAB/Metal Concentrate Peroxidase Kit. Thermo Fischer, cat. number 1859346 and 1856090). Finally, slides were lightly counterstained with hematoxylin and then dehydrated in

opposite ascending series and mounted with DPX Mountant (Sigma, cat. number 06522-100).

2.1.5 Heme quantification

To extract heme from perfused mouse tissues, a minimum of 30 mg of caudal epididymides (either three or four pooled together), an entire testis or seminal vesicle were dounce homogenized fresh in a minimum of five volumes of lysis solution containing 50 mM Tris/HCl pH 8.0, 5 mM $CaCl_2$, 50 mM NaCl, 1% Triton X-100 and 0.5% Proteinase K. Proteinase K was added fresh to the buffer and the homogenate was incubated overnight at 37°C with moderate shaking. The next day the Proteinase K digest is sonicated for 1 min (10 W, pulse 0.5 sec), centrifuged at 11,000 *x g* for 45 minutes and then the supernatant was collected for heme quantification. 20 µl of the tissue lysate sample is mixed with 180 µl of 2 M oxalic acid and sample tubes are then heated in a water bath set at 100°C for 30 minutes while a duplicate set of samples remain at room temperature as blank controls. Fluorescence of porphyrins were then read using Ex400/10nm, Em645/40nm on a BioTek microplate reader (BioTek, Synergy HT) and heme content calculated based off of a heme standard curve and subtraction of blank values (parallel unheated samples in oxalic acid) from samples.

2.1.6 EIF2α phosphorylation quantification

Eight age matched wildtype and double knock out male mice were sacrificed by cervical dislocation, and whole testes were dissected out and rinsed in ice cold PBS. A single testis was then homogenized in 500 µl standard lysis buffer with 5x protease inhibitors and 3x phosphatase inhibitors, via 8 strokes in a 20 gauge 2 ml glass duall

dounce homogenizer, transferred to 1.5 ml Eppendorf tube and placed on ice for 15 minutes, vortexing for 15 seconds every 5 minutes. Afterward, the homogenate is then sonicated for 10 seconds, twice, prior to proceeding with standard clarifying spin for SIM. For all samples, 150 µg of protein was then separated on Criterion Precast Gradient 4-15% SDS-PAGE gels (Bio-Rad, cat. number 5671083) and probed for phosphorylated EIF2α protein levels with rabbit anti-Eif2a S51 phosphorylation polyclonal antibody (1:500 dilution) (Cell Signaling Technologies, cat. number D9G8) and Total EIF2α protein levels with rabbit anti-Eif2a polyclonal antibody (1:10,000 dilution) (Cell Signaling Technologies, cat. number D7D3). Additional blots were probed with rat anti-MRP5 NC3 monoclonal antibody (1:200) and rat anti-MRP9 M9I-27 monoclonal antibody (1:200). Quantification of EIF2α S51 phosphorylation was performed by Image Lab 6.1 software (BioRad) and normalized to total EIF2α protein.

2.2 Mouse reproduction studies

2.2.1 Breeding schema for general fecundity and fertility

All breeding studies were performed in harem setups with one stud male mouse and two female mice per cage. These harems were monitored over a period of at least 6 months to track breeding of *ABCC5/ABCC12* double knockout mice (-/-, -/-) as well as the requisite control intercrosses of heterozygous-homozygous (+/-, -/-) and homozygous-heterozygous (-/-, +/-) mice. Once successful pregnancies were determined, females were separated from males and individually housed for monitoring fecundity. New female mice were then rotated in the male mice cages to maintain

setups of two female mice per stud male. Males unable to produce any pregnancies after two months were removed and replaced. Pregnant dams were monitored at least twice daily for birth of pups and overall health, litter size was recorded at birth and any subsequent mortality logged through weaning was reported. Fecundity was calculated based off the number of breeding setups required to achieve same number of pregnancies as well as the number of offspring per litter and average productivity of litters per harem breeding setup. All genetic segregation and statistics for MRP5 and MRP9 alleles were calculated on weaned P21 mice.

2.2.2 *In vitro* fertilization (IVF) and general sperm characterization

All IVF was conducted in HTF media (EmbryoMax, Sigma, cat. number MR-070), supplemented with 3 mg/ml of BSA. Males were mated with females and assessment of mating was determined by the presence of a vaginal plug. Males that were listed as plug positive were allowed to rest a total of three days prior to IVF. Spermatozoa was collected from individual males and placed in 90 µl of TYH media supplemented with beta-methyl-cyclodextrin to induce capacitation [158]. Sperm samples were allowed to capacitate for a total of 45-60 minutes. A 10 µl sample was diluted in 1400 µl of IVF media and assessed on an IVOS system (Hamilton Thorne CASA - Computer Assisted Sperm Analyzer). Total sperm concentration, percent progressive motility and percent rapid motile cells was calculated. Visual assessment of morphology was assessed, and percentage of proximal tail bends and distal tail bends were determined. IVF was conducted and standardized to an insemination dose of 1.0 x 10^6 sperm/ml for each male processed. Oocytes and sperm were incubated for a total of 5 hours. Presumptive zygotes were rinsed through HTF media to remove accessory

sperm and cultured overnight in KSOM media plus amino acids [159]. The next morning, total number of two cell embryos were determined and a fertilization rate calculated based on the number of two cell embryos per total number of oocytes inseminated (these experiments were performed by Charles River Labs).

2.2.3 Sperm "swim-out" collection for advanced imaging

Age matched male mice were sacrificed by cervical dislocation, and entire reproductive tracts were dissected out intact to isolate the caudal epididymis. Caudal epididymides (CE) were trimmed away from fat pads and the testes, rinsed once quickly (dipping) in DPBS and then dabbed dried (single touch) on a kimwipe before being placed in a 35 mm dish with mineral oil. Prewarmed DPBS with added 100 mg/L $MgCl_2$ and $CaCl_2$ (swim-out solution) to 37°C was then added to the mineral oil in close proximity to the CEs for sperm swim-out. Swim-out was achieved by snipping the CEs with dissecting micro-scissors and dragging the exposed globule with a 22G needle from the mineral oil into the swim-out solution. The entire petri dish was then covered and then placed in the 37°C incubator for 30min to allow for purified sperm to fully swim-out into the solution. Then sperm were collected with a 1ml pipettor and spun down gently in a 1.5 ml Eppendorf tube at 333 *x g* for 3 minutes, followed by resuspension in fresh swim-out buffer and rocked gently for 2 minutes. This rinsing was repeated the same way again twice, and after the third rinse and spin down the sperm are resuspended in a final 4% PFA (for label-free heme imaging) or 2% PFA and 1% Glutaraldehyde (for transmission electron microscopy [TEM] imaging) solution. For pilot testing of label-free heme imaging of sperm, fixed sperm samples were then smeared on microscope slides and imaged via transient absorption (TA)

microscopy in collaboration with Dr. Ji-Xin Cheng's Lab at Boston University following previously established protocols [160,161]. An N of > 30 individual whole intact wildtype sperms were imaged for testing heme content and quantification by concentration per total sperm or volumetrically per cubic nanometer. TEM imagery of sperm was done in collaboration with Dr. John Phillips' Lab and the University of Utah Health Sciences Center Core where embedding, sectioning and imaging of sperm was conducted by Ms. Nancy Chandler. Representative cross-sectional planes of the sperm midpieces were taken using a JEOL JEM 1400plus microscope at 6000x magnification for an n > 15 FOVs for each animal sample.

2.3 Mammalian cell culture methods

All mammalian cells were cultured continuously at 37°C in a humidified incubator with 5% CO_2. Immortalized fibroblasts were generated from mouse embryos isolated at E12.5 by sacrificing pregnant females and culturing the mouse embryonic fibroblasts (MEFs) as described previously [82,162]. Once established, these primary cells from wildtype, MRP9 single knockout and double knockout mice were immortalized by retroviral infection of MEFs with conditioned media from Ψ2-U195 cells producing the SV40 large T antigen and cell lines were genotyped using the same MRP5 and MRP9 primers listed in **Appendix II**. For overexpression in cell culture, plasmids for either *ABCC5* or *ABCC12* constructs were transfected into cell lines using PolyJet transfection reagent (SignaGen Laboratories, cat. number SL100688). Previously, human *ABCC5* ORF was cloned into pcDNA3.1(+)zeo and pEGFP-N1 plasmids for mammalian expression [82]. Likewise, human *ABCC12* ORF was cloned

into pcDNA3.1(+)zeo via EcorI and XbaI in a similar manner and subsequently epitope tagged with FLAG. Cells that were transfected with either vector or MRP expressing constructs could then be harvested up to 48 hours later for western blotting (protein expression), microscopy (localization) or other downstream assays. For attempting induction of endogenous expression of MRP5 or MRP9 in cell lines possibly capable of production (i.e. T-47D, A549, HCT116 and GC-2spd), cells were treated for 24 hours with 2 mM Sodium Butyrate (NaB) following methods from Bin Shi et al 2020 and then analyzed for expression and subcellular localization [157]. For western blotting, cells were harvested in standard lysis buffer and followed SIM as described above. For polarization of MDCKII cells, trypsinized cells were seeded onto transwell cell culture inserts (Corning, COSTAR Polystyrene 6 well plates 24mm inserts, cat. number 3450) and allowed to grow to a monolayer in standard growth media (DMEM supplemented with 10% FBS) changed daily. Prior to reaching confluence, MDCKII cell's monolayer integrity was determined daily by measuring the transepithelial electrical resistance (TEER) using an EVOM^2 Epithelial Voltohmmeter device (World Precision Instruments, cat. number EVOM2). MDCKII cells were considered polarized and used for imaging when TEER values exceeded 200 Ω/cm^2 resistance and were validated by checking for markers of polarization. Immunofluorescence was performed as follows: cells seeded onto coverslips (or transwells) were rinsed with ice cold DPBS (and subsequently in between each additional step) and immediately fixed in freshly prepared 4% PFA for greater than 30 minutes; cells were then quenched with 0.1 M ethanolamine for 5 minutes, twice; permeabilized with 0.1% Triton-X 100 in DPBS solution for 10 minutes; and blocked in blocking solution of 3% BSA:Superblock

(SuperBlock Buffer in PBS, Thermo Scientific, cat. number 37515) for greater than one hour at room temperature or overnight at 4°C; incubated with primary antibody (rat monoclonal anti-MRP9 M9I-38, 1:10 in blocking solution) overnight at 4°C; secondary antibody (Alexa fluorophore-conjugated goat anti-rat, 1:2000 in blocking solution) for 1 hour at RT; and subsequently counterstained with DAPI (1:30,000 of 5 mg/ml) for 3 minutes and mounted using Antifade reagent (ProLong Gold Antifade Reagent, Invitrogen, cat. number P36934). Images were taken and processed using an Airyscan980 SR confocal microscope (Zeiss) and we acknowledge the Imaging Core Facility in the department of Cell Biology and Molecular Genetics at the University of Maryland, College Park supported by Award Number 1S10OD025223-01A1 from the National Institutes of Health.

2.4 Metabolomics methods

2.4.1 Global untargeted metabolomics of mouse testes

Tissue was first extracted either in aqueous or organic methods. For aqueous extractions, 10 volumes of methanol:H_2O (3:1) was added to the tissue sample and homogenized with ceramic beads (Precellys®24-Dual, PeqLab). Then 200 µl of the homogenate was transferred to a new tube where it was then vortexed and centrifuged at 15,000 RPM for 10 min at 4°C. The supernatant was transferred to sample vial for ultra high performance liquid chromatography coupled with mass spectrometry (UHPLC-MS) analysis. Analytes were separated with either a CSH C18 column or a BEH amide column for more nonpolar and polar species, respectively. For the first

aqueous method, separation was achieved using an ACQUITY UPLC CSH C18 Column (1.7 µm, 2.1 mm X 100 mm). Mobile phase A was water (contained 0.1% formic acid) and mobile phase B was acetonitrile (contained 0.1% formic acid). The gradient was: 0 to 1 min, 5% B; 1.1 to 10 min, 5% to 95 % B; 10.1 to 13 min, 95 % B; 13.1 to 13.5 min, 95 to 5% B; 13.6 to 15 min, hold at 5% B. The flow rate was 0.5 mL/min. The column was maintained at 50°C and the auto-sampler was kept at 10°C. A 5 µL injection was used for all samples. For the second method of aqueous analysis, the separation was achieved using an ACQUITY UPLC BEH amide Column (1.7 µm, 2.1 mm X 100 mm). Mobile phase A was water (contained 0.1% formic acid) and mobile phase B was acetonitrile (contained 0.1% formic acid). The gradient was: 0 to 1 min, 99% B; 1 to 10 min, 99% to 30 B; 10.1 to 12 min, hold at 99% B. The flow rate was 0.5 mL/min. The column was maintained at 45°C and the auto-sampler was kept at 10°C. A 5 µL injection was used for all samples. For both aqueous sample preps, data was acquired in both positive (HDMSe) and negative (HDMSe) mode. The capillary voltages were separated for positive (0.8 kV) and negative (0.8 kV) and sampling cone voltage was 40 V. Nitrogen at a flow of 800 L/h was used as the desolvation gas with a constant desolvation temperature of 500°C. The source temperature was set at 150°C. Data were acquired over the *m/z* range of 50-1000. For organic extraction (lipid) methods, likewise 10 volumes of methanol:H_2O (3:1) was added to the tissue sample and homogenized with ceramic beads (Precellys®24-Dual, PeqLab). However, now after homogenization 400 ul was transferred to a new tube and 500 µL of ice-cold methyl-tert-butyl ether (MTBE) is added, prior to incubation at 650 RPM for 1 hour. Additionally, 500 µL of ice-cold water was then added and incubated

at 650 RPM for 15 min before phase separation was completed by centrifugation for 8 min at 8,000 RPM at 4°C. The top (organic) layer was removed and dried at room temperature under nitrogen. The recovered lipids were reconstituted in 200 µL of isopropanol:acetonitrile:water (2:1:1, v/v/v) and were transferred to sample vial for UPLC-MS analysis. The separation was achieved using a CORTECS HILIC Column (2.7 µm, 2.1 mm X 100 mm). Mobile phase A was water/acetonitrile (5:95, v/v) with 10 mM ammonium acetate and mobile phase B water/acetonitrile (50:50, v/v) with 10 mM ammonium acetate. The gradient was ramped from 0.1% to 20% B in 10 min, ramped to 80% B in 3 min, ramped back down to 0.1% B and held for 3 min. The flow rate was 0.5 mL/min. The column was maintained at 30°C and the auto-sampler was kept at 10°C. A 5 µL injection was used for all samples. Like the aqueous phase, data was acquired in both positive (HDMSe) and negative (HDMSe) mode. The capillary voltages were separated for positive (2.8 kV) and negative (1.9 kV) and sampling cone voltage was 30 V. Nitrogen at a flow of 900 L/h was used as the desolvation gas with a constant desolvation temperature of 550°C. The source temperature was set at 120°C. Data were acquired over the *m/z* range of 100-1500. Positive and negative mode data were basally analyzed by Progenesis QI and putative metabolite identification was searched by using HMDB and LIPID MAPS databases (delta < 5 ppm). The output marker lists were then manually sorted and annotated for more sophisticated downstream analysis with MetaboAnalyst [163-165]. Multivariate data analysis, volcano plots, Variable Importance in Projection (VIP) heat maps and mummichog algorithm analysis to putatively annotate metabolites were performed using

MetaboAnalyst 4.0 [166]. All metabolomics species extractions and data collection here and below were performed by the Kane Lab, UMB School of Pharmacy.

2.4.2 Measurement of retinoids from reproductive tissues

Two separate analyses were performed to determine the retinoid profile in wild type and double knockout mice. Testes and seminal vesicles were assayed for retinoic acid isomers and retinol and total retinyl esters. Tissue samples were stored in -80°C until processed. Only glass containers, pipettes, and syringes were used to handle retinoids. Extraction of retinoids was performed under yellow lights using a two-step liquid-liquid extraction that has been described in detail previously using 4,4-dimethyl-RA as an internal standard for RA and retinyl acetate as an internal standard for retinol and total retinyl ester [167-170]. Briefly, for the extraction of retinoids, tissue was homogenized in 1 mL of 0.9% NaCl (normal saline) and to each homogenate aliquot, 3 mL of 0.025 M KOH in ethanol was added to the homogenate followed by addition of 10 mL hexane to the aqueous ethanol phase. The samples were vortexed and centrifuged for 1 to 3 min at 1,000 rpm in a Dynac centrifuge (Becton Dickinson) to facilitate phase separation and pellet precipitated protein. The hexane (top) phase containing nonpolar retinoids [retinol and total retinyl esters (RE)] was removed. Then 4 M HCl (200 μL) was added to the remaining aqueous ethanol phase, samples were vortexed, and then polar retinoids (RA) were removed by extraction with a second 10 mL aliquot of hexane as described above. Organic hexane phases were evaporated under nitrogen while heating at approximately 30°C in a water bath (model N-EVAP 112, Organomation Associates, Berlin, MA, USA). All samples were resuspended in 60 μL acetonitrile.

Levels of RA were determined by liquid chromatography-multistage tandem mass spectrometry (LC-MRM^3) which is an LC-MS/MS method utilizing two distinct fragmentation events for enhanced selectivity [167]. RA was measured using a Shimadzu Prominence UFLC XR liquid chromatography system (Shimadzu, Columbia, MD) coupled to an AB Sciex 6500+ QTRAP hybrid triple quadrupole mass spectrometer (AB Sciex, Framingham, MA) using atmospheric pressure chemical ionization (APCI) operated in positive ion mode as previously described [167]. For the LC separation, the column temperature was controlled at 25°C, the autosampler was maintained at 10°C and the injection volume was typically 20 µL. All separations were performed using an Ascentis Express RP-Amide guard cartridge column (Supelco, 50 × 2.1 mm, 2.7 µm) coupled to an Ascentis Express RP-Amide analytical column (Supelco, 100 × 2.1 mm, 2.7 µm). Mobile phase A consisted of 0.1% formic acid in water, and mobile phase B consisted of 0.1% formic acid in acetonitrile. Endogenously occurring retinoid isomers including all-trans-retinoic acid (RA), 9-*cis* retinoic acid, 13-*cis* retinoic acid, and 9,13-di-*cis* retinoic acid are resolved using a gradient separation at a flow rate of 0.4 mL min^{-1} with gradient conditions described previously [167]. The APCI source conditions and MRM^3 detection parameters were as previously described where the MRM^3 transition for RA was *m/z* 301.1 → *m/z* 205.1 → *m/z* 159.1 and for 4,4-dimethyl RA was *m/z* 329.2 → *m/z* 151.2 → *m/z* 100.0 [167].

Levels of retinol and total retinyl esters (RE) were quantified via HPLC-UV according to previously published methodology [170,171]. Note: total retinyl esters is 90+% retinyl palmitate. Retinol and RE were resolved by reverse-phase chromatography (Zorbax SB-C18, 4.6 × 100 mm, 3.5 µm) on a Waters Acquity UPLC

H-class system and were quantified by UV absorbance at 325 nm. Analytes were separated at 1 mL min^{-1} with a gradient separation as described previously with a typical injection volume of 30 μL. The amount of retinoic acid (RA), retinol (ROL) and total retinyl ester (RE) was normalized per gram of tissue.

2.4.3 Targeted metabolomics of subcellular fractionation of testes

High Throughput Targeted Metabolomics were performed on subcellular fractions isolated from WT and DKO testes. This subcellular fractionation was performed as described above with minor modifications, generating "Total Homogenate", "740 *x g*", "Membrane Prep", "Mitochondria" and "MAMs" fractions. In order to maintain compatibility with downstream mass spectrometry analysis, each fraction was collected in ice cold 0.9% saline for its final centrifugation and subsequently was rinsed and diluted in ice cold 0.9% saline instead of lysis buffer prior to freezing. The concentration of metabolites and lipids were then determined with mass spectrometry using MxP® Quant 500 kit (Biocrates Life Sciences AG, Innsbruck, Austria). The kit enables quantification of approximately 630 endogenous metabolites belonging to 26 different biochemical classes: alkaloids (1), amine oxides (1), amino acids (20), amino acids related compounds (30), bile acids (14), biogenic amines (9), carbohydrates (1), carboxylic acids (7), cresols (1), fatty acids (12), hormones (4), indoles and derivatives (4), nucleobases and related compounds (2), vitamins (1), acylcarnitines (40), lysophosphatidylcholines (14), phosphatidylcholines (76), sphingomyelins (15), ceramides (28), dihydroceramides (8), hexosylceramides (19), dihexosylceramides (9), trihexosylceramides (6), cholesteryl esters (22), diglycerides (44), triglycerides (242). The method combines direct infusion coupled with tandem

mass spectrometry (DI – MS/MS) and reverse phase liquid chromatography coupled with tandem mass spectrometry workflows (LC – MS/MS). Extraction was carried out per manufacturer's instructions. Tissue samples were homogenized with ceramic beads (Precellys®24-Dual, Bertin Technologies SAS, France) prior to analysis. Briefly, mitochondrial fractions and tissue homogenates were thawed over ice and 30 µl of the sample was loaded onto the filter plate in 96 well format, impregnated with deuterated internal standards and dried under a stream of nitrogen in a positive pressure manifold. A 5% solution of phenylisothiocyanate in ethanol:water:pyridine (1:1:1, v:v:v) was added for derivatization of metabolites. Extraction was done with 5mM ammonium acetate in methanol. The extracts were eluted with positive pressure manifold, followed by dilution steps for LC-MS/MS and DI-MS/MS acquisitions. The tandem mass spectrometry platform consisted of a Waters I Class Ultra performance liquid chromatography (UPLC) coupled to a Waters TQ-XS tandem quadrupole mass spectrometer (Waters Corporation, Milford, MA). MetIDQ software (Biocrates Life Sciences AG, Innsbruck, Austria) was used to register the samples, analyze the data and validate the assay. All reagents used were of analytical grade and mobile phases used were of LC-MS grade.

2.5 Transcriptomics and associated methods

2.5.1 Global RNAseq of mouse tissues

RNA was extracted from frozen tissues following standard Trizol chloroform protocol (Invitrogen, cat. number 15596026) and aqueous fractions were then taken

directly into Qiagen RNA plus extraction kit (Qiagen, cat. number 74136) for maximum purity. Total RNA quality and quantity were tested on an Agilent Bioanalyzer 2100 System (Agilent cat. number G2939BA) using RNA Nano Chip On-Chip Electrophoresis trays for samples with RIN scores greater than 8 prior to processing for library prep/construction and sequencing. RNA-seq was performed at NISC using Illumina NovaSeq6000. FastQC, version 0.11.7, was used as an additional bioinformatics quality control on output reads from sequencing. The reads were then aligned to the mouse mm10 GRCh38 reference genome for gene annotation using STAR (Spliced Transcripts Alignment to a Reference), version 2.7.0f, and numbers of reads in transcripts per million (TPM) mapped to genes were counted generating matrixes for all samples. Differentially expressed genes were then identified via both manual export, sorting and fold change annotation, as well as processed via DESeq2, version 1.12.3, for more complex analysis. DESeq2 was run using R (version 3.6.1) and Bioconductor (version 3.4) with BioInstaller (version 1.24.0) for volcano plotting and statistical analysis of differential changes utilizing adjusted *P* value < 0.01 and False Discovery Rate (FDR) cutoffs of 0.05.

2.5.2 Pathway analysis

Gene Ontology (GO) enrichment and network analysis of RNAseq results were performed using both Ingenuity Pathway Analysis (IPA) software package (Qiagen version 1-16) and manually developed excel pipeline workflows. For IPA analysis, statistically significant gene lists by tissue were manually filtered for minimum threshold of 10 TPM, sorted by *P* value and uploaded along with gene expression fold change for analysis. For pipeline pathway analysis, gene lists for GO terms and

associated pathways of interest were downloaded from MGI [172-174], RGD [175] as well as manually added from literature review of relevant publications. These all-encompassing lists were then used as target gene IDs for filtered call look up functions from RNAseq gene expression RSEM matrixes. In brief, genes with matching IDs which passed threshold of expression in at least one sample condition and were statistically significant, were output in a heatmap with *P* value and relative fold change displayed.

2.5.3 Motif analysis

The MEME Suite and HOMER motif platforms were used to unbiasedly identify conserved motifs via discovery analysis of enriched sequences from differentially expressed genes. More specifically, we generated gene lists (either globally or mitochondria targeted) and divided them into upregulated and downregulated genes and extracted their associated sequence FASTA files. Then 1000bp upstream of ORF and 50bp downstream were used to run MEME or HOMER via pearl scripts on NIH High Performance Cluster (HPC) to discover the top 5 ungapped enriched putative motif sequences. These sequences were then further analyzed with the web-based suite tools TomTom and GoMo for MEME motif findings and manually curated for motif verification, which were further validated by checking and annotating output from the HOMER suite. This work, as well as some of the RNAseq processing, was done in collaboration with the Bodine Lab utilizing the computational resources of the NIH HPC Biowulf cluster (http://hpc.nih.gov).

2.6 Statistical analyses

All data throughout are expressed as means ± SEM unless otherwise stated. Means of groups were assessed by using two-sided, unpaired student's t-test or the equivalent analyses where applicable unless otherwise stated. A *P* value of <0.05 when compared to baseline values or genotypes (WT) was considered statistically significant. All analyses were performed using Prism 9 software (GraphPad, version 9.1.0).

3 Chapter 3: The Function of MRP9 and MRP5 in Male Reproduction

3.1 Summary

Previous studies in *C. elegans* have demonstrated that the heme transporter MRP-5 is essential for male fecundity in worms, however MRP5 knockout mice do not show any male reproductive deficits. Here, we show that loss of both MRP5 and its close homolog MRP9 (ABCC12) recapitulate male reproductive phenotypes in mice. Even though MRP9 is solely expressed in maturating spermatozoa in mice, MRP9 knockout males reveal no overt reproductive phenotypes unless MRP5 is also eliminated. Concomitant with the reproductive phenotype, both MRP9 and MRP5 are highly enriched in mitochondrial-associated membranes in the testes. Loss of MRP9 and MRP5 (DKO) disrupts mitochondrial homeostasis and regulatory pathways, resulting in ineffective sperm with reduced reproductive fitness and abnormal mitochondria. RNA-seq and metabolomic analyses of DKO testes reveal large-scale perturbation in genes and metabolism related to mitochondrial function. Taken together, our results establish a concerted and critical role for MRP9 and MRP5 in male reproduction and mitochondrial metabolism.

3.2 Results

The generation of MRP9 KO and MRP9/5 DKO mice

MRP9 mutant mice were generated via CRISPR/Cas9 by injecting guide RNAs targeted to the second exon of *ABCC12* (**Figure 3.1A and Appendix 1)**. DNA sequencing of founder animals revealed various indels in 11 animals at the target site; a 17 bp insertion was selected for further characterization **(Figure 3.1B & C)**. RT-PCR confirmed that the frameshift-inducing mutation was transcribed but no alternate start sites or splice variants were identified **(Figure 3.1C)**. *ABCC12*$^{-/-}$ animals are viable and reach adulthood with no overt phenotypes. Immunoblots of lysates from testes from adult mice showed no detectable MRP9 protein **(Figure 3.2A)**. Immunohistochemistry of tissue sections showed that MRP9 is specifically detected in both the maturing and developed spermatozoa of seminiferous tubules and caudal epididymis, respectively **(Figure 3.2B)**, consistent with the findings reported by Ono et al [114].

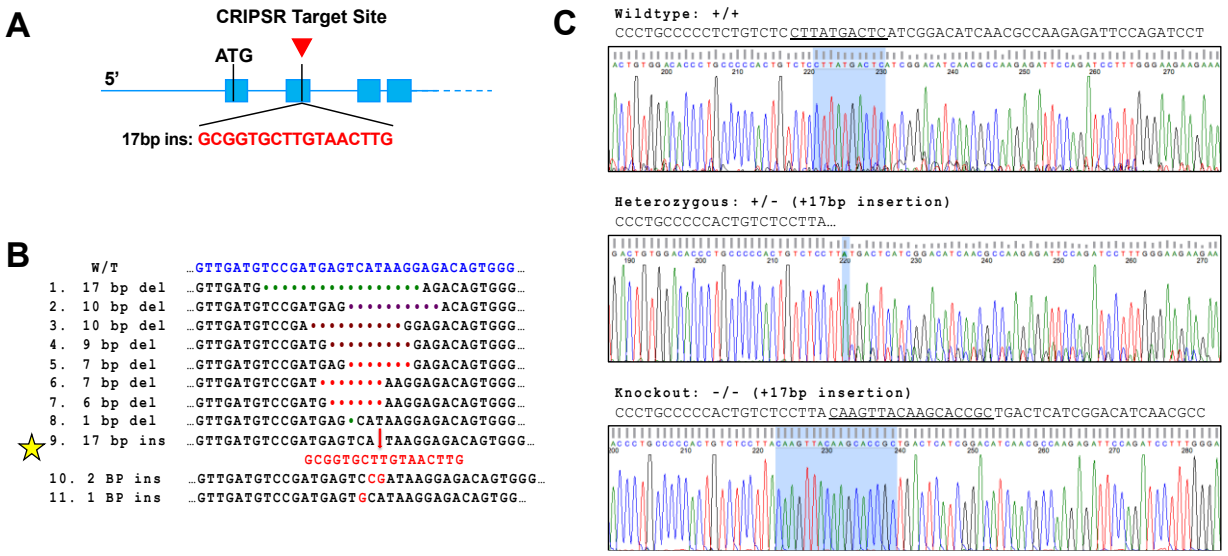

Figure 3.1 Generation of the *ABCC12*$^{-/-}$ mouse

(A) Gene loci of *ABCC12* indicating the CRISPR target site in second exon.

(B) DNA sequence of *ABCC12* CRISPR target site indicating the mutations generated in the founder animal lines.

(C) Sequencing of RT-PCR from testes of *ABCC12* WT, HET and KO mice confirming mutation.

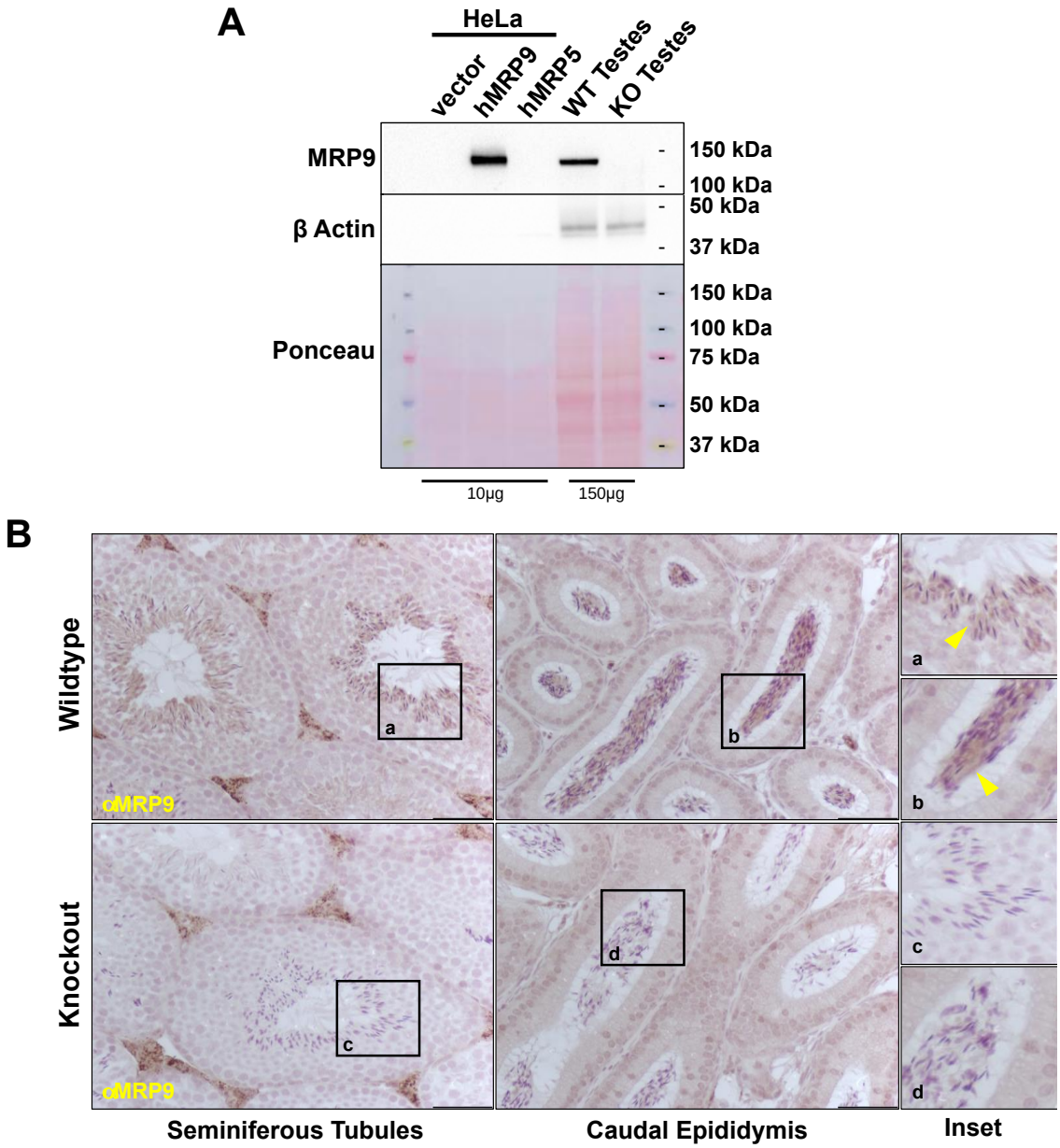

Figure 3.2 MRP9 is highly expressed in the maturating sperm of the testes and caudal epididymis

A) Immunoblot analysis of lysates from transfected HeLa cells and mouse testes; membrane probed for MRP9 and beta-actin following SIM.

B) MRP9 immunohistochemistry analysis of paraffin-embedded testes tissue sections from WT and KO mice. Tissue sections were probed for MRP9 and lightly counterstained with hematoxylin. Images are representative of at least 3 mice and two different anti-MRP9 antibodies. Scale bar equals 100 μm.

Single cell RNAseq datasets of the testis niche **(Figure 3.3A)** further confirmed this finding as the gene expression profile of *ABCC12* is distinctly germ cell specific **(Figure 3.3B)** [153]. This is in contrast to *ABCC5*, which is expressed in early spermatogonia precursors as well as Sertoli and Leydig cells **(Figure 3.3B)** [153]. Immunoblotting of lysates from additional tissues of wildtype and KO mice revealed the testes as the only organ with any appreciable amounts of both MRP9 and MRP5 **(Figure 3.4)**. Nevertheless, single knockouts did not show any statistically significant defects in reproduction, with expected litter size and normal Mendelian segregation of progeny with intercrosses capable of producing DKO animals **(Figure 3.5)**.

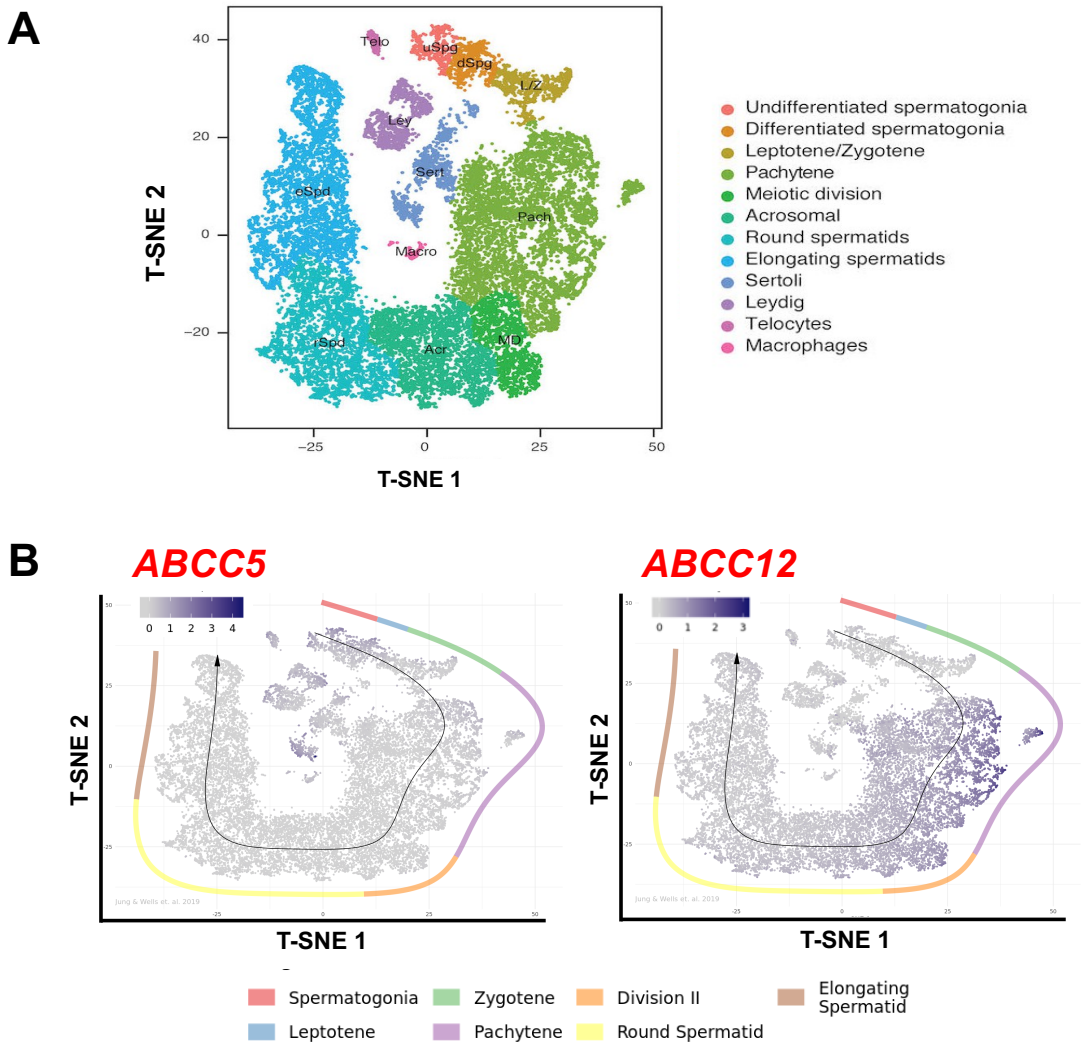

Figure 3.3 Single cell testes RNAseq atlas reveals distinct temporospatial expression of *ABCC5* and *ABCC12*

A) Single cell RNAseq atlas reference output of distinct marker cell populations within the testes taken from Jung et al 2019 [153].

B) *ABCC5* (left) and *ABCC12* (right) gene expression profiles along the temporospatial axis of spermatid maturation [153].

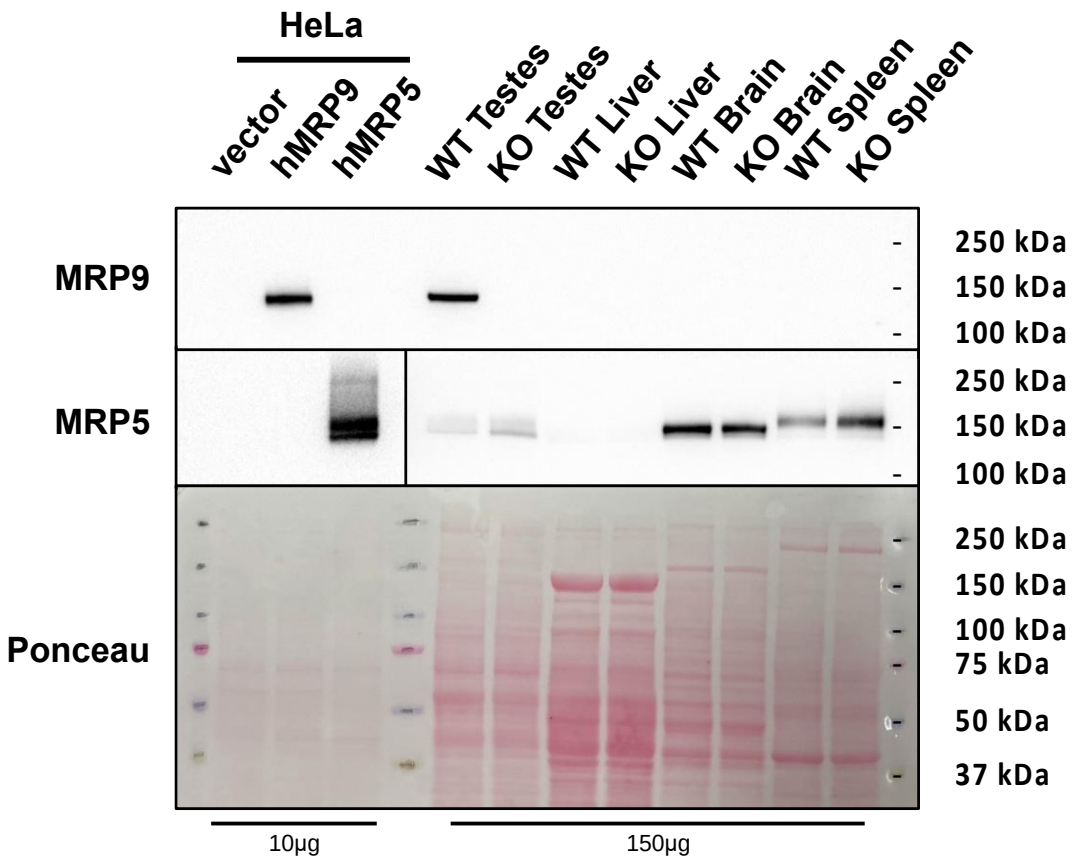

Figure 3.4 MRP5 is present in the testes at low levels in WT and MRP9 KO mice, the primary tissue of MRP9 protein expression

Immunoblot of protein lysates wildtype and MRP9 KO tissues; membrane is probed for MRP9 and MRP5 following SIM.

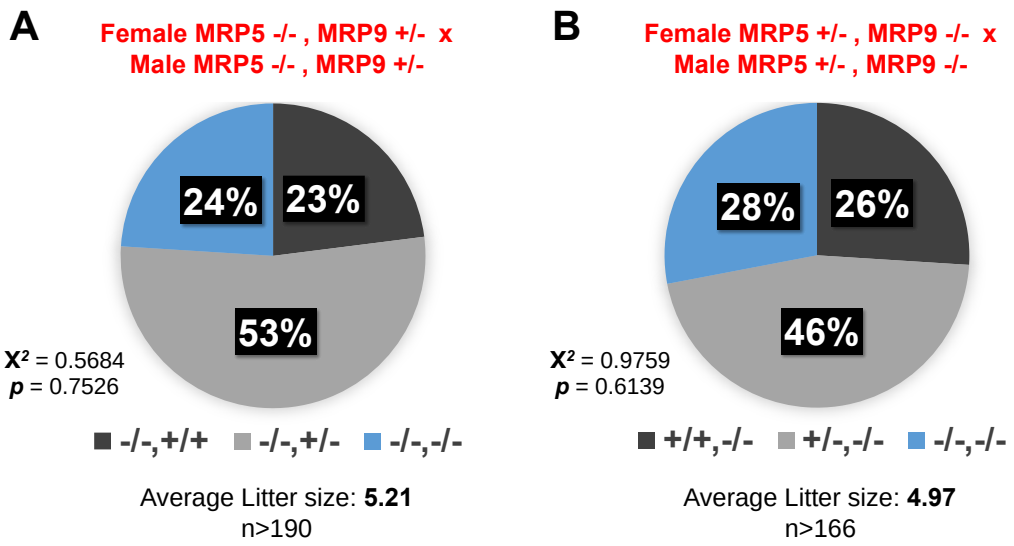

Figure 3.5 Progeny from MRP9 and MRP5 knockouts show normal Mendelian segregation of offspring and viability of DKO mice

a) Genotyped progeny from MRP5-/- and MRR9+/- intercrosses, Chi-squared and *P* values calculated with Prism 9 (GraphPad).

b) Genotyped progeny from MRP5+/- and MRR9-/- intercrosses, Chi-squared and *P* values calculated with Prism 9 (GraphPad).

MRP9 and MRP5 are required for male reproductive fitness

Although DKO mice were clearly viable, upon attempting to breed them we quickly ascertained they were highly deficient in their reproductive capacity. Both the number of pups born **(Figure 3.6A)** and number of pups weaned **(Figure 3.6B)** from DKO litters were significantly reduced compared to WT, requiring over three times the number of pregnancies to produce equivalent numbers of animals **(Figure 3.6C)**. Furthermore, DKO male mice had high incidences of penile prolapse and clogging of the urogenital track with seminal coagulum (five DKO compared to zero WT studded mice), regardless of female genotype **(Figure 3.7A)**. This prompted closer investigation into male fitness as a possible culprit in DKO fecundity. Indeed, sperm from DKO mice had significantly lower *in vitro* fertilization rates compared to wildtype **(Figure 3.7B)** despite no differences in total sperm production **(Figure 3.7C)**. Though not significant, this possibly can be attributed to sperm fitness as DKO sperm showed decreased motility trends **(Figure 3.7D & E).**

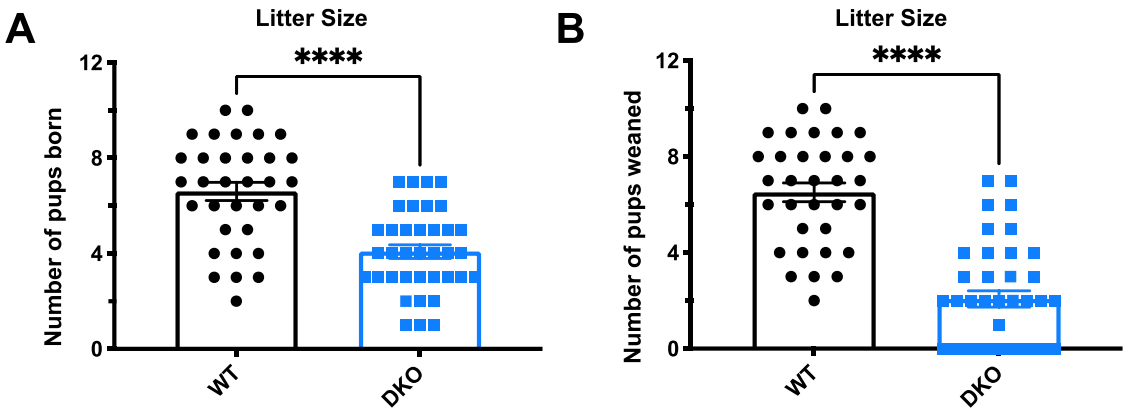

C

Male x Female Genotype	Pregnancies	Pups Born	Pups Weaned	Survival	Litter Size
WT X WT	33	218	215	**0.99**	**6.52**
DKO x DKO	44	151	83	**0.55**	**1.89**

Figure 3.6 MRP9 and MRP5 double knockout mice are viable but have reduced reproductive fitness and fecundity

a) Quantification of the number of pups born per litter of WT vs DKO mice, **** = $P < 0.0001$.

b) Quantification of the number of pups weaned per litter of WT vs DKO mice, **** = $P < 0.0001$.

c) Numbers of breeding setups and percentage of pup survival from double knock out mice compared to wildtype pairings quantified in panel A and panel B.

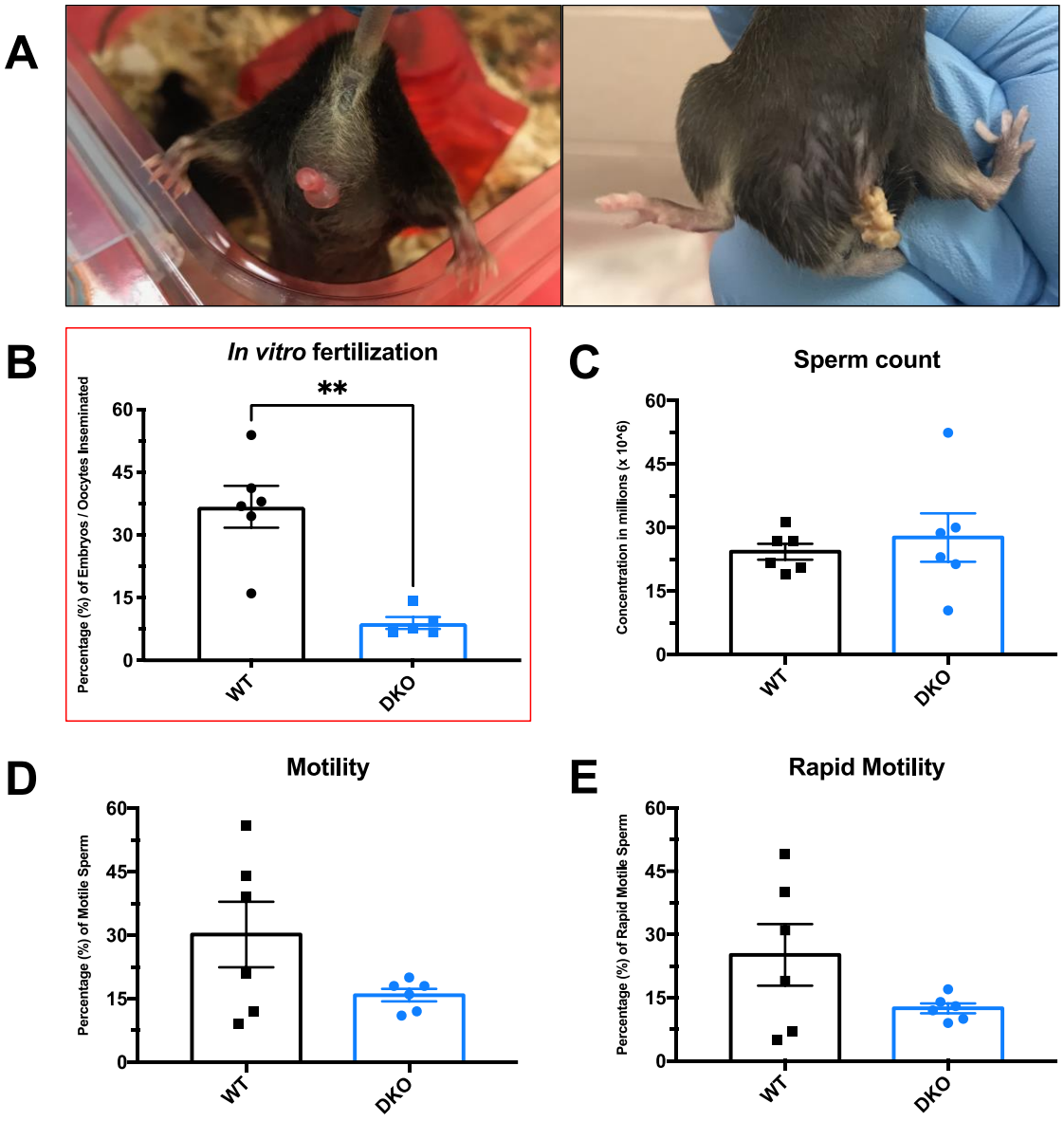

Figure 3.7 Double knockout mice reveal significant defect in male reproductive fitness

A) Representative images of penile prolapse (left) and seminal coagulum (right) in DKO male mice setup for breeding.

B) *In vitro* fertilization rate of WT and DKO sperm incubated with WT oocytes for 5 hours at a concentration of 1.0 x 10^6 sperm/ml. Next day total number of two cell

embryos were determined and a fertilization rate was calculated based on the number of two cell embryos divided by the total number of oocytes inseminated for each male, ** = $P < 0.002$.

C) Total concentration of spermatozoa calculated by IVOS system computer assisted sperm analyzer.

D) Percentage of "progressive motile" capacitated sperm assessed by IVOS system computer assisted sperm analyzer.

E) Percentage of "rapid motile" capacitated sperm assessed by IVOS system computer assisted sperm analyzer.

MRP9 is associated with the mitochondria in the testes

To understand why DKO male mice have reduced fecundity and sperm fitness we looked to further characterize the function of these proteins in this context. Given the distinct spatiotemporal gene expressions **(Figure 3.3)**, we hypothesized that MRPs may play redundant subcellular roles during spermatid maturation. As discussed earlier, MRP9 had been previously described to localize to the sperm midpiece, the location of the mitochondrial sheath, while transfection in cells most closely resembled an ER localization, not plasma membrane [114]. To examine MRP9 localization, crude subcellular fractionation was first performed on lysates from mouse testes followed by immunoblotting. MRP9 protein was significantly enriched in 9,000 *x g* fractions which pellet mitochondria **(Figure 3.8A)**. Given this surprising finding, we further separated these crude mitochondrial fractions via Percoll-based differential centrifugations based

on Weickowski et al [176]. Modifications for isolation of testes tissue allowed for the successful separation of nuclei and debris (740 *x g* spin), plasma membrane, lysosomes/microsomes and cytosolic components (100,000 *x g* Membrane Prep), purified mitochondria, and mitochondrial-associated membranes (MAMs). Immunoblots on these fractions revealed that MRP9 was not present in purified mitochondria but rather is significantly enriched in MAMs, the associated contact sites of the ER and mitochondria, which are characterized by the markers Mitofusin 2 and Calnexin **(Figure 3.8B)**. We further confirmed that MRP9 was specifically enriched in the MAMs of the testes using MRP9 antibodies targeting different epitopes **(Figure 3.9)**. Interestingly, probing these membranes with anti-MRP5 antibody showed MRP5 protein was also present in the MAMs as well as total membranes **(Figure 3.9)**.

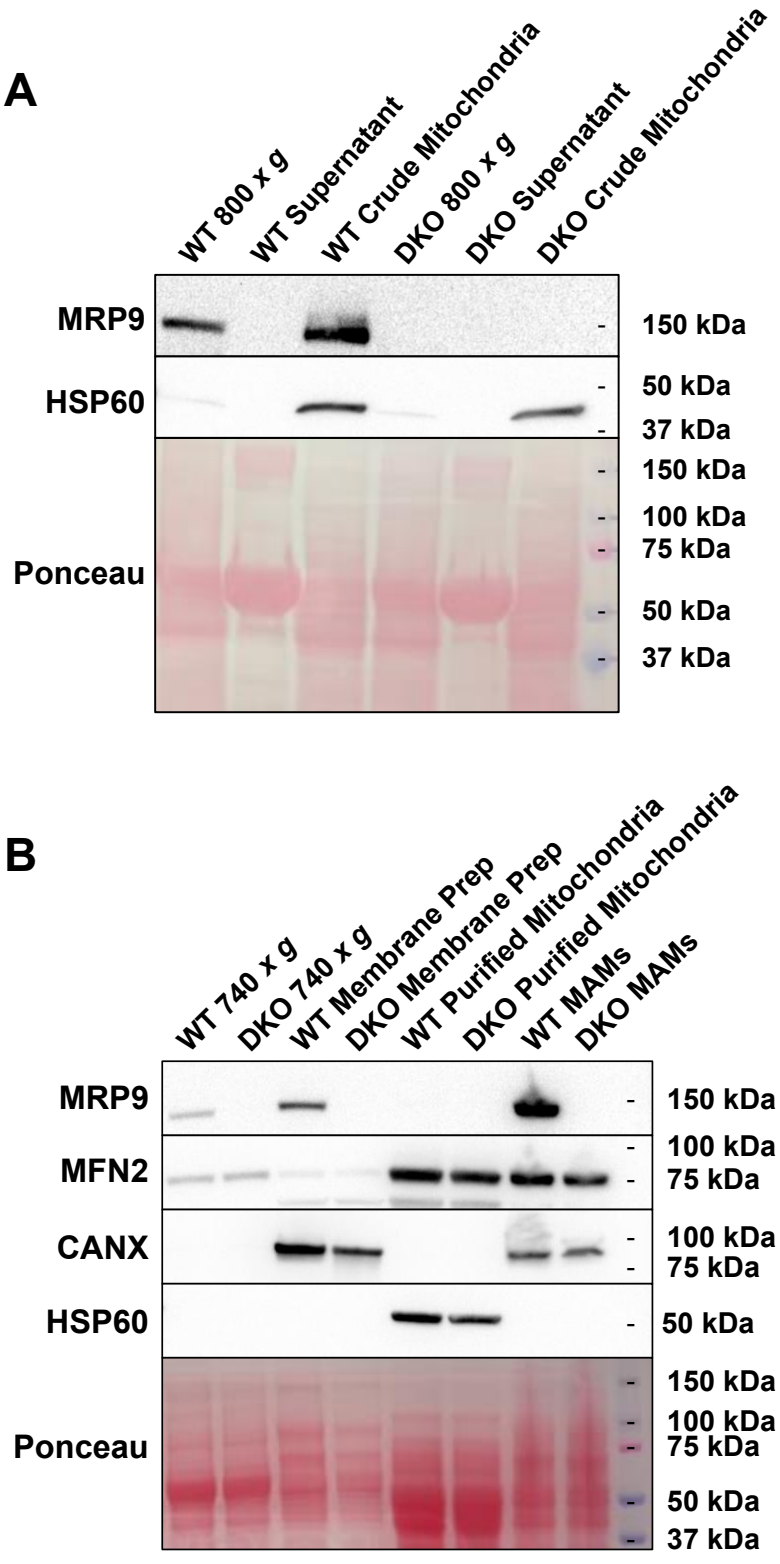
A
WT 800 x g
WT Supernatant
WT Crude Mitochondria
DKO 800 x g
DKO Supernatant
DKO Crude Mitochondria
MRP9
HSP60
Ponceau
150 kDa
50 kDa
37 kDa
150 kDa
100 kDa
75 kDa
50 kDa
37 kDa
B
WT 740 x g
DKO 740 x g
WT Membrane Prep
DKO Membrane Prep
WT Purified Mitochondria
DKO Purified Mitochondria
WT MAMs
DKO MAMs
MRP9
MFN2
CANX
HSP60
Ponceau
150 kDa
100 kDa
75 kDa
100 kDa
75 kDa
50 kDa
150 kDa
100 kDa
75 kDa
50 kDa
37 kDa

Figure 3.8 Subcellular fractionation of testes homogenates shows enrichment of MRP9 in the Mitochondrial-Associated Membranes (MAMs) fraction

A) Immunoblot analysis of crude mitochondrial fractionation from testes of mice. Membrane was probed for MRP9 (M9II-3 antibody) and HSP60, a mitochondrial matrix protein marker.

B) Immunoblot analysis of subcellular fractionation from testes of mice. Membranes were probed for MRP9 and MFN2, CANX, HSP60 markers of outer mitochondrial membrane, ER membrane, and mitochondrial matrix respectively.

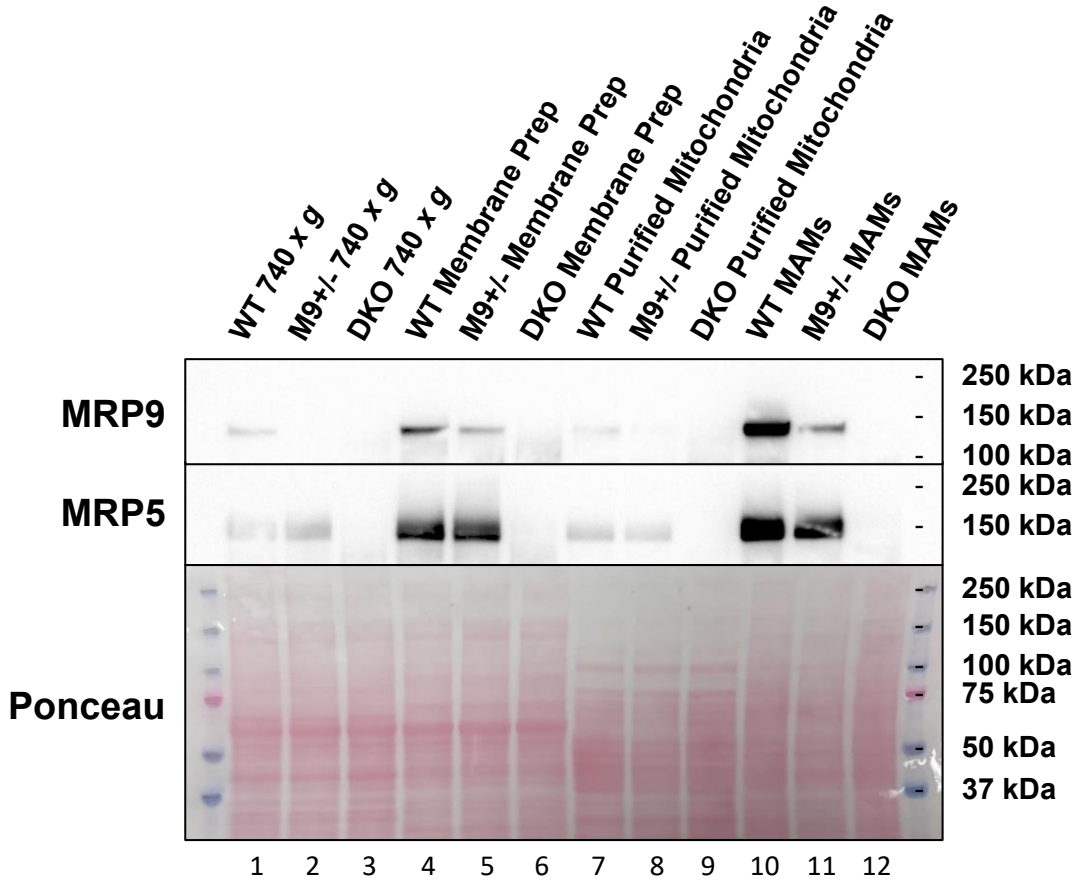

Figure 3.9 Subcellular fractionation of testes homogenates confirms enrichment of MRPs in MAMs fractions

Immunoblot of subcellular fractionation from testes of wildtype, MRP9 heterozygous and double knockout mice. Membranes were probed for MRP9 (M9I-27 antibody) and MRP5.

MRP9 is located in close proximity to the mitochondria and ER

Given this novel subcellular localization for a 12 TMD ABCC transporter, we sought to further characterize MRP9 function and confirm its localization *in cellula*. A recent study by Shi et al showed that sodium butyrate (NaB) may induce MRP9 expression in certain cell lines. We attempted to recapitulate these results to evaluate endogenous MRP9 expression and localization in cells [157]. In addition to the two cancer cell lines described in their publication (A549 and HCT116), we also tested immortalized mouse embryonic fibroblasts (MEFs) from WT and DKO mice plus nine other cell lines to evaluate expression of MRP9 in response to NaB treatment **(Figure 3.10A)**. Immunoblots of these lysates showed no detectable MRP9 expression in MEFs even after NaB treatment; other cell lines showed a significantly higher molecular weight (200 kDa) signal then the expected mouse or human MRP9 (≈150 kDa) **(Figure 3.10A)**. Additionally, from the cell lines which appeared to have prominent bands, there was little consistency in the pattern of protein expression or induction after treatment (compare Caco-2 [lanes 11 and 12] to Hep G2 [lanes 13 and14]) **(Figure 3.10A)**. To determine if this higher molecular weight band was in fact a modified version of MRP9, we used siRNA-mediated knockdown of *ABCC12* in Caco-2 and Hep G2 cells **(Figure 3.10B and Appendix III)**. *ABCC12* depletion had no impact on the higher molecular weight signal despite robust knockdown of *GAPDH* control target, indicating that the published NaB results were an artifact.

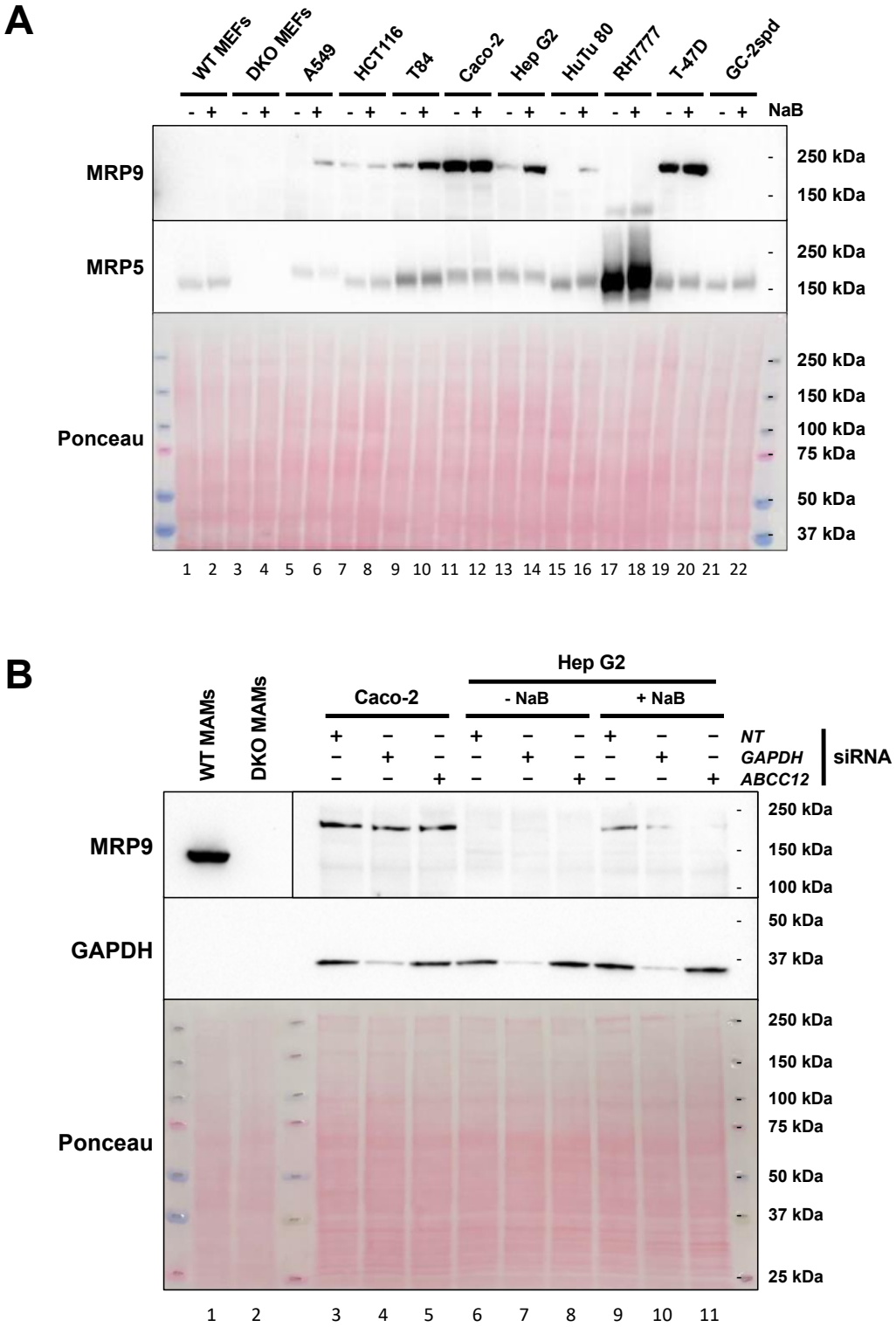
A
WT MEFs
DKO MEFs
A549
HCT116
T84
Caco-2
Hep G2
HuTu 80
RH7777
T-47D
GC-2spd
NaB
MRP9
MRP5
Ponceau
250 kDa
150 kDa
100 kDa
75 kDa
50 kDa
37 kDa
1 2 3 4 5 6 7 8 9 10 11 12 13 14 15 16 17 18 19 20 21 22
B
WT MAMs
DKO MAMs
Caco-2
Hep G2
- NaB
+ NaB
NT
GAPDH
ABCC12
siRNA
MRP9
GAPDH
Ponceau
250 kDa
150 kDa
100 kDa
75 kDa
50 kDa
37 kDa
25 kDa
1 2 3 4 5 6 7 8 9 10 11

Figure 3.10 Endogenous expression of MRP9 cannot be detected or induced in cell culture

A) Immunoblot of cell lines treated with either 2mM NaB or PBS control for 24 hours; membrane was probed for MRP9 and MRP5 following SIM.
B) Immunoblot analysis of selected cell lines with or without 4mM NaB and treated with Non-Targeted (NT), *GAPDH* or *ABCC12* siRNA for 48hours; membrane was probed for MRP9 and GAPDH protein levels.

To confirm that MRP9 partitions with MAMs, we transiently transfected human *ABCC12* into HeLa cells. Airyscan super resolution microscopy and 3D rendering revealed MRP9 located in close proximity to the mitochondria (Mitotracker) and ER (Calnexin) **(Figure 3.11)**. Furthermore, polarization of cells did not alter this intracellular distribution of MRP9, which is in stark contrast to MRP5 that redistributes to the basolateral surface of the plasma membrane in polarized MDCKII cells **(Figure 3.12)**.

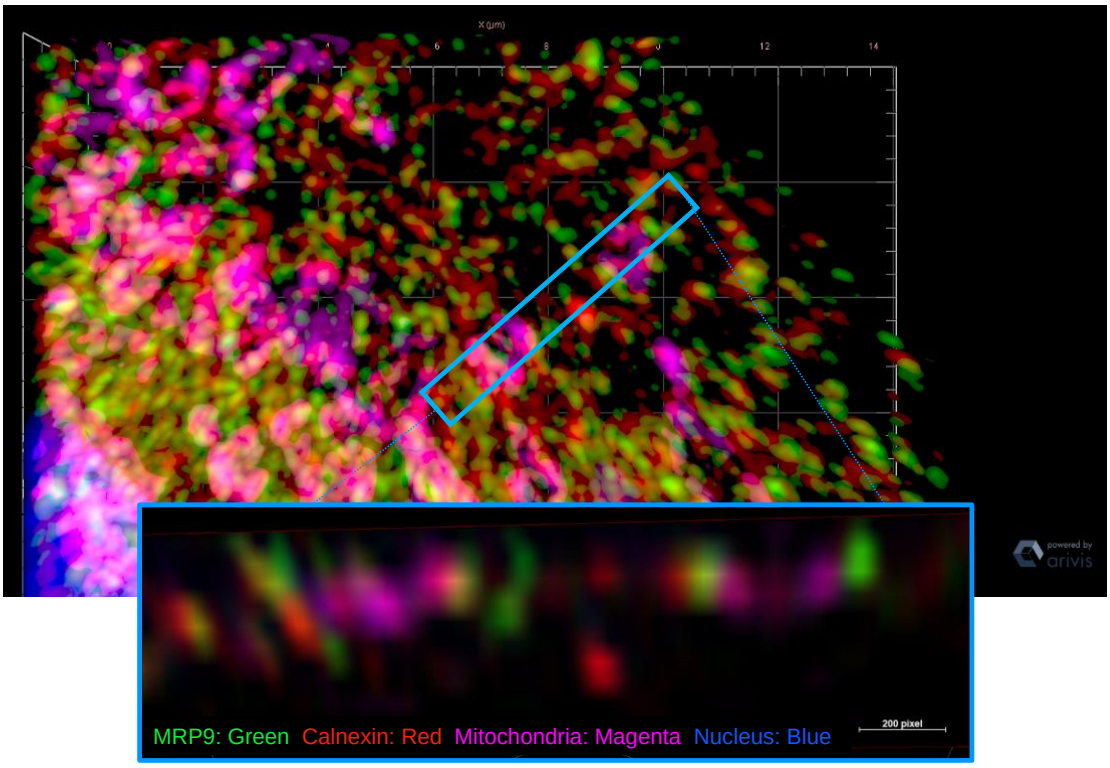

Figure 3.11 Immunofluorescence of cells transfected with MRP9 confirms novel subcellular localization in close proximity to mitochondria

Airyscan super resolution microscopy and 3D rendering of HeLa cells transfected with human ABCC12 for 48 hours and treated with Mitotracker Deep Red FM immediately prior to fixation and immunofluorescence. Antibody probing for MRP9 and Calnexin was followed by Alexa-488 and Alexa-568 secondary antibodies respectively followed by DAPI counter staining prior to mounting.

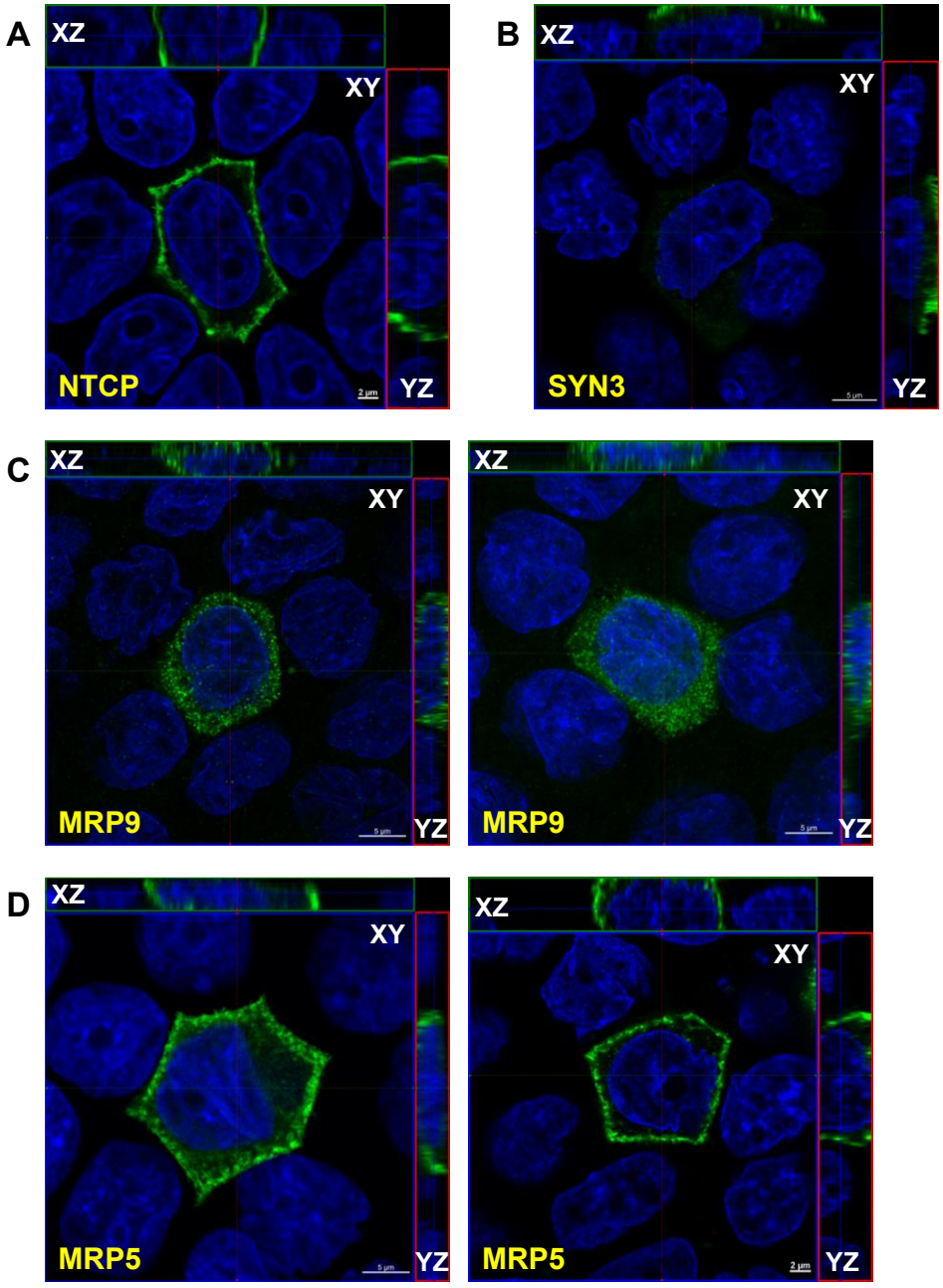

Figure 3.12 MRP9 shows distinct intracellular localization in polarized MDCKII cells compared to MRP5

Confocal images of MDCKII cells grown on transwell filters transfected with A) basolateral marker Sodium taurocholate cotransporting polypeptide (NTCP)

NTCP-GFP; B) apical marker Syntaxin 3 SYN3-GFP; and C) human ABCC12 or D) human ABCC5. Polarization of the monolayer was additionally confirmed prior to fixation by measurement of trans-epithelial electrical resistance. A representative confocal section (XY) is depicted along with the composite stacks in the side panel views (XZ and YZ).

Metabolomics and RNAseq show significant global perturbations in the testes of DKO mice

In order to systematically dissect why the combined loss of MRP9 and MRP5 manifests in male reproductive dysfunction, we sought to understand what substrates may be transported by these proteins and how their absence may impact homeostatic pathways in the testes. To achieve this, we performed unbiased metabolomics and RNAseq in tandem from the same mice to integrate any differential metabolites and gene expression changes in the DKO testes. Global untargeted metabolomics of testes indicated significant perturbation in metabolites, with a remarkable 24 of the top 25 differential species from aqueous phase extraction showing accumulation in DKO testes **(Figure 3.13A)**. These dramatic differences in metabolite profiles were evident regardless of the extraction method (aqueous vs organic) or the mode of acquisition (negative vs positive) **(Figure 3.14)**. Analysis of these putative species of interest allowed for the identification of individual time of flights and masses (*m/z*) of hyper accumulated and significant candidate metabolites **(Figure 3.13B)**. However, any given *m/z* could be representing any number of actual biological compounds that share the same mass, including non-endogenous metabolites which require filtering. Doing

so for those candidate species highlighted in **Figure 3.13B**, we found classes of metabolites that could potentially include glucosphingolipids, phosphatidylserines and acid ethyl esters **(Figure 3.13C)**. As a means to associate this information with specific metabolites, all *m/z*'s identified from our six untargeted testes metabolomics datasets were pooled and processed using MetaboAnalyst Mummichog analyses [166]. Of the species analyzed, 65 statistically significant metabolites were assigned putative KEGG IDs (**Table 3.1)**. Included in the list of metabolites is the heme precursor succinyl-CoA with a 16-fold increase in DKO testes compared to WT.

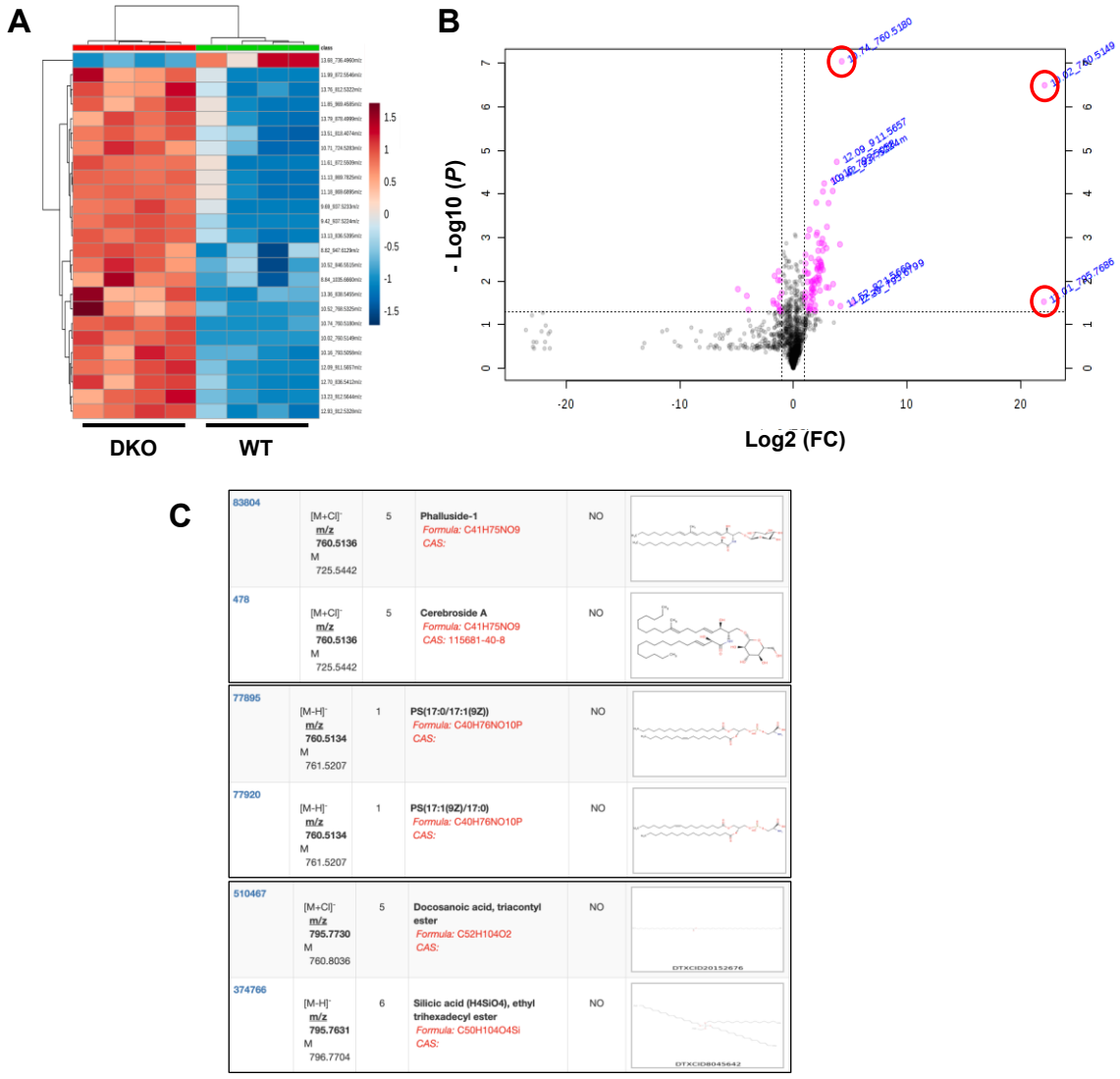

Figure 3.13 Metabolomics of testes from DKO and WT mice indicate significant perturbation in metabolites and identify putative species of interest

A) Variable Importance in Projection (VIP) Heatmap of the top 25 differential metabolites in testes from aqueous phase extractions on C18 column run in negative mode.

B) Volcano plot of aqueous extracted negative mode metabolites, highlighting individual time of flight/masses of putative species with extreme differences in fold change and *P* value.

C) Highlighting putative candidate metabolite classes from panel B volcano plot with similar *m/z*. Classes of relevant biological compounds include glucosphingolipids, phosphatidylserines and acid ethyl esters.

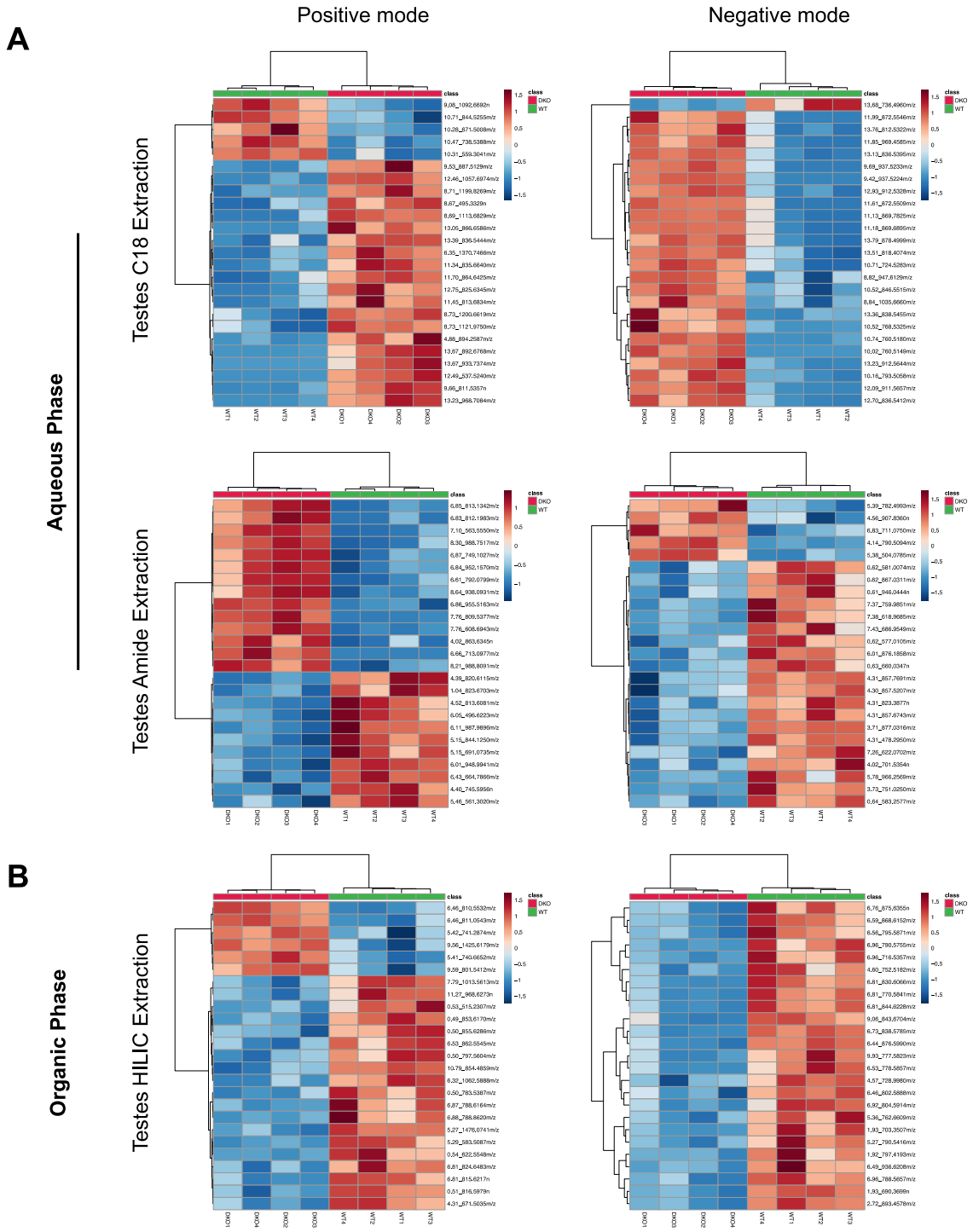

Figure 3.14 Global untargeted metabolomics testes show dramatic differences in metabolites in both aqueous and organic phase extractions

A) Variable Importance in Projection (VIP) heatmaps of differential metabolites from aqueous phase extractions on C18 (top) or amide (bottom) columns. Samples run through mass spectrometer in positive (left) or negative (right) mode testes in WT and DKO mice.

B) Variable Importance in Projection (VIP) Heatmaps of differential metabolites from organic phase extractions on HILIC columns. Samples run through mass spectrometer in positive (left) or negative (right) mode testes in WT and DKO mice.

Table 3.1 Identifiable metabolites from MetaboAnalyst mummichog processing

Extraction Method	Compound KEGG ID	Matched form	Name / ID	pValue	Fold Change
Aqueous Pos	G00526	M+NaCl[1+]	**Glycan - (GlcA)2 (GlcNAc)2**	0.0006	3.3345
Amide Pos	C11039	M+CH3COO[-]	**2'-Deoxy-5-hydroxymethylcytidine-5'-triphosphate**	0.0009	-2.1258
Amide Pos	C15976	M+Cl[-]	**2-Methyl-1-hydroxypropyl-TPP**	0.0017	2.7099
Amide Pos	C11039	M-H2O-H[-]	**2'-Deoxy-5-hydroxymethylcytidine-5'-triphosphate**	0.0022	-2.0490
Amide Pos	C00127	M+Br[-]	**Oxidized glutathione**	0.0034	-2.4940
Amide Pos	G00044	M+CH3COO[-]	**IV2-a-Fuc-Lc4Cer; Type IH glycolipid**	0.0057	-2.8923
Amide Pos	G00055	M+CH3COO[-]	**IV2-a-Fuc-nLc4Cer; Type IIH glycolipid**	0.0057	-2.8923
Amide Pos	G00060	M+CH3COO[-]	**III3-a-Fuc-nLc4Cer; Lacto-N-fucopentaosyl III ceramide**	0.0057	-2.8923
Amide Pos	G10770	M-2H[2-]	**(GlcNAc)3 (LFuc)1 (Man)3 (Asn)1**	0.0060	-2.3658
Amide Pos	C05261	M(S34)-H[-]	**3-Oxotetradecanoyl-CoA**	0.0061	-2.9834
Amide Pos	C05261	M(Cl37)-H[-]	**3-Oxotetradecanoyl-CoA**	0.0061	-2.9834
Amide Pos	C04646	M-H+O[-]	**Thioinosinic acid**	0.0064	-2.1401
Amide Pos	C16618	M-H[-]	**6-Thioxanthine 5'-monophosphate**	0.0064	-2.1401
Amide Pos	C00387	M+Br[-]	**Guanosine**	0.0064	-2.0488
Aqueous Pos	C05504	M+NaCl[1+]	**Estriol-16-Glucuronide**	0.0070	-2.6085
Aqueous Pos	C11376	M-HCOOH+H[1+]	**SN38 glucuronide**	0.0070	-2.6085
Aqueous Pos	C16327	M(C13)+2H[2+]	**OPC8-CoA**	0.0070	-2.6085
Amide Pos	C00655	M+Br[-]	**Xanthylic acid**	0.0078	8.4958
Amide Pos	C21750	M+Cl37[-]	**5-Fluorodeoxyuridine diphosphate**	0.0078	8.4958
Amide Pos	C14855	M+Br81[-]	**4,5-Dihydro-4-hydroxy-5-S-glutathionyl-benzo[a]pyrene**	0.0080	7.1469
Amide Pos	C14856	M+Br81[-]	**7,8-Dihydro-7-hydroxy-8-S-glutathionyl-benzo[a]pyrene**	0.0080	7.1469
Aqueous Pos	G01945	M[1+]	**(Gal)2 (GlcNAc)2 (S)3**	0.0082	3.8200
Amide Pos	G00159	M-H2O-H[-]	**(Gal)2 (GalNAc)1 (GlcA)2 (Xyl)1 (Ser)1**	0.0085	-3.2323
Amide Pos	G00163	M-H2O-H[-]	**(Gal)2 (GlcA)2 (GlcNAc)1 (Xyl)1 (Ser)1**	0.0085	-3.2323
Amide Pos	C11174	M-H2O-H[-]	**1-Diphosinositol pentakisphosphate**	0.0086	-2.5534
Amide Pos	C11526	M-H2O-H[-]	**5-Diphosphoinositol pentakisphosphate**	0.0086	-2.5534
Amide Pos	C00091	M(C13)-H[-]	**Succinyl-CoA**	0.0089	16.1675
Amide Pos	C00683	M(C13)-H[-]	**Methylmalonyl-CoA**	0.0089	16.1675
Amide Pos	C01213	M(C13)-H[-]	**L-methylmalonyl-CoA**	0.0089	16.1675
Amide Pos	C03691	M+Cl37[-]	**CMP-N-glycoloylneuraminate**	0.0096	-3.3747
Amide Pos	C00877	M-H[-]	**Crotonoyl-CoA**	0.0113	-2.3923
Amide Pos	C01144	M-H2O-H[-]	**(S)-3-Hydroxybutyryl-CoA**	0.0113	-2.3923
Amide Pos	C03460	M-H[-]	**Methacrylyl-CoA**	0.0113	-2.3923
Amide Pos	C06000	M-H2O-H[-]	**(S)-3-Hydroxyisobutyryl-CoA**	0.0113	-2.3923
Amide Pos	G00005	M(S34)-H[-]	**(GlcNAc)2 (Man)3 (PP-Dol)1**	0.0116	3.6595
Amide Pos	G00005	M(Cl37)-H[-]	**(GlcNAc)2 (Man)3 (PP-Dol)1**	0.0116	3.6595
Amide Pos	G00066	M(S34)-H[-]	**(Gal)2 (Glc)1 (GlcNAc)2 (Cer)1**	0.0116	3.6595
Amide Pos	G00066	M(Cl37)-H[-]	**(Gal)2 (Glc)1 (GlcNAc)2 (Cer)1**	0.0116	3.6595
Amide Pos	G00095	M(S34)-H[-]	**IV3GalNAca-Gb4Cer**	0.0116	3.6595
Amide Pos	G00095	M(Cl37)-H[-]	**IV3GalNAca-Gb4Cer**	0.0116	3.6595
Amide Pos	G00889	M(S34)-H[-]	**(Gal)2 (GalNAc)1 (Glc)1 (GlcNAc)1 (Cer)1**	0.0116	3.6595
Amide Pos	G00889	M(Cl37)-H[-]	**(Gal)2 (GalNAc)1 (Glc)1 (GlcNAc)1 (Cer)1**	0.0116	3.6595
Amide Pos	G02977	M(S34)-H[-]	**(Gal)2 (GalNAc)2 (Glc)1 (Cer)1**	0.0116	3.6595
Amide Pos	G02977	M(Cl37)-H[-]	**(Gal)2 (GalNAc)2 (Glc)1 (Cer)1**	0.0116	3.6595
Amide Pos	C05264	M+CH3COO[-]	**(S)-Hydroxydecanoyl-CoA**	0.0117	3.1082
Amide Pos	C00327	M+K-2H[-]	**Citrulline**	0.0118	3.1441
Amide Pos	C05266	M-H+O[-]	**(S)-Hydroxyoctanoyl-CoA**	0.0127	-3.7376
Aqueous Neg	G00149	M+Br81[-]	**(GlcN)1 (Ino(acyl)-P)1 (Man)3 (EtN)1 (P)1**	0.0144	3.1562
Amide Pos	C01832	M+HCOO[-]	**Lauroyl-CoA**	0.0172	3.5276
Aqueous Pos	C18043	M(S34)+H[1+]	**Cholesterol sulfate**	0.0177	-3.0325
Aqueous Pos	C18043	M(Cl37)+H[1+]	**Cholesterol sulfate**	0.0177	-3.0325
Amide Pos	C00183	M+Na-2H[-]	**L-Valine**	0.0224	-2.1317
Amide Pos	C00719	M+Na-2H[-]	**Betaine**	0.0224	-2.1317
Amide Pos	G00026	M+Cl[-]	**(Gal)1 (GalNAc)1 (Neu5Ac)1 (Ser/Thr)1**	0.0228	-8.3344
Aqueous Pos	G00158	M+HCOONa[1+]	**(Gal)2 (GalNAc)1 (GlcA)1 (Xyl)1 (Ser)1**	0.0235	-2.4856
Aqueous Pos	G00162	M+HCOONa[1+]	**(Gal)2 (GlcA)1 (GlcNAc)1 (Xyl)1 (Ser)1**	0.0235	-2.4856
Aqueous Neg	G00157	M+Br[-]	**(Gal)2 (GlcA)1 (Xyl)1 (Ser)1**	0.0237	-2.2724
Organic Pos	C16338	M+HCOOK[1+]	**3-Oxo-OPC4-CoA**	0.0251	1.8715
Amide Pos	C04646	M-H+O[-]	**Thioinosinic acid**	0.0292	-2.7960
Amide Pos	C16618	M-H[-]	**6-Thioxanthine 5'-monophosphate**	0.0292	-2.7960
Organic Pos	G13036	M[1+]	**(GlcA)2 (GlcN)1 (GlcNAc)1 (S)3**	0.0423	2.4015
Amide Pos	C02843	M(C13)-H[-]	**Long-chain acyl-CoA**	0.0429	-1.9489
Aqueous Neg	C05791	M+Cl[-]	**D-Urobilinogen**	0.0454	-2.2582
Amide Pos	C00942	M(Cl37)-H[-]	**Cyclic GMP**	0.0455	2.0594
Aqueous Pos	G00063	M[1+]	**IV3NeuAc,III3Fuc-nLc4Cer**	0.0480	1.9138

Fold change and *P* values for statistically significant species identifiable to KEGG IDs based on mummichog analysis from all six untargeted metabolomics datasets of the testes [166].

RNAseq analysis on the paired testis of the same aged-matched mice utilized for metabolomics studies found 3,736 differentially expressed genes between WT and DKO **(Figure 3.15A)**. Stringent filtering for higher levels of significance and fold-change allowed for the identification of a number of top genes including uncharacterized and testis-specific predicted genes (Gm10354, Gm9758, 5430401F13Rik) as well as mitochondrial respiratory genes (Atp5k, Ndufa1, Atp5e) **(Figure 3.15A)**. To unbiasedly determine the pathways and Gene Ontology (GO) terms most significantly affected in these mice we performed Ingenuity Pathway Analysis (IPA, Qiagen) **(Figure 3.15B and Appendix IV)**. The vast majority of the top GO canonical pathways were intimately interconnected and overlapped with mitochondrial function **(Figure 3.15B & C).** Of note, the top two pathways identified, EIF2 Signaling and Protein Ubiquitination, are critical for mitigating unfolded protein response and mitochondrial dysfunction associated with iron and heme deficiencies, and both had significance values of -log(*P* value)>10 **(Appendix IV)** [177].

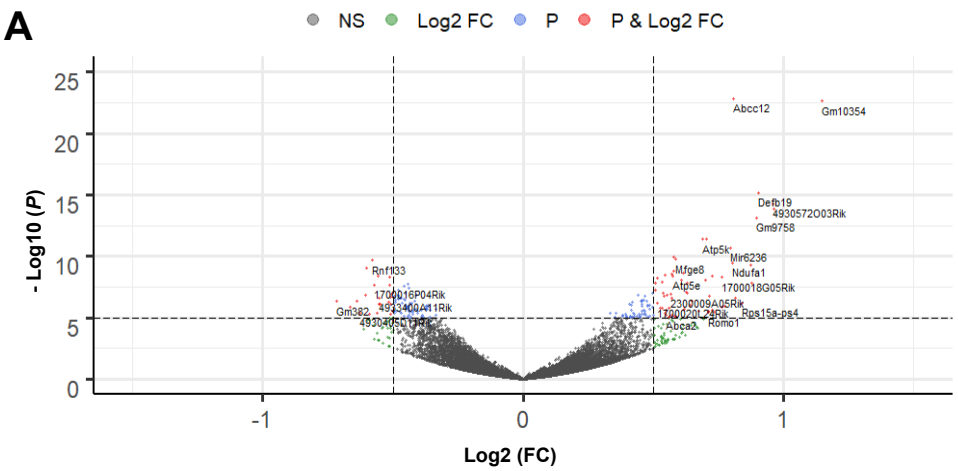

B

	INGENUITY PATHWAY ANALYSIS (IPA)
1	EIF2 Signaling
2	Protein Ubiquitination
3	Estrogen Receptor Signaling
4	mTOR Signaling
5	NRF2-mediated Oxidative Stress Response
6	Sirtuin Signaling
7	Reg of eIF4 & p70SK Signaling
8	Oxidative Phosphorylation
9	Huntington's Disease Signaling
10	Germ Cell-Sertoli Cell Junction Signaling
11	Mitochondrial Dysfunction
12	Nucleotide Excision Repair

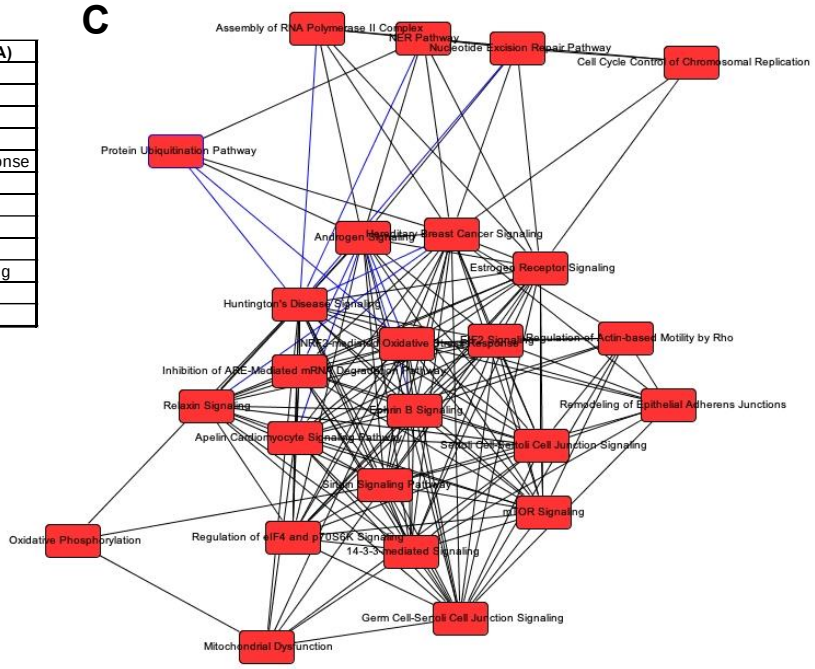

Figure 3.15 RNAseq analysis provides relevant genes and pathways with significant expression perturbation in testes

A) Volcano plot of gene expression changes from DKO and WT testes; significance threshold set at -log(*P* value) > 5.

B) Top twelve Gene Ontology (GO) Pathways perturbed in testes based on Qiagen IPA analysis.

C) Key overlapping canonical pathways in testes based on Qiagen IPA analysis.

We next determined whether DKO mice had similar dysfunctions in tissues other than the testis. RNAseq from spleen, brain and liver did show differences in gene expression **(Figure 3.16A)**, however none to the extent or significance that was observed in the testes **(Figure 3.16B & C)**. Furthermore, IPA analysis of these differentially expressed genes from other organs did not recapitulate the same pathway perturbations found in the testes **(Figure 3.16G)**. This is not surprising as MRP9 is most highly expressed in male germ cells.

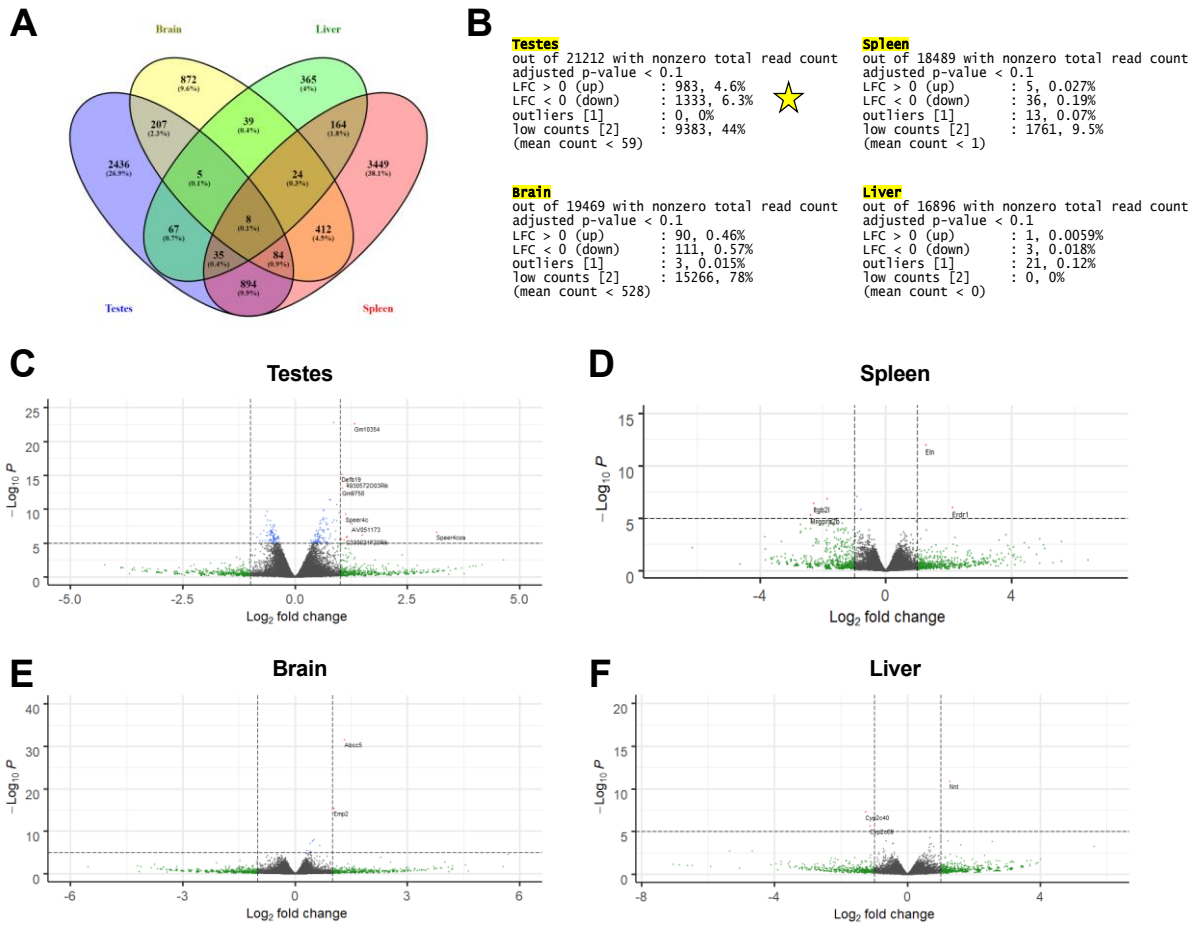

G

INGENUITY PATHWAY ANALYSIS (IPA)
For a TPM >10 threshold

Rank:	TESTES	SPLEEN	BRAIN	LIVER
1	EIF2 Signaling	B Cell Receptor Signaling	Glioma Signaling	Sirtuin Signaling
2	Protein Ubiquitination	PI3K Signaling in B Lymphocytes	Superpathway of Cholesterol Biosynthesis	Superpathway of Cholesterol Biosynthesis
3	Estrogen Receptor Signaling	Systemic Lupus Erythematosus in B Cell Signaling	CXCR4 Signaling	tRNA Charging
4	mTOR Signaling	Death Receptor Signaling	Thrombin Signaling	Superpathway of Geranylgeranyl Diphosphate Biosynthesis
5	NRF2-mediated Oxidative Stress Response	Huntington's Disease Signaling	Breast Cancer Regulation by Stathmin1	Ketogenesis
6	Sirtuin signaling	Estrogen Receptor Signaling	Molecular Mechanisms of Cancer	Mevalonate
7	Reg of eIF4 & p70SK signaling	NF-kB Signaling	RAR Activation	Methyl Thiopropionate Biosynthesis
8	Oxidative Phosphorylation	Lymphotoxin B Receptor Signaling	Chronic Myeloid Leukemia Signaling	Acetyl-CoA Biosynthesis 3 (from Citrate)
9	Huntington's Disease Signaling	Role of RIG1-like Receptors in Antiviral Innate Immunity	Cholesterol Biosynthesis 1	D-myo-inositol (1,4,5,6) Tetrakisphosphate Biosynthesis
10	Germ Cell-Sertoli Cell Junction Signaling	Role of NFAT in Regulation of the Immune Response	Cholesterol Biosynthesis 2	D-myo-inositol (3,4,5,6) Tetrakisphosphate Biosynthesis
11	Mitochondrial Dysfunction	NF-kB Activation by Viruses	Cholesterol Biosynthesis 3	Insulin Receptor Signaling
12	Nucleotide Excision Repair	NGF Signaling	Thrombopoetin Signaling	3-phosphoinositide Degradation

Figure 3.16 RNAseq analysis from additional tissues indicates the testes as the organ with most significant perturbation in DKO mice

A) Venn Diagram of all differentially expressed genes across testes, brain, liver and spleen.

B) DESeq statistical analysis of each organ's adjusted total gene numbers and fold changes.

C) Volcano plot of gene expression changes from DKO and WT testes; threshold significance set at -log(*P* value) > 5.

D) Volcano plot of gene expression changes from DKO and WT spleens; threshold significance set at -log(*P* value) > 5.

E) Volcano plot of gene expression changes from DKO and WT brains; threshold significance set at -log(*P* value) > 5.

F) Volcano plot of gene expression changes from DKO and WT livers; threshold significance set at -log(*P* value) > 5.

G) Top twelve Gene Ontology (GO) Pathways perturbed in all organs analyzed by Qiagen IPA.

To generate metabolite-gene relationships, we integrated the metabolomics data with RNAseq using MetaboAnalyst. The merged data revealed mitochondrial pathway dysfunction with energy production components of the cell (TCA Cycle, Pyruvate Metabolism, and Glycolysis) showing the highest impact and significance (**Figure 3.17 and Table 3.2).** Taken together, these findings further enforce a role for MRP9 and MRP5 in mitochondrial metabolism specifically in the testes.

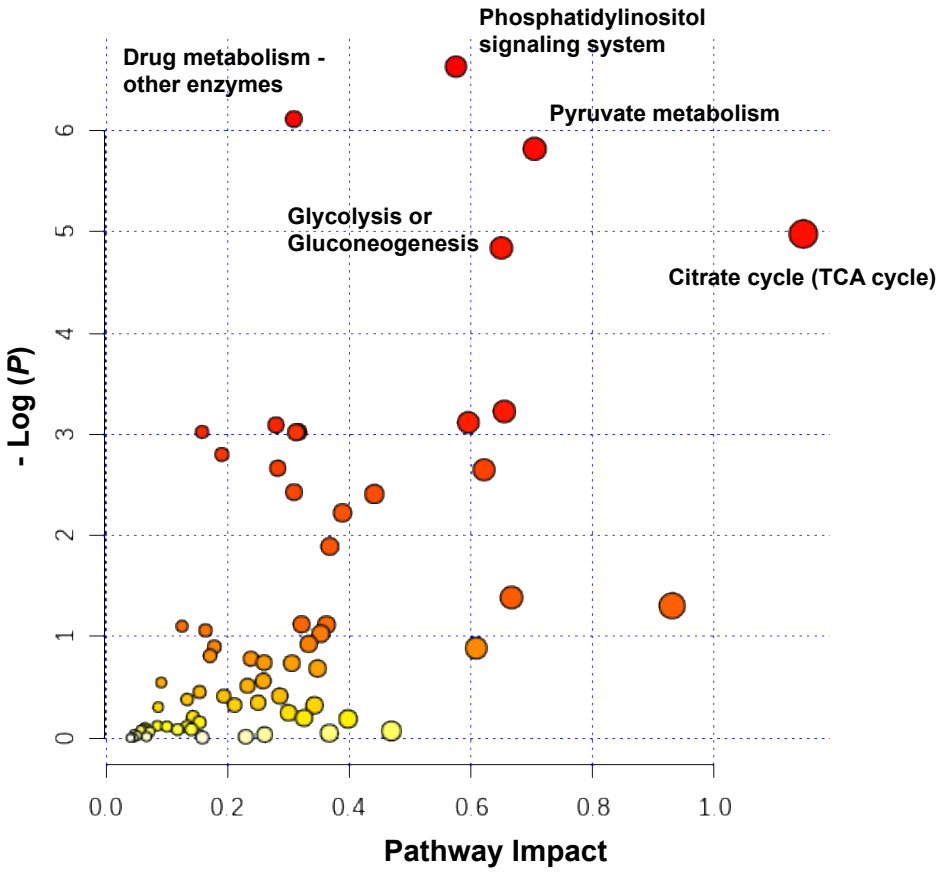

Figure 3.17 Integrative analysis of metabolome and transcriptome reveals evident mitochondrial pathway dysfunction

MetaboAnalyst combined analysis of RNAseq differential gene expression changes and metabolomics mummichog putative KEGG IDs to create overview pathway impact for testes; top five pathways by *P* value are annotated.

Table 3.2 All statistically significant pathways identified by integrative MetaboAnalyst analysis of metabolomics and RNAseq

MetaboAnalyst Testes Pathways	Total	Expected	Raw p	-LOG(p)	FDR	Impact
Phosphatidylinositol signaling system	74	5.1195	0.0013121	6.6362	0.082863	0.57534
Drug metabolism - other enzymes	69	4.7736	0.0022033	6.1178	0.082863	0.30882
Pyruvate metabolism	45	3.1132	0.0029594	5.8228	0.082863	0.70455
Citrate cycle (TCA cycle)	42	2.9057	0.0068637	4.9815	0.13233	1.1463
Glycolysis or Gluconeogenesis	61	4.2201	0.0078766	4.8439	0.13233	0.65
Purine metabolism	169	11.692	0.039654	3.2276	0.37186	0.65476
Propanoate metabolism	48	3.3208	0.044216	3.1187	0.37186	0.59574
Inositol phosphate metabolism	69	4.7736	0.045331	3.0938	0.37186	0.27941
Drug metabolism - cytochrome P450	39	2.6981	0.048529	3.0256	0.37186	0.15789
Ether lipid metabolism	39	2.6981	0.048529	3.0256	0.37186	0.31579
Lysine degradation	49	3.3899	0.048696	3.0222	0.37186	0.3125

Output of all statistically significant pathways determined by MetaboAnalyst combined analysis of RNAseq gene lists with differential expression changes and metabolomics mummichog putative KEGG IDs.

Elucidating the mechanisms behind dysfunction in DKO mice

We identified mitochondrial dysfunction as the overarching factor from our integrative analysis. To determine the specific mechanisms that underlie this dysfunction in the testes, we built an analysis pipeline of all genes associated with any given pathway from published GO databases (such as RGD and MGI) and curated fold change findings into heat map tables **(Figure 3.18A)**. Genes associated with mitochondrial function served as a positive control for analysis and confirmed significant perturbation in DKO testes with over 200 individual genes identified **(Figure 3.18B)**.

A

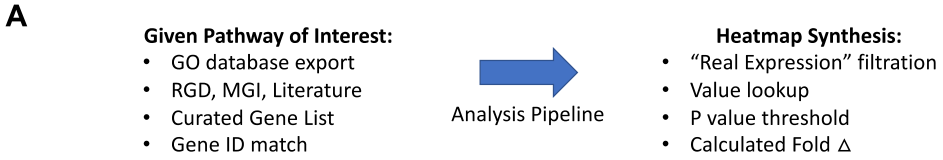

B

SYMBOL	PVALUE	FC	SYMBOL	PVALUE	FC	SYMBOL	PVALUE	FC	SYMBOL	PVALUE	FC	SYMBOL	PVALUE	FC	SYMBOL	PVALUE	FC
Mief1	0.0004	1.0953	1810043G02	0.0069	-1.2508	Mul1	0.0144	-1.1801	Adcy10	0.0213	1.1538	Rnf144b	0.0296	1.1320	Ppa2	0.0378	-1.0811
Tomm40	0.0007	-1.2444	Efhd1	0.0072	1.1456	Dld	0.0146	1.3118	Pacs2	0.0218	-1.1602	Cisd1	0.0299	-1.2525	Wwox	0.0378	-1.2227
Gadd45gip1	0.0009	-1.2072	Mrps24	0.0073	-2.2120	Mtch2	0.0153	-1.0823	NDUFB9	0.0220	-1.2733	Acsl5	0.0299	1.3138	NDUFV2	0.0379	-1.0802
Mrps12	0.0012	-1.3526	Chpf	0.0074	-1.4239	COX5B	0.0153	-1.2139	Vat1	0.0223	-1.2351	D10Jhu81e	0.0301	-1.3699	Clpp	0.0379	-1.3285
Timm13	0.0020	-1.3934	Slc25a33	0.0075	-1.1482	Vrk2	0.0153	1.4574	Hagh	0.0227	-1.1748	Hax1	0.0302	1.0943	Actb	0.0393	-1.1927
Agtpbp1	0.0025	1.1799	Mrpl15	0.0076	-1.3290	Polrmt	0.0153	-1.3106	Dnaja1	0.0227	1.2146	Tomm22	0.0304	1.1649	Mrpl45	0.0396	1.1832
Atp5d	0.0027	-1.3937	Nsun4	0.0078	-1.3024	Gatc	0.0157	1.1092	Ndufc1	0.0228	1.2169	Pgs1	0.0308	-1.1040	L2hgdh	0.0401	1.1787
Mrpl55	0.0031	-1.1810	Pet100	0.0083	-1.3873	Pld6	0.0158	-1.3146	Cycs	0.0228	1.2837	Pfdn2	0.0308	-1.4429	Cox16	0.0401	1.0935
Spata5	0.0032	1.1378	COX4I1	0.0083	-1.3127	Fkbp8	0.0159	-1.1967	Hsdl1	0.0229	-1.2459	Etfb	0.0308	-1.4433	Fh1	0.0404	-1.1726
Slc25a37	0.0032	1.2235	Uqcrq	0.0083	-1.3204	Coq10b	0.0159	1.4860	Osgepl1	0.0230	1.2436	Gstp1	0.0309	-1.6693	Ghitm	0.0409	1.2048
Mapk10	0.0032	-1.0820	Mrpl4	0.0086	-1.2524	NDUFA1	0.0160	-1.4864	Fez1	0.0235	1.3950	Usp8	0.0311	1.1444	Dctn1	0.0415	-1.1988
Arl2	0.0034	-1.4531	Ndufs6	0.0091	-1.1662	Mrpl43	0.0161	-1.4383	Timm10	0.0238	-1.3038	Glyctk	0.0312	-1.1461	Cox20	0.0425	1.6560
Tdrkh	0.0038	1.1965	Ndufa6	0.0098	-1.3561	Mrpl28	0.0162	-1.2460	Cox5a	0.0241	-1.2152	Dmpk	0.0313	-1.4675	Dlat	0.0427	1.1566
Tbrg4	0.0040	-1.1145	Mrps5	0.0099	1.1577	Mrpl1	0.0164	1.2279	Slc25a31	0.0242	1.2552	Mrps18c	0.0318	1.2708	Gfer	0.0427	-1.1732
Ak2	0.0042	-1.1286	Mrpl33	0.0099	1.3133	Park7	0.0164	-1.1511	Chchd7	0.0243	-1.0724	Pnkd	0.0318	-1.2358	2410015M20	0.0428	-1.1378
Sod2	0.0043	-1.2667	NDUFA4L2	0.0100	-1.1529	Ndufa9	0.0165	-1.1929	ATP5O	0.0247	-1.1116	Acot9	0.0321	1.2023	Ccdc90b	0.0436	1.2581
Mrps34	0.0044	-1.3827	Timm10b	0.0102	-1.6526	COX7B2	0.0168	1.3161	Ppp2r2b	0.0247	1.1764	Elac2	0.0322	-1.1356	Atg4d	0.0441	-1.0693
Mrps26	0.0045	-1.2151	Tomm7	0.0108	-1.3137	Slc25a25	0.0171	-1.2091	Sord	0.0249	1.1104	Ndufaf3	0.0323	-1.1286	Dynll1	0.0447	-1.1547
Mpg	0.0046	-1.1623	Bloc1s1	0.0114	-1.5885	Bad	0.0173	-1.1532	Silrp	0.0250	-1.2222	Immt	0.0325	1.0957	Mrpl48	0.0458	1.1516
Alkbh7	0.0047	-1.3726	Txn2	0.0114	-1.1589	Mtpap	0.0177	1.3151	Dync1h1	0.0256	-1.2701	Isca2	0.0329	1.2530	Idh3b	0.0462	-1.1794
Eral1	0.0051	-1.2571	Mtch1	0.0115	-1.4608	Gk2	0.0179	1.2004	Sdhc	0.0257	-1.2429	Ranbp2	0.0333	1.3195	Pi4kb	0.0465	-1.1539
NDUFS7	0.0059	-1.2813	Mterf3	0.0115	1.3142	Sucla2	0.0180	1.2647	Hadhb	0.0259	1.1909	Mrps22	0.0341	1.0896	Akap10	0.0466	1.1565
NDUFA2	0.0060	-1.6707	2010107E04	0.0115	1.7208	Spg7	0.0183	-1.0920	Uqcc3	0.0263	-1.3110	Mrpl27	0.0343	-1.4362	Rhot1	0.0467	1.2255
Afg3l1	0.0060	1.1185	Mrpl54	0.0118	1.2334	Mpc2	0.0189	1.2403	Crat	0.0266	-1.1401	Atpaf2	0.0347	-1.1318	Coa4	0.0467	-1.1360
Coa6	0.0062	-1.1670	Atp5l	0.0118	-1.2691	Prelid1	0.0190	-1.1862	Dync1li2	0.0268	1.1089	Slc35f6	0.0347	-1.1659	Mtif2	0.0473	1.2521
Tmem11	0.0063	-1.4467	Chchd6	0.0122	-1.1485	Letm2	0.0191	1.1335	Mcat	0.0272	-1.1299	Stk11	0.0350	-1.1368	Pdhb	0.0477	1.1008
Phb	0.0063	-1.3395	Star	0.0123	-1.8074	Mrpl53	0.0191	-1.2066	Mrps17	0.0276	-1.4064	Clpx	0.0352	1.2008	Cox6a1	0.0485	-1.2080
Uqcr10	0.0064	-1.7782	Tfam	0.0125	1.3135	Pdk3	0.0192	1.3719	Slc25a10	0.0276	-1.3000	Mfn1	0.0356	1.1373	Tomm20l	0.0485	1.2965
Cbr4	0.0066	1.1989	Ndufs8	0.0126	-1.6010	Actr10	0.0193	1.2201	Abcg2	0.0276	1.3762	Trp53	0.0356	-1.2506	Dynlrb1	0.0485	-1.3742
Capza1	0.0066	1.1801	Mrpl10	0.0130	-1.3607	Lias	0.0193	1.1592	Letm1	0.0282	-1.1211	Cabs1	0.0357	1.3121	ATP5C1	0.0489	1.1369
Apex1	0.0067	-1.2404	Ptpmt1	0.0131	-1.2303	Sqrdl	0.0194	1.1733	Apoo	0.0285	1.5286	Atad3a	0.0357	-1.4089			
Dynll2	0.0068	-1.4417	Uqcrc2	0.0138	1.1274	Mrps31	0.0196	1.3443	9430016H08	0.0285	1.2594	Dap3	0.0360	1.1239			
Mrpl57	0.0069	-1.5369	Nt5m	0.0141	-1.1367	Vdac3	0.0197	1.3218	Cyc1	0.0291	-1.2995	Mrpl32	0.0373	1.2965			
NDUFB8	0.0069	-1.1551	NDUFB10	0.0143	-1.4712	Mrpl47	0.0209	1.3530	Slc25a28	0.0296	-1.1956	Romo1	0.0374	-1.7206			

Figure 3.18 RNAseq Analysis Pipeline confirms mitochondria and mitochondrial dysfunction associated genes are highly perturbed in DKO testes

A) Simplified schematic for pathway pipeline analysis: gene lists of interest were curated for integration with RNA expression data. Real expression was validated by thresholding a minimum 10 transcripts per million and statistically significant genes ($P < .05$) fold change were output in heatmaps.

B) Output of analysis pipeline investigating all "mitochondria" and "mitochondrial disfunction" GO pathway gene lists. 200 total genes identified, sorted by ascending *P* value.

With the analysis pipeline we then asked what individual genes or pathways are involved in responding to this level of disruption. Given the top-related pathway identified from our IPA studies was EIF2 signaling, we investigated all genes associated with EIF2, translation and translational regulation, and found 95 genes that were differentially regulated **(Table 3.3)**.

Table 3.3 EIF2a and associated translational regulation pathways are significantly altered in DKO testes

SYMBOL	PVALUE	FC	SYMBOL	PVALUE	FC	SYMBOL	PVALUE	FC
Eif4e	0.0022	1.1282	Pop5	0.0112	-1.2006	Xpo1	0.0294	1.2834
Riok3	0.0031	1.1060	Pelo	0.0114	-1.3602	Gtpbp4	0.0302	1.2063
Spata5	0.0032	1.1378	Rps8	0.0114	-1.2486	Nxt2	0.0308	1.4189
Nop10	0.0032	-1.3394	Rps29	0.0117	-1.5442	Wdr75	0.0313	1.1472
Rpl31	0.0035	-1.5499	Rpl29	0.0124	-1.1646	Uba52	0.0322	-1.4261
Rps16	0.0037	-1.4641	Hbs1l	0.0126	1.1278	Sbds	0.0337	1.1121
Nck2	0.0037	-1.3262	Eef1b2	0.0126	1.0781	Eif2s1	0.0344	1.2027
Rpl8	0.0038	-1.3988	Fcf1	0.0130	-1.1199	Nmd3	0.0356	1.2202
Rpl28	0.0040	-1.1876	Rpl9	0.0136	1.3013	Rexo1	0.0359	-1.0897
Eif3i	0.0048	-1.3023	Imp3	0.0163	-1.3514	Klhl25	0.0363	-1.2171
Nxf2	0.0050	1.2737	Eif1a	0.0179	1.2296	Eef2	0.0366	-1.1573
Rpl38	0.0052	-1.2651	Eif4ebp2	0.0179	-1.2373	Pop4	0.0372	1.1602
Rps15a	0.0052	-1.4904	Rpp38	0.0180	1.1535	Rplp0	0.0373	-1.2090
Rps12	0.0052	-1.3531	Rara	0.0195	-1.1871	Xrn1	0.0377	1.3024
Polr2d	0.0061	-1.2028	Fbl	0.0198	-1.4356	Rps15	0.0388	-1.2027
Rpl18a	0.0061	-1.3778	Eif4a2	0.0201	1.2541	Drosha	0.0396	-1.1002
Eif4g2	0.0065	1.1627	Eif3e	0.0204	1.4014	Eif3d	0.0403	-1.0670
Rplp2	0.0075	-1.4350	Dis3	0.0209	1.1906	Rrp12	0.0406	-1.1628
Rps13	0.0087	-1.3671	Eif1b	0.0215	1.1580	Rpl30	0.0407	-1.1839
Rpl26	0.0089	-1.2391	Eif4ebp3	0.0221	-1.4873	Rps21	0.0423	-1.1592
Rps18	0.0091	-1.5232	Eif2s3y	0.0226	1.1986	Rpl36a	0.0428	-1.5183
Eif3k	0.0092	-1.3322	Rpsa	0.0227	-1.2841	Rpl12	0.0439	1.0578
Rpl35	0.0093	1.4495	Riok2	0.0229	1.1716	Rpl3	0.0458	-1.1457
Rpp30	0.0098	1.2495	Rpl10a	0.0234	-1.4035	Mtif2	0.0473	1.2521
Rplp1	0.0100	-1.7267	Gar1	0.0234	-1.3500	Rpl21	0.0475	-1.1863
Rps7	0.0100	1.2074	Eif3c	0.0246	-1.0539	Etf1	0.0478	1.2466
Rps14	0.0101	-1.2565	Npm1	0.0247	1.1328	Fbll1	0.0479	-1.6294
Rps5	0.0106	-1.2407	Rpl24	0.0247	1.2138	Rpl27	0.0481	-1.1962
Ppp1r15b	0.0108	1.1830	Taf9	0.0256	-1.1037	Mpp6	0.0488	1.3307
Rpl37a	0.0109	-1.2912	Tbl3	0.0261	-1.4080	Utp14b	0.0490	1.1892
Rpl37	0.0111	-1.9127	Paip1	0.0271	1.2616	Nvl	0.0499	1.2134
Rps28	0.0112	-1.7270	Rbm28	0.0288	1.1249			

Output of analysis pipeline investigating all “EIF2 Signaling” and all “Translational Regulation” GO pathway gene lists. 95 total genes identified, sorted by ascending *P* value.

As mentioned previously, EIF2 signaling and EIF2a phosphorylation by the heme responsive kinase HRI (*Eif2ak1*) is a primary mechanism for regulating translation to reduce mitochondrial stress and unfolded protein response (UPR) in situations of intracellular heme deficiency [177-180]. These studies are all focused on the erythron, where heme is critical as it becomes the limiting factor for incorporation into hemoglobin for red blood cell differentiation. Limited studies have characterized a similar role in mitigating mitochondrial dysfunction in neurons, but very little is known about HRI and EIF2a signaling in any other tissue [178,181-184]. We analyzed the single cell RNAseq datasets of the testes and found that both factors are expressed during spermatid maturation **(Figure 3.19A)** [153]. Immunoblotting of total testes homogenates confirmed significant EIF2a protein expression. Importantly, EIF2a phosphorylation was significantly altered in the DKO mice **(Figure 3.19B & C)**, substantiating the involvement of the EIF2a pathway in mitigating UPR and mitochondrial dysfunction in the testes.

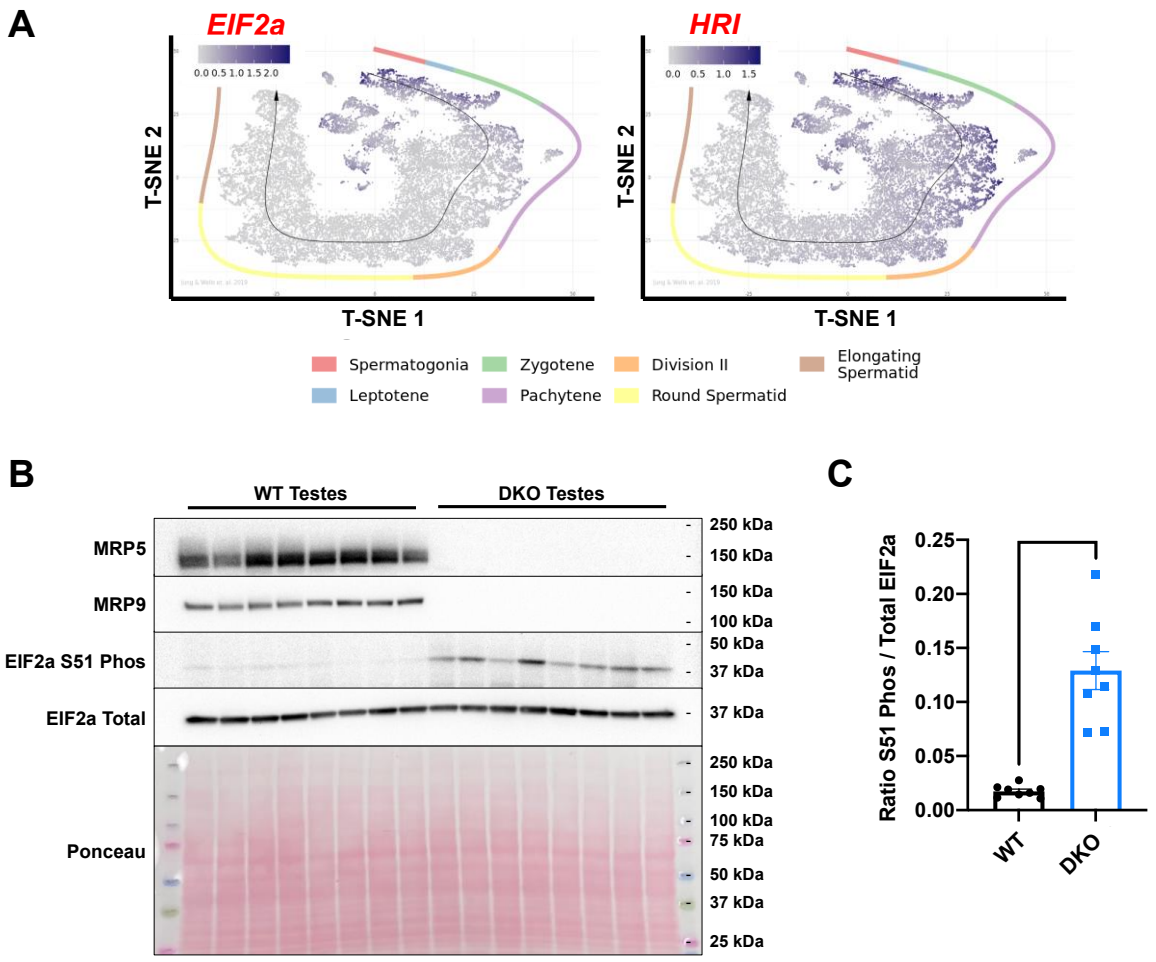

Figure 3.19 Heme responsive components of the erythroid translational regulation system are expressed and significantly modulated in DKO testes

A) Gene expression profiles for *Eif2a* (left) and *Eif2ak1* (right) along the temporospatial axis of spermatid maturation from single cell RNAseq of the testes [153].

B) Immunoblot analysis of testes lysates from DKO and WT mice following SIM. Membranes were probed for Serine 51 phosphorylated EIF2a and total EIF2a as well as MRP5 and MRP9 controls. Blot is representative of three separate experiments, each lane represents an individual mouse, n=8 mice per genotype.

C) Quantification of phosphorylated EIF2a normalized to total EIF2a protein in DKO testes compared to WT, **** = $P < 0.0001$.

We next asked if the observed EIF2 signaling in the testes of DKO mice was in response to heme deficiency, as is the hallmark of the erythroid condition. If so, one would expect that iron/heme homeostasis should also be perturbed in the testes of these mice. Subsequent probing with our pipeline pathway analysis revealed 30 heme and iron homeostasis related genes were in fact significantly altered in DKO testes compared to WT, including a large number of which indicate iron deficiency **(Table 3.4)**. For example, the top hit was *BOLA2*, a multiple mitochondrial dysfunctions syndrome (MMDS) protein essential for FeS cluster assembly [185,186].

Table 3.4 Heme/Iron homeostasis related genes are also significantly perturbed in DKO testes compared to WT

SYMBOL	PVALUE	FC
Bola2	0.0030	-1.4343
Slc25a37	0.0032	1.2235
Sod2	0.0043	-1.2667
Thap4	0.0048	-1.0670
Pcbp2	0.0113	-1.1312
Trim27	0.0117	-1.0530
Cyb561d2	0.0123	-1.3346
Cyb5r4	0.0146	1.3079
Hmox2	0.0172	1.1150
Pcbp1	0.0174	-1.2135
Atp6v1a	0.0181	1.1048
Cyp2d26	0.0218	-1.2632
Cycs	0.0228	1.2837
Sod1	0.0230	-1.2531
Cyc1	0.0291	-1.2995
Fth1	0.0293	-1.3578
Slc25a28	0.0296	-1.1958
Cisd1	0.0299	-1.2525
Trf	0.0303	-1.3973
Pgrmc2	0.0305	-1.0740
Scara5	0.0306	-1.2911
Ncoa4	0.0323	1.1137
Tfrc	0.0326	1.2393
Nubp1	0.0330	-1.2011
Neo1	0.0355	-1.1542
Urod	0.0375	-1.2805
Cyp46a1	0.0385	-1.3452
Snx3	0.0420	-1.0587
Cyp51	0.0430	1.2406
Slc39a8	0.0441	1.0960

Output of analysis pipeline investigating all “Iron Homeostasis”, “Heme” and “Heme Binding” GO pathway gene lists. 30 total genes identified, sorted by ascending *P* value.

To determine if heme levels were in fact altered in male reproductive tissues, we quantified total heme by the oxalic acid method. Although heme levels in whole testes and seminal vesicles showed no difference **(Figure 3.20A & B)**, caudal epididymides, the storage sites for mature sperm showed a significant decrease in the DKO, suggestive of insufficient heme in the spermatozoa of DKO mice **(Figure 3.20C)**.

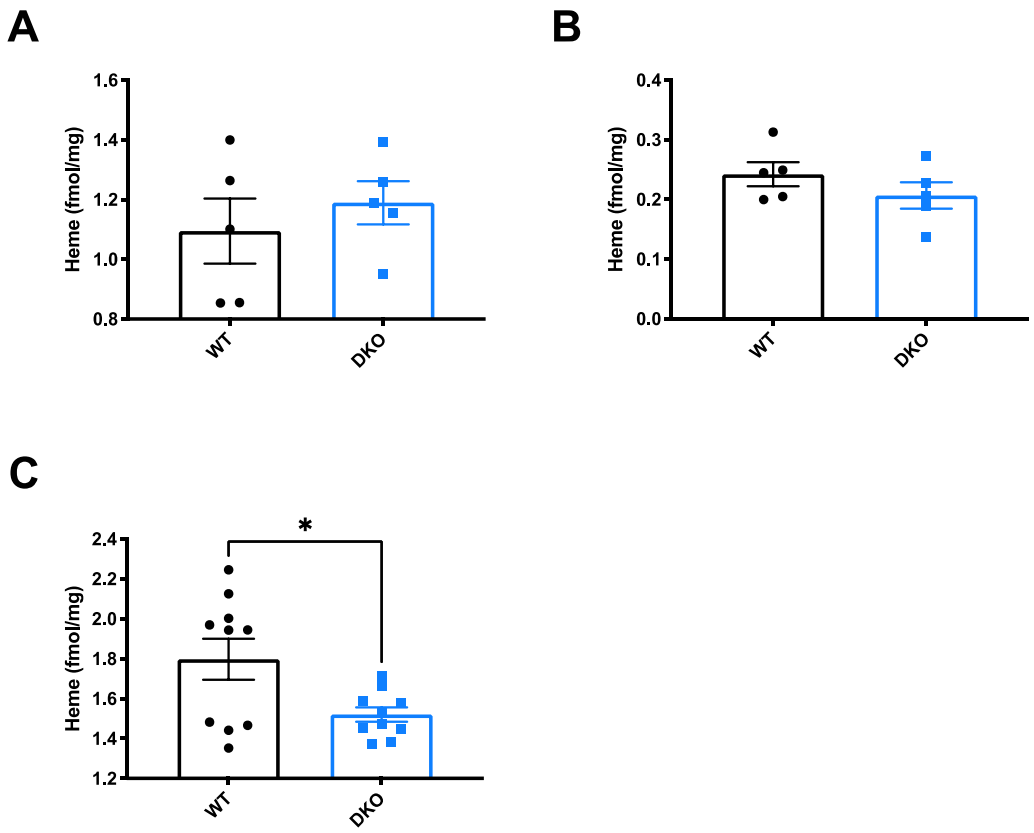

Figure 3.20 Heme quantification of male reproductive tissues demonstrate reduced heme levels in caudal epididymis

A) Heme content of whole testis from DKO and WT mice by oxalic acid quantification, n=5 animals per genotype.

B) Heme content of seminal vesicles from DKO and WT mice by oxalic acid quantification, n=5 animals per genotype.

C) Heme content of pooled caudal epididymides from DKO and WT mice by oxalic acid quantification, n=15 animals per genotype (1.5 mice or 3 epididymides per replicate), * $P = 0.0275$.

A critical component of EIF2 signaling for maintaining mitochondrial function and redox homeostasis is the repression of the mTOR signaling cascade to inhibit proliferation and enable differentiation [177,187]. Indeed, the mTOR signaling pathway was also one of the most significant GO terms from IPA of the testes **(Figure 3.15B)**, with 23 of 31 genes significantly decreased in DKO testes compared to WT **(Table 3.5)**. Upregulation by some of these remaining genes is not surprising as *EIF-4E* is a highly abundant translation regulation factor in the testes which has been shown to play an important role in spermatogenesis through regulation of capping stage-specific mRNAs during germ cell development [188].

Table 3.5 mTOR signaling cascade is significantly downregulated in DKO testes

SYMBOL	PVALUE	FC
Eif4e	0.0022	1.1282
Mlst8	0.0042	-1.2628
Nras	0.0045	1.1204
Mapk3	0.0048	-1.2147
Hras	0.0049	-1.3347
Pik3r2	0.0055	-1.2891
Tsc2	0.0140	-1.1764
Pik3r3	0.0140	1.2058
Lamtor2	0.0159	-1.3638
Lamtor4	0.0169	-1.7561
Nprl2	0.0170	-1.1422
Poldip3	0.0171	-1.1275
Mapkap1	0.0203	-1.0839
Lamtor1	0.0220	-1.2689
Cycs	0.0228	1.2837
Ywhag	0.0234	-1.3266
Rptor	0.0262	-1.2289
Prkaa1	0.0265	1.2390
Ccne1	0.0295	-1.1385
Wdr24	0.0327	-1.2272
Strada	0.0333	-1.1417
Rps6ka6	0.0343	1.2828
Mios	0.0346	1.1789
Stk11	0.0350	-1.1368
Rac1	0.0351	-1.2483
Eef2	0.0366	-1.1573
Akt1	0.0375	-1.2934
Fkbp1a	0.0435	-1.0919
Rheb	0.0459	1.2548
Ywhaz	0.0477	-1.0763
Ywhae	0.0478	-1.0606

Output of analysis pipeline investigating all “mTOR Signaling” GO pathway gene lists.

31 total genes identified, sorted by ascending *P* value.

Retinoic acid regulation at the intersection of mitochondrial dysfunction and male reproduction

Growing evidence reveals an interconnection between translational regulation pathways and retinoid signaling; retinoic acid has been shown to regulate the mTOR/EIF-4E cascade to modulate protein synthesis in response to axon damage and remodeling [189]. Retinoic acid is an essential metabolite of vitamin A which also serves as a critical signaling molecule in a variety of biological contexts [190-192]. One of the key roles of retinoic acid is the regulation of gene expression that impacts mitochondrial function [193]. Principal targets of this retinoic acid signaling include key OxPhos and respiratory genes such as NADH dehydrogenase subunits, cytochrome c oxidases and the ATPases, which are some of the most differentially expressed genes in the DKO testes **(Figure 3.15A)** [193,194]. Therefore, we hypothesized that retinoic acid homeostasis/signaling may play an essential role in the phenotype observed in the DKO testes.

RNAseq showed that retinoic acid signaling/metabolism associated gene expression is significantly perturbed in the testes of DKO mice **(Table 3.6)**. Interestingly, among these changes are decreases in the cytosolic chaperone Crabp1, responsible for delivering retinoic acid for catabolism, as well as binding receptors (RAR, RXRs), suggestive of retinoic acid deficiency [195-197]. Retinoic acid is essential for male germ cell differentiation and reproductive fecundity, and vitamin A deficiency a well-established cause of male infertility both in mice and humans [198,199]. Defects in retinoid homeostasis are critical due to the impact on retinoic acid signaling, which exerts key control over meiotic initiation and spermatogenesis to

maintain testes function [198,200,201]. Given then the gene expression changes observed and the male reproductive phenotype in these mice, we asked what was the status of retinoids in male reproductive tissues? Quantification of the three major components of the retinoid pathway, vitamin A esters, vitamin A (retinol) and retinoic acid, revealed significant differences in Vitamin A metabolism. DKO mice showed elevated levels of the nutrient retinol in their seminal vesicles, while the active metabolite retinoic acid was decreased in both testes and seminal vesicles **(Figure 3.21)**.

Table 3.6 Retinoic acid signaling/metabolism associated genes are significantly perturbed in the testes of DKO mice

SYMBOL	PVALUE	FC
Crabp1	0.0054	-1.5406
Sdf2l1	0.0075	-1.3796
Adh1	0.0088	-1.5492
Ncor2	0.0123	-1.3468
Rxrb	0.0163	-1.2426
Fabp9	0.0177	1.3635
Trim24	0.0192	1.1793
Rara	0.0195	-1.1871
Rdh11	0.0240	1.0804
Scarb1	0.0267	-1.1486
Dhrs7b	0.0268	-1.2188
Dnajb11	0.0316	1.1495
Fabp5	0.0320	-1.6633
Bco1	0.0360	1.0767
Rbp4	0.0373	-1.2553
Erp29	0.0403	-1.0859

Output of analysis pipeline investigating all “Retinoic Acid”, “Retinoid Metabolism”, “Retinoic Acid Signaling” and assorted GO pathway gene lists. 16 total genes identified, sorted by ascending *P* value.

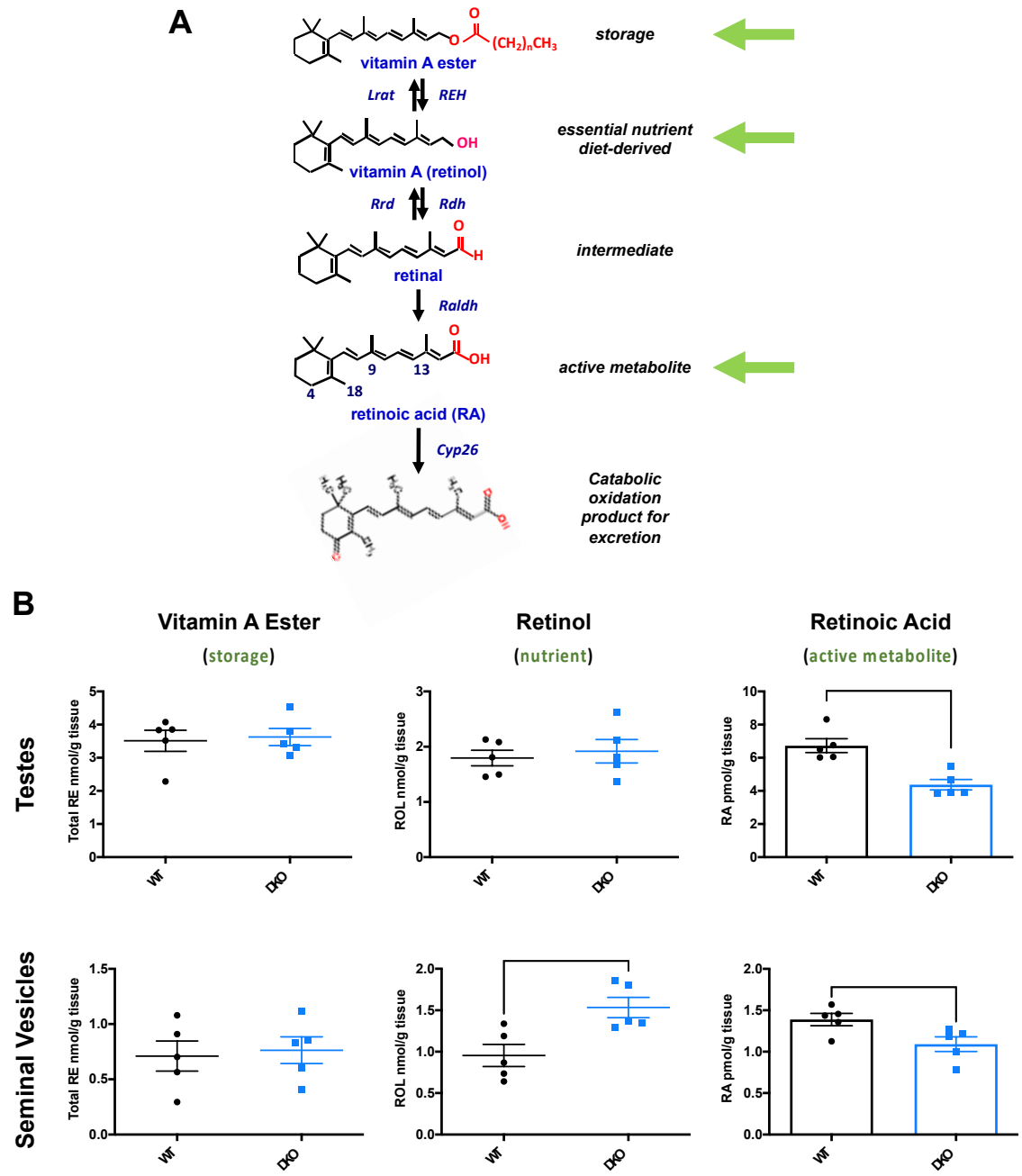

Figure 3.21 Retinoid pathway determination from DKO and WT mice show significant differences in vitamin A metabolism

A) Schematic of vitamin A metabolism pathway and annotated retinoid species (green arrows) quantified below in panel B from testes.

B) Quantification of vitamin A metabolism components in testes (top) and seminal vesicles (bottom); * = $P < 0.05$, ** = $P < 0.01$.

Given that the total levels of vitamin A and storage esters are not perturbed in the testes, we assume these animals are not nutritionally deficient - meaning that at least Sertoli cells are still able to acquire, produce and distribute retinoic acid to spermatogonia. Reinforcing this notion is the fact that DKO mice are not completely sterile and are still able to produce sperm, with no blocks on meiosis or spermatogenesis. What then is the significance behind retinoic acid depletion in these reproductive tissues? To explore the implications of this decrease in retinoic acid levels we performed a deeper analysis of RNAseq on the full signaling network. Ontology network mapping by IPA generated the Retinoic Acid Receptor (RAR) activation pathway and confirmed aberrant retinoic acid signaling/metabolism in the testes of DKO mice **(Figure 3.22)**. Additionally, network mapping verified systemic cascade downregulation, specifically in the case of the binding receptors responsible for activation and suppression of target genes (RARs, RXRs, SMRT and SMADs).

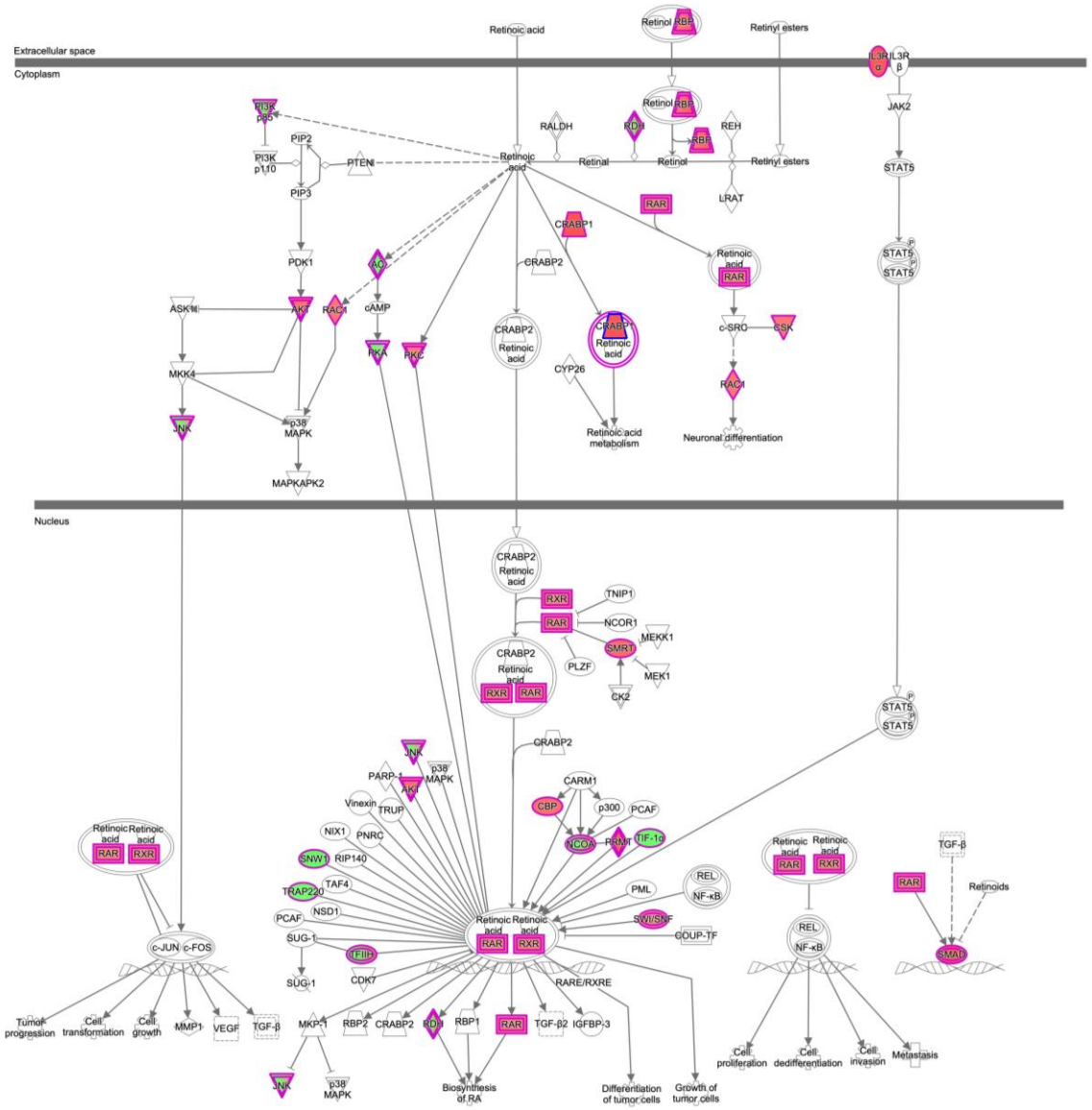

Figure 3.22 RAR activation pathway ontology genes further confirm retinoic acid signaling / metabolism are aberrant in the testes of DKO mice

IPA analysis of Retinoic Acid Receptor (RAR) ontology network of gene expression fold changes from RNAseq of WT and DKO testes; red – downregulated genes, green – upregulated genes.

To determine if retinoic acid binding transcription factors and cascade regulators were impacting our mitochondrial genes of interest, we performed unbiased motif discovery of all the genes from our mitochondrial dysfunction heat map (**Figure 3.18**). To perform this analysis, we extracted upstream regulatory sequence (5` 1000bp) from all significantly up-regulated and down-regulated genes and processed either with MEME **(Figure 3.23A)** or HOMER **(Figure 3.23B)** suites to identify enriched un-gapped sequences conserved across transcripts (**Appendix V)**. The top five statistically significant DNA sequences of each were then analyzed and aligned for querying against known binding motifs (**Figure 3.23)**. We identified significant enrichment of retinoic acid related binding motifs in the genes dysregulated in the DKO mice [202]. Importantly, these motifs were found from both analysis platforms and included putative RARs, RXRs, and VDR vitamin D receptor binding sequences, the last of which also exerts its function via RXRs [202,203]. Of note, the RHOXF1 binding motif, known for modulating expression of target genes involved in spermatogenesis and male infertility, also aligns with enriched sequences [204,205]. These findings reveal specific DNA binding motifs that are conserved amongst our highly dysregulated mitochondrial genes, providing a direct mechanistic link between retinoic acid and mitochondrial status.

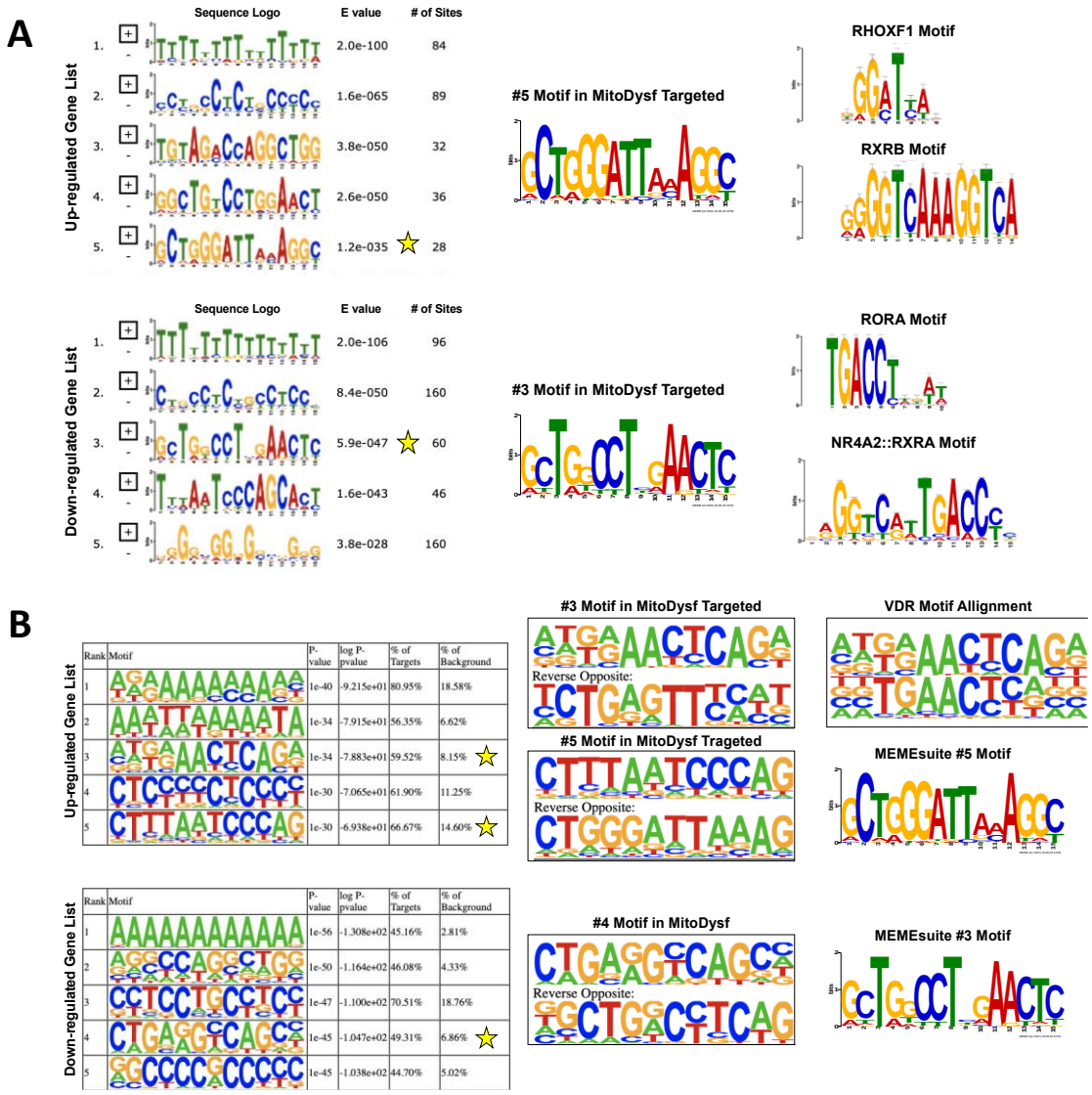

Figure 3.23 Targeted motif discovery of mitochondrial dysfunction pathway genes identifies critically conserved retinoic acid related binding motifs

A) Output of MEME suite motif discovery analysis of top five un-gapped enriched sequences from mitochondrial dysfunction gene list transcripts upregulated (top) or downregulated (bottom) in DKO testes. TomTom motif blast output used for candidate sequences alignment and predictions.

B) Output of HOMER motif discovery analysis of top five un-gapped enriched sequences from mitochondrial dysfunction gene list.

Ablation of MRP9 and MRP5 significantly impacts mitochondrial function

To characterize mitochondrial dysfunction in the DKO mice, we first analyzed mitochondria oxidative phosphorylation complexes. All five complexes appeared to be normal in the testes of both genotypes **(Figure 3.24)**. We wondered whether differences may only manifest in the spermatozoa themselves instead of the whole testes, given our heme content quantifications. Sperm therefore were collected from the caudal epididymis by "swim-out" method for transmission electron microscopy (TEM) imaging. Strikingly, TEM cross sections of sperm midpieces revealed DKO mice had highly vacuolated and aberrant mitochondria, in contrast to the ubiquitously electron dense cristae in the WT (**Figure 3.25A)**. These defects were not observed in the single KOs or double heterozygous animals **(Figure 3.25B)**.

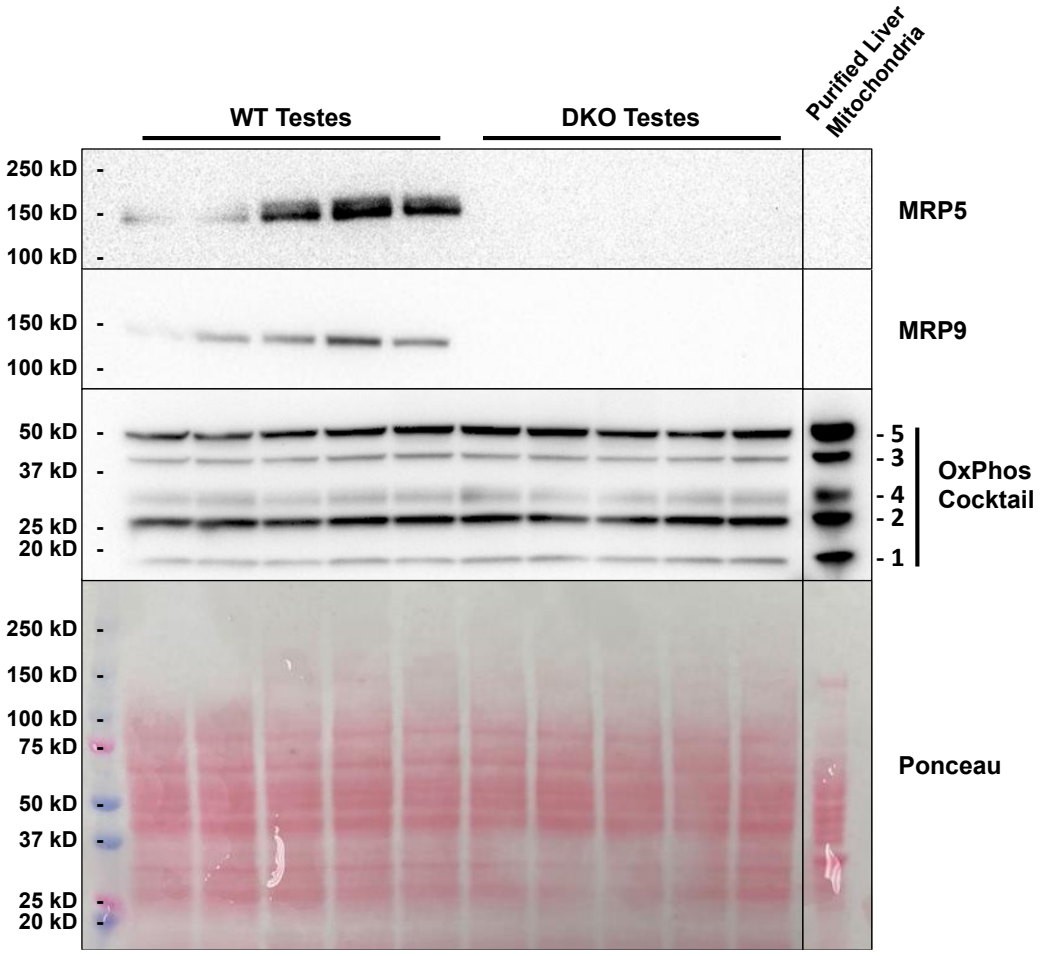

Figure 3.24 Probing testes of WT and DKO mice for OxPhos complex deficiencies reveal no differences

Immunoblotting of testes total lysates with anti-Total OxPhos Complex Kit, MRP5 and MRP9 antibodies following SIM. Complex Kit cocktail targets are premixed mouse monoclonal antibodies (#1 – Complex I, C-I-20 ND6; #2 – Complex II, C-II-30 FeS; #3 – Complex III, C-III-Core 2; #4 – Complex IV, C-IV-1; #5 – Complex V, C-V-a) and targets are labeled 1-5 on right hand side of the immunoblot.

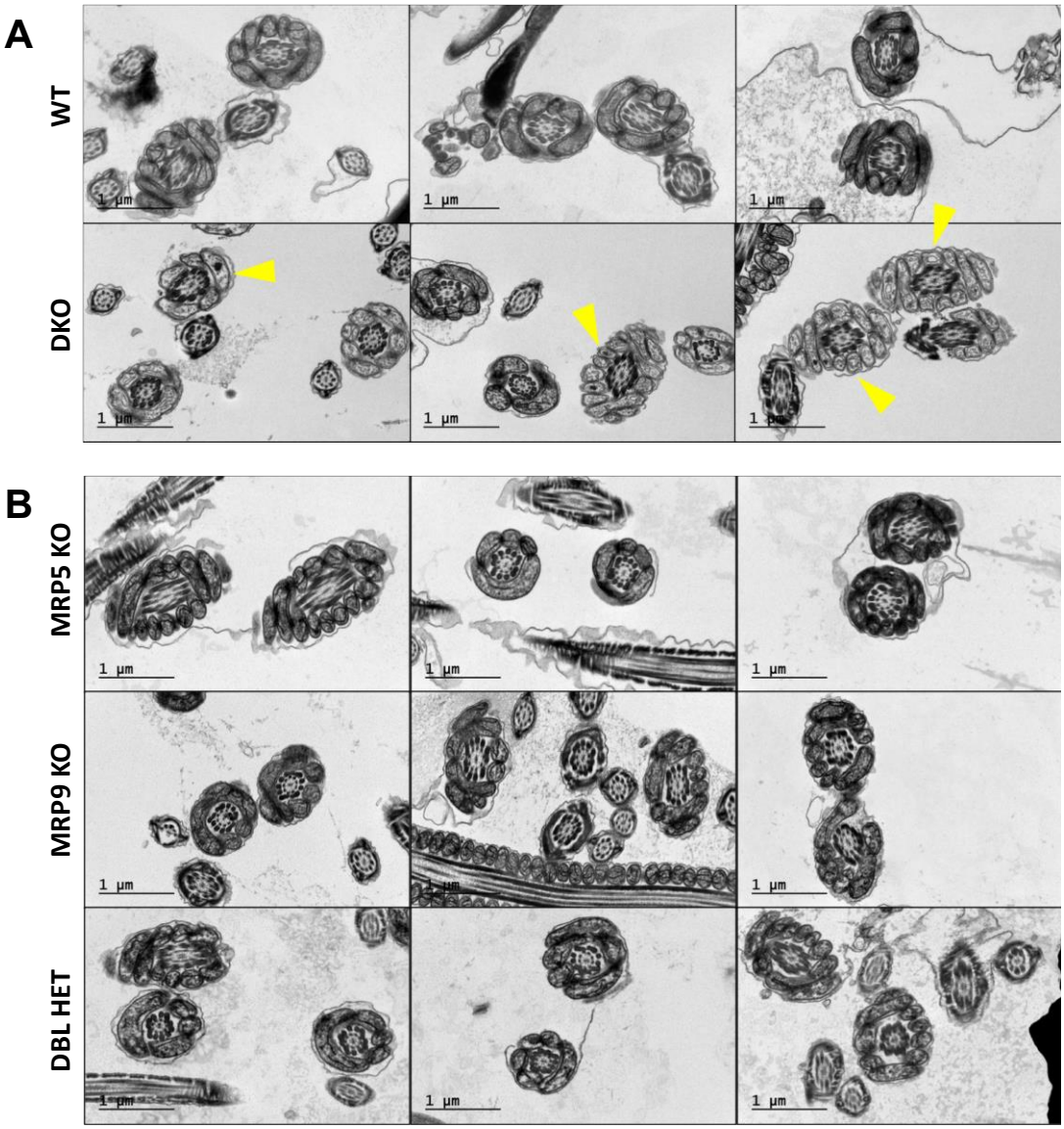

Figure 3.25 Genetic disruption of both MRP9 and MRP5 in mice causes aberrant mitochondria in the midpiece of caudal epididymal sperm

A) TEM of swum-out caudal epididymal spermatozoa from WT (top) and DKO (bottom). Cross sections of the sperm midpiece visualize cristae and mitochondrial morphology of the mitochondrial sheath. Yellow arrow heads highlight vacuolated and aberrant mitochondria. Representative images from at least 15 FOVs per sample.

B) TEM of swum-out caudal epididymal spermatozoa from MRP5 KO (top), MRP9 KO (middle), and Double Het (bottom). Cross sections of the sperm midpiece visualize cristae and mitochondrial morphology of the mitochondrial sheath. Representative images from at least 15 FOVs per sample.

3.3 Discussion

MRP9 in many ways is a very perplexing ABCC transporter: a unique expression pattern, no known drug substrates, and the last in the ABCC class still to be characterized [91,114,115]. In the current study, we fill in some of the gaps in our knowledge of MRP9 by generating the first MRP9 knockout mouse model. We find that MRP9 is highly expressed in the mouse spermatogenic lineage and reveal its subcellular location. Unlike other MRPs, MRP9 does not localize to the plasma membrane irrespective of cell polarization, consistent with the intracellular location published by Ono et al [114]. However, MRP9 localization is not truly ER as they had postulated. We provide evidence that MRP9 partitions to mitochondrial-associated membrane fractions. This makes physiological sense as MRP9 is localized to developing and mature spermatozoa which are known to be devoid of traditional ER structures [206,207]. Though the ER is depleted in the process of differentiation, vestiges of ER membranes likely remain, particularly those in tight contact with mitochondria, and have been postulated to concentrate in the neck of the sperm mid-piece to serve as a store for Ca^{2+} necessary for sperm activation [207,208]. Indeed, ER resident proteins such as ERp29 and Calreticulin have also been demonstrated to be present in sperm and play essential roles in acrosome reaction, fertilization and stress

responses [207,208]. Therefore, we envision MRP9 may reside at these interfaces adjacent to mitochondria, effluxing substrates essential for regulating mitochondrial function and/or trafficking metabolites between these compartments as spermatogonia develop.

MRP9 is not expressed in any of the cell lines tested including MEFs. Our results also refute the findings of Shi et al that the histone deacetylase inhibitor sodium butyrate increases MRP9 abundance, especially since they did not reveal the molecular weight of their protein nor did they perform gene knockdowns to show protein specificity [157]. Even probing of GC-2spd cells, a SV40 large T antigen immortalized cell line of spermatocyte precursors, shows no detectable levels of MRP9 by western blotting [209,210]. These premeiotic cells display spermatid characteristics despite arresting at meiosis, having lost their full differentiation potential, indicating that MRP9 expression may be explicitly tied to differentiation/sperm maturation [211]. Nevertheless, ablation of MRP9 alone show no overt male reproductive phenotypes in mice despite complete loss of detectable protein by western blotting and immunohistochemistry utilizing antibodies which targeted either the N-terminus or ATP binding cassettes. Inspection of these histological sections of testis and epididymis reveal effective spermatogenesis, with normal spermatid progression in seminiferous tubules and mature sperm in the convoluted ducts. Unsurprisingly, we also see no morphological defects evident in electron microscopy of sperm from MRP9 single knockouts, as these male mice are perfectly capable of siring progeny even in an MRP5 heterozygous background. Therefore, any discernable impact on reproduction is only found when both MRP9 and MRP5 are both ablated.

DKO mice show a significant decrease in reproductive output, as measured by litter size and pregnancy rates as a consequence of DKO sperm's inability to effectively fertilize, since IVF rates with wildtype oocytes are drastically reduced. In addition to a trend in decreased motility, the morphological abnormality of their mitochondria at the ultrastructural level is remarkable. As discussed previously, these changes in mitochondrial function can have a significant impact on male fecundity. It was therefore reasonable that we focused the mutant characterization on male mice particularly because they showed reproduction phenotypes and that MRP9 is abundantly expressed in the testes. We cannot fully rule out the possibility that there might be a maternal component to the low number of DKO pups that survive to weaning (**Figure 3.6**).

Fortunately, the viability of DKO mice afforded the possibility of investigating the mechanisms behind their reproductive dysfunction. From the untargeted metabolomics, it became obvious that there were substantial changes in the composition of metabolites retained in the testis, highlighting a number of putative substrates that may be inappropriately trafficking in the combined loss of MRP5 and MRP9. In agreement with the metabolomic results, RNAseq from the same tissue samples revealed significant perturbations in gene expression. Importantly, integrative analysis of both datasets revealed that energy production and mitochondrial function were the top two terms impacted in the DKO.

The top pathway identified by our gene expression analysis was EIF2 signaling, which we validated *in vivo* as a response to mitochondria dysfunction and/or induced by alterations in heme levels in maturing sperm. Indeed, heme and iron related genes

were differentially expressed in the testes, and quantification of heme in the caudal epididymis of DKO mice showed significantly decreased levels. In a similar vein to the well-established models of unfolded protein response in the erythron, we envisage a necessity for heme sharing and partitioning as mitochondria are rapidly being recruited and cells are undergoing proliferation for spermatogenesis and differentiation. Though this translational regulation via EIF2 signaling has been well studied in other contexts, virtually nothing is known about its role in the testes. The only published study relates to EIF2s3y, which was shown to be essential for regulating protein proliferation in spermatogenesis [212]. It is yet to be determined whether or not this subunit has any direct relation to our findings here, although its gene expression is also significantly upregulated in the DKO testes ($P = 0.022$).

Beyond EIF2 signaling, IPA identified several additional pathways: Protein Ubiquitination (essential for unfolded protein response), mTOR Signaling, Regulation of EIF4, Oxidative Phosphorylation, Germ Cell-Sertoli Cell Junction Signaling (an essential component of sperm differentiation), and Mitochondrial Dysfunction. It is plausible that retinoic acid may be a critical regulator in all these pathways for the following reasons: 1) it is essential in male fertility as one of the primary signaling molecules from Sertoli cells for progression of spermatogenesis; 2) it is critical for regulating gene expression of essential oxidative phosphorylation and mitochondrial genes; and 3) it has been shown to modulate mTOR and EIF4 regulation [189,193,198]. Consistent with this notion, we find genes associated with retinoids and retinoic acid levels significantly decreased in DKO testes. Furthermore, targets of gene expression perturbation have significant enrichment of RA binding motifs for transcriptional

regulation, thereby demonstrating a viable means for interconnecting regulation across all these pathways.

Taken together, we postulate the following model for a concerted role for MRP9 and MRP5 in the testes **(Figure 3.26)**: In the absence of MRP9 and MRP5, metabolites such as heme and/or other substrates are inappropriately trafficked or distributed causing mitochondrial damage. This dysfunction induces signaling through the EIF2 and mTOR pathways to regulate protein translation and UPR with corresponding changes in retinoic acid levels and signaling. Germ cells differentiate into mature spermatozoa, but these are functionally defective as they fail to fertilize normal oocytes due to mitochondrial insufficiencies.

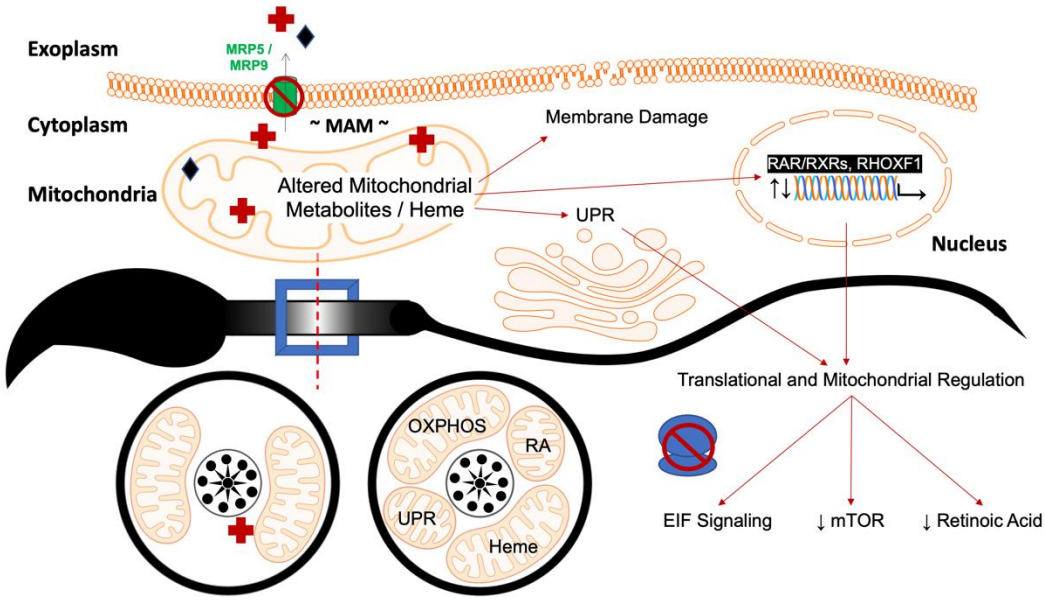

Figure 3.26 Proposed model for MRP5 and MRP9 function in male germ cells

Aberrant heme/metabolite trafficking causes partitioning defects and mitochondrial dysfunction impacting downstream pathways and overall sperm reproductive fitness, see text for details.

An outstanding question that still remains, however, is precisely how and when are these transporters active? Given the differences in the temporospatial gene expression patterns of MRP9 and MRP5, it is tempting to speculate that MRP5 functions may precede MRP9 as germ cells differentiate and undergo meiosis. This may explain why single knockout animals show no phenotype - if metabolites are unable to reach their destination at one point during maturation, then they are compensated via an alternate pathway during development.

4 Chapter 4: Discussion

4.1 Conclusions

MRP5 is a conserved metazoan heme exporter that is essential for male fecundity in *C. elegans*, however, MRP5 KO mice have no overt reproductive phenotypes [82,107]. MRP9, the closest ABCC homolog of MRP5, is highly expressed in the testes and is the last mammalian MRP whose function remains uncharacterized [114]. The goal of this project was to determine the impact(s) of MRP9 ablation, and to elucidate the endogenous functions of MRP9 and MRP5 as they relate to reproduction and genetic compensation in a mammalian model. The major findings of our study are delineated below:

1) MRP9 is specifically expressed in developing spermatids and mature spermatozoa in mice. Loss of MRP9 however, has no discernable impact on male reproductive function and knockout mice are viable.
2) The combined loss of MRP5 and MRP9 in mice results in significant reproductive failure due to decreased male fecundity. Defects in sperm fertilization rates and high incidences of penile prolapse and seminal coagulum clogging contribute to reduced litter sizes in DKO mice.
3) Subcellular fractionation demonstrates that MRP9 and MRP5 are highly enriched in mitochondrial-associated membranes of the testes, a distinct compartment characterized by mitochondrial outer membrane and endoplasmic reticulum markers.

4) Contrary to reported studies, MRP9 protein cannot be induced by sodium butyrate treatment. *In vitro* immunofluorescence studies utilizing transient transfection in HeLa cells confirm that MRP9 is localized to mitochondrial-associated membranes and does not traffic to the plasma membrane.
5) Untargeted metabolomics and RNAseq of testes reveal widespread and significant differences in both the global metabolome and transcriptome of DKO mice. Integrative analysis of both datasets show substantial perturbations in mitochondrial homeostasis and energy production.
6) EIF2 Signaling and Protein Ubiquitination are the top two pathways identified by RNAseq. We find that heme content is decreased in the caudal epididymis from DKO mice and testes. EIF2a protein phosphorylation is significantly attenuated in DKO mice, suggestive of the involvement of this pathway in UPR and mitochondria insufficiencies.
7) Genes associated with vitamin A metabolism are significantly perturbed in the testes of DKO mice. Retinoid signaling genes and retinoic acid levels themselves are also significantly decreased, corresponding with an enrichment of retinoic acid binding motifs in genes related to mitochondrial dysfunction that are differentially expressed in the RNAseq. These findings suggest a combined mechanism for interconnecting mTOR, EIF and mitochondrial regulation by retinoic acid, a nutrient essential for governing spermatogenesis.
8) Caudal epididymal sperm of DKO mice have highly vacuolated and aberrant mitochondria by TEM imaging, in stark contrast to the ubiquitously electron dense cristae of WT and single knockout animals. These results indicate that

loss of both transporters manifest in mitochondrial dysfunction and confirm concerted compensation of multidrug drug resistance proteins in male reproductive fitness.

4.2 Future Directions

Targeted functional metabolomics of subcellular fractions

In this study we performed untargeted metabolomics of total testes to determine global metabolite profiles and identify if any species of interest were grossly perturbed in the organ. However, identification of individual species from unbiased mass spec data can be extremely challenging, given the only information we glean are mass to charge ratios (time of flight through the machine). In our case, this resulted in myriads of differentially accumulated species we could quantify; however, the majority of which could not be associated with a distinct KEGG ID and therefore were not included in subsequent analysis. Additionally, given that at least in the testes these MRPs are highly enriched in mitochondrial-associated membranes, it is likely that some, if not most, of the significant changes are not at the total organ level, but rather in the subcellular partitioning within the testes themselves. Therefore, we sought to address this by performing subcellular fractionation of the testes tissue. We then performed targeted high throughput metabolomics, utilizing plates with known standard curves for over 600 individual species. We propose that this dataset (actively under investigation) will allow for the identification of specific differences within each subcellular organelle or niche and in particular, associate the exact species that may be

sequestered inside the mitochondria because they cannot be effluxed at the MAMs interface.

Modulation of MAM homeostasis to further characterize MRP9

Here we show that MRP9 both *in vitro* and in the testes is enriched in mitochondrial associated membranes or MAMs. We therefore wondered if targeting to this subcellular localization is dependent on MAM status and/or if alterations in MAM proteins possibly interacting with MRP9 may also affect this localization. We propose investigating this further in future studies by expressing MRP9 ectopically in Mitofusin 1/2 knockouts and wildtype MEFs *in vitro* [130,213]. As discussed previously, Mitofusin 2 is a unique outer mitochondrial membrane GTPase which is essential for mitochondrial elongation and fusion (like Mitofusin 1), but also intercalates in the membrane of the ER, acting as a tether between these two organelles [129,213,214]. Though there are conflicting findings associated with the ablation of Mitofusin 2 and its impact on MAMs themselves, we are interested to determine if immunofluorescence of MRP9 is altered in the absence of these proteins, altering mitochondrial dynamics [215,216]. If so, we would also be highly interested in performing immunoprecipitations of these proteins to see if they are interacting in this tight membrane interface.

Label-free heme imaging of spermatozoa

In this study we performed heme quantification of caudal epididymis as a proxy for heme content in sperm themselves as the convoluted ducts are the storage reserve site for mature sperm. This is partly due to the fact that the quantity of sperm that could be extracted via epididymal swim-out was insufficient and would have required large numbers of mice. Even with whole caudal epididymides, we required tissue from at least two mice (three epididymides) to consistently measure heme content. Naturally, these results then are not without caveats, as conceivably the differences in heme could be from the principal cells, epithelial cells, or the fibromuscular tissue that make up the actual structure of the epididymal duct [217,218]. Little is known about heme and heme trafficking in those tissues, and though we could not detect MRP9 protein by IHC in those cell types, we do not know the status of MRP5 as the anti-MRP5 antibodies did not work in IHC. To bypass these issues and more accurately measure heme content in free swimming spermatozoa, we proposed imaging heme directly via transient absorption (TA) microscopy [161]. In previous collaborations with the Dr. Ji-Xin Cheng's group, we have been able to successfully label-free image heme in *C. elegans*, demonstrating distinct storage and dynamic distribution in a living organism [160]. Therefore, we sought to similarly image heme from sperm of DKO and WT mice and determine if its partitioning within the mid-piece is perturbed. Preliminary results from WT sperm show heme signal through the entirety of the sperm midpieces, reminiscent of our TEM results visualizing the electron dense mitochondria **(Figure 4.1)**. In future studies we plan on both imaging and quantifying heme content with caudal epididymal

sperm from WT and DKO mice to validate our findings and further identify possible heme differences at the cellular level.

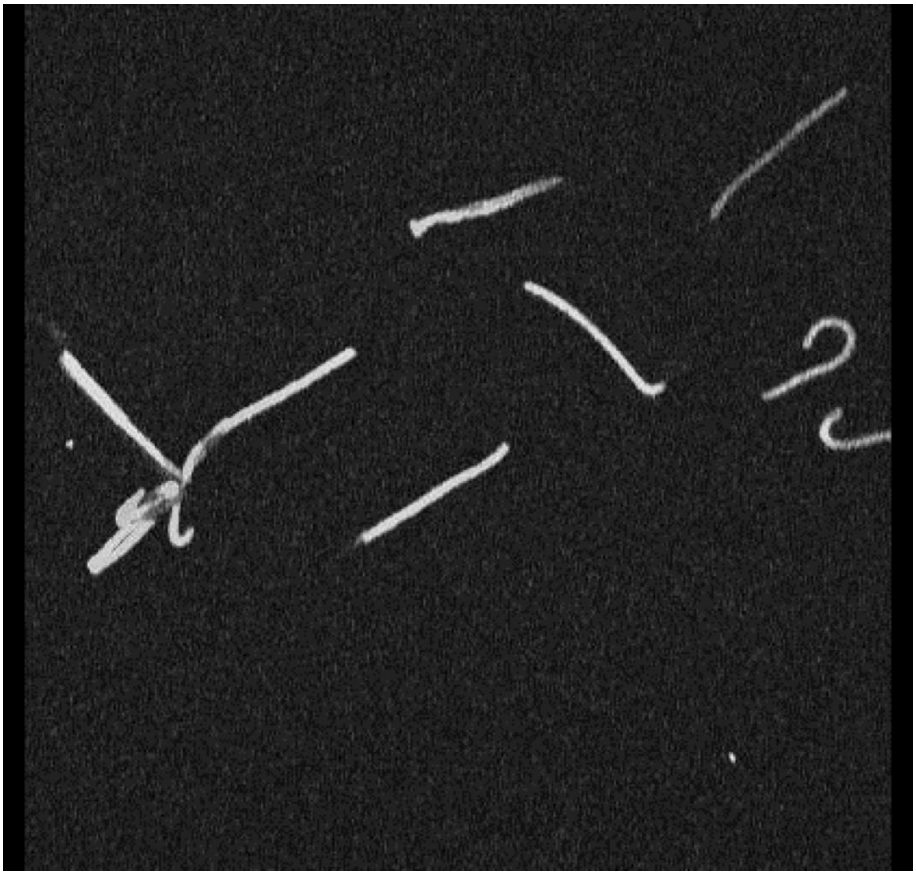

Figure 4.1 Label-free heme imaging of wildtype spermatozoa

Representative still-shot of a 3D projection of volumetric heme imaging. Wildtype sperm swum-out from the caudal epididymis were fixed and imaged by transient absorption microscopy.

Rescue of the male phenotype

The results presented here give insight into the consequences of ablating both MRP5 and MRP9 together in the mouse model. Alterations in mitochondrial homeostasis clearly have significant ramifications on spermatozoa and consequently, male fertilization and fecundity. Within these findings however, we have not explored means of ameliorating the mitochondrial dysfunction to rescue male reproductive phenotypes in the DKO mice. To address this, we propose future studies that may be able to answer this question both chemically and genetically. Primary and secondary mitochondrial disorders are a target of over 230 clinical trials as of 2019, and a number of nutritional interventions as well as novel experimental drugs have shown to have significant promise in amending these disease states *in vivo* [219]. In particular, antioxidant molecules have been a focus of drug development for decades because oxidative stress induced by mitochondrial dysfunction and reactive oxygen species (ROS) production has widespread effects from energy production to lipid peroxidation and total cellular health [219-221]. All of these factors also have detrimental impacts on sperm fertility, so it would be of significant interest to test these ROS inhibitors as well as common antioxidant treatments (such a coenzyme Q10) to determine if any are able to improve DKO sperm fertilization rates [123]. Indeed, loss of the MAM tether protein Mitofusin 2 leads to impaired mitochondrial respiration which can be rescued by coenzyme Q10 supplementation, giving further support to this idea [222].

An additional avenue of inquiry for rescuing this male phenotype is to return to *C. elegans*. *mrp-5* male worms have defective reproductive sensilla (rays) and copulatory spicules, which are established phenotypes that cause male reproductive

failure in *C. elegans [108]*. Some of these defects, such as the shrunken fan with reduced ray formation, are undoubtably more developmental and morphological in nature than our initial characterization in mice [108]. The failure observed in spicule retraction and the overall sterility, however, broadly phenocopy DKO male mice penile prolapse and IVF rates [223]. It therefore would be interesting to determine if either of these distinct defects seen in male *mrp-5* worms are interrelated and rescuable. Therefore, future studies could include expressing MRP9 in the *mrp-5(ok2067)* mutant worms to determine if mouse MRP9 can rescue the worm male reproductive phenotypes.

Direct evidence of heme transport by MRP5 and MRP9

Though MRP5 has been established by our lab as a heme exporter, we have yet to directly demonstrate binding of heme or determine the biochemical mechanism for heme transport. Our analysis of MRP5 and MRP9 protein sequences uncover no regions of similarity to canonical heme binding domains or motifs present in other heme transporters. Given the promiscuity of ABCC transporters and the variability of their putative substrates, it is possible that MRP5 and MRP9 may lack these highly specific signatures found in other heme transporters. Nevertheless, we sought to uncover any unique differences that may elucidate mechanisms for heme efflux and performed *in silico* analysis of *C. elegans* MRP-5 and all human MRPs. Alignment and manual annotation of protein sequences identified several conserved residues in MRP5 and MRP9, which are not present in other ABCC family members (**Figure 4.2**). Furthermore, the recent discovery of the structural basis for substrate recognition of

MRP1 by cryo-EM allowed us to perform threaded modeling of human MRP5 and human MRP9 (**Figure 4.3**) [224-226]. These models suggest that hydrophobic binding pockets in MRP5 and MRP9 may be capable of transporting heme (**Figure 4.4**) [100,224,225]. Therefore, we propose future studies to evaluate these residues to determine if they are truly responsible for heme transport and confirm if heme efflux is indeed specific to these MRPs function. A means of investigating this would be to generate MRP5 and MRP9 with site-directed mutations in these putative heme-binding residues as well as mutations in the conserved ABC transporter components (such as the nucleotide binding domains and walker motifs) to serve as positive controls for disruption of transport activity [227]. The mutant proteins can be tested in transport assays established in our lab using yeast to determine if heme efflux is abolished. If so, it is worth noting there are numerous human SNP variants found in MRP5 and MRP9 (**Figure 4.2**) [228]. These mutants can also be investigated to determine if humans with missense variants in MRP5 and MRP9 show male infertility.

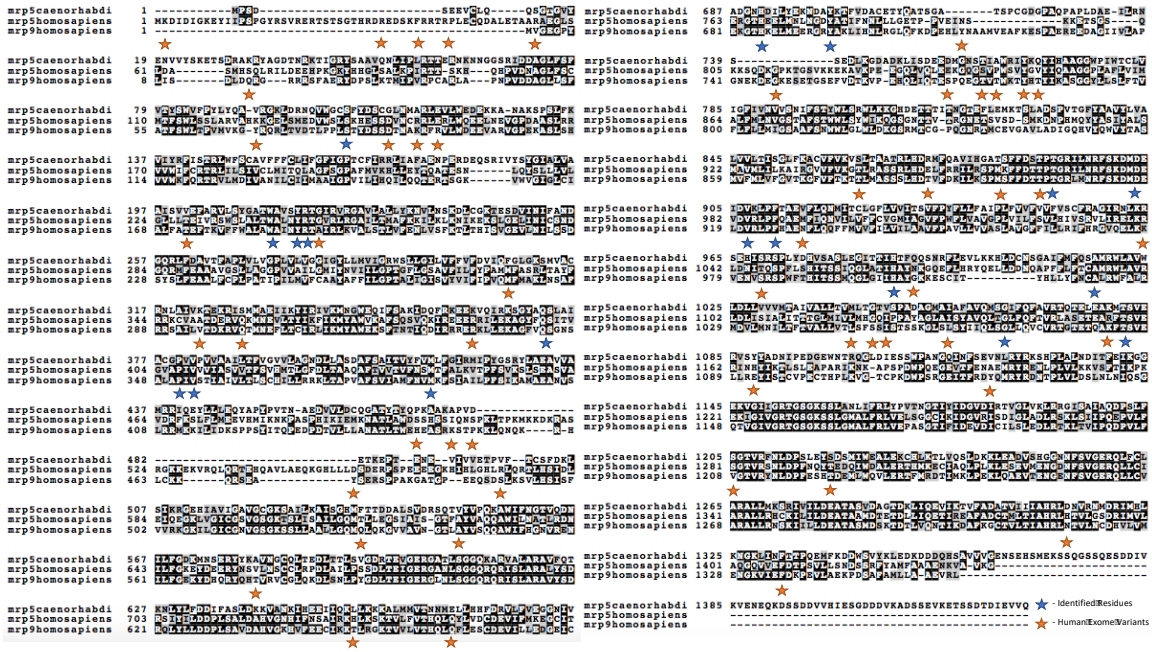

Figure 4.2 Identification of conserved residues in MRP5 and MRP9 that may be responsible for heme binding and transport

Alignment of protein sequences of *C. elegans* MRP-5, human MRP5 and human MRP9. Residues conserved in these three proteins but different in all other human ABCCs are highlighted by a blue star. Human variants identified in gnomAD database highlighted by an orange star [228].

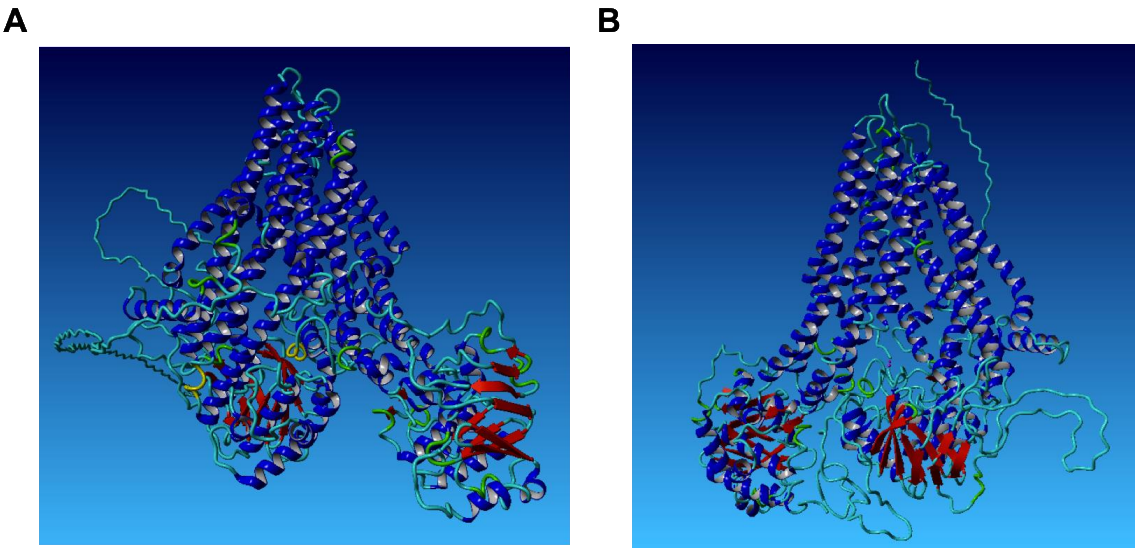

Figure 4.3 Phyre2 threaded modeling of human MRP5 and human MRP9

A) Human MRP5 and B) human MRP9 modeled with Phyre2 software utilizing 5UJA_pdb (MRP1) crystal structure file as a model [226].

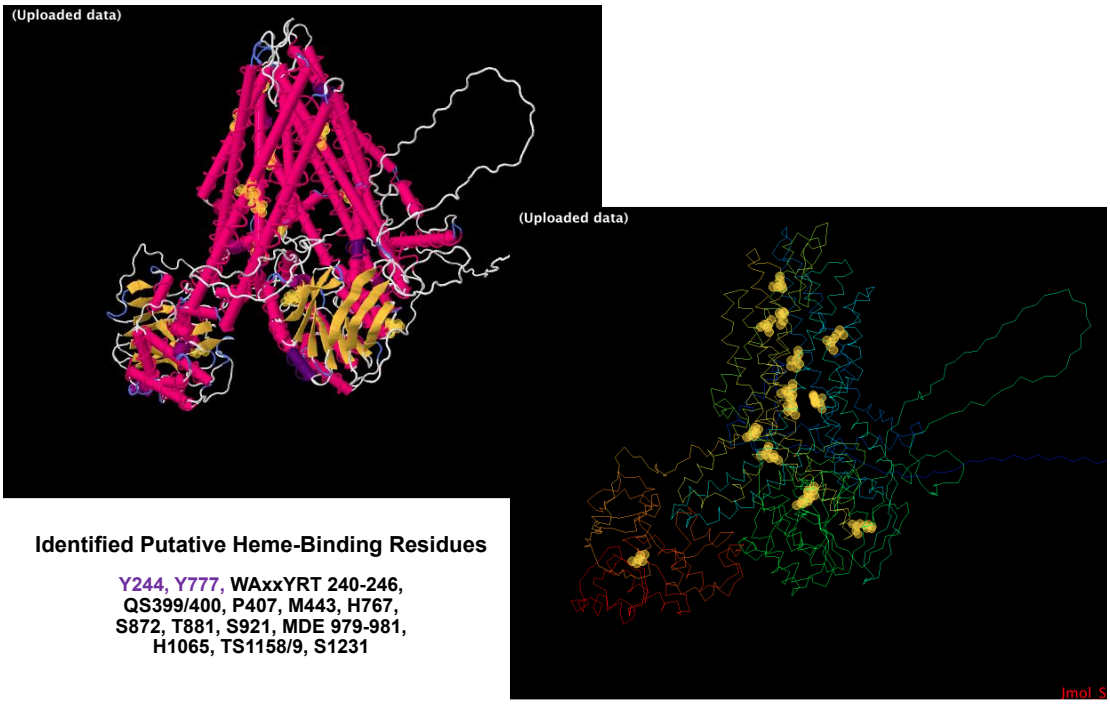

Figure 4.4 Annotation of *in silico* modeling with putative heme-binding residues demonstrating a possible mechanism for heme transport

Jmol software annotation of Phyre2 threaded modeling of human MRP5 with the putative heme-binding functional residues identified *in silico* analysis. A conceivable binding pocket and substrate channel is visible in the bundle of the transmembrane domains for transport.

4.3 Significance

As mentioned previously, ABCC proteins are one of the most well-studied class of transporters due to their critical roles in cancer biology, multidrug resistance and associated human diseases [90,229,230]. Since the generation of the MRP1 knockout mouse nearly 25 years ago, all the remaining members of this group have been ablated and characterized, save one - MRP9 [231,232]. To our knowledge, we generated the first MRP9 knockout mouse in the *ABCC12* gene. *ABCC12*$^{-/-}$ homozygous mice are surprisingly viable and fertile, demonstrating that MRP9 is dispensable in the mouse despite its high expression levels in the testes. Additionally, creation of these null animals allowed for the confirmation of MRP9's specific expression in male germ cells and the discovery of its subcellular localization, enriched in mitochondrial associated membranes. These results are unique and novel amongst ABCC transporters and sets MRP9 apart from traditional MRPs.

MRP9's closest homolog, MRP5 or ABCC5, is a conserved heme exporter that is genetically dispensable in the mouse model [82,84,233,234]. As discussed earlier, given MRP5's weak gene expression in male reproductive tissues, no studies had examined protein levels or endogenous function in the testes of mice prior to our findings [234]. To our knowledge, the only study that has probed for MRP5 in male reproductive tissues was Klein et al in their investigation of MRPs at the blood testes barrier (BTB) where they see weak signal in Leydig cells of rats but nothing in macaque or human testis [152]. Here we show for the first time that not only is MRP5 protein detectable in the testes, but that it also appears to be enriched in mitochondrial associated membranes along with MRP9. Though MRP5 still localizes to basolateral

plasma membranes in cell culture, the tissue fractionation studies bring to light the possibility of additional novel tissue dependent expression patterns and subcellular localizations for this transporter. We envision that these results may have significant implications when it comes to cancer and the roles MRP5 may play dependent upon tissue and cell type.

Though MRP5 knockout mice have no overt phenotypes, loss of the homolog *mrp-5* in *C. elegans* results in severe male reproductive deficiencies [82,107]. The hypotheses generated to explain this discrepancy revolve around the evolution of a more complex system in higher order vertebrates with redundancies in their transporters (i.e. MRP9), thus enabling them to genetically compensate for the loss of MRP5 where worms cannot. We show that the combined ablation of MRP9 and MRP5 in a mammalian system effectively recapitulates this male phenotype seen in worms, answering our original question. This finding is seminal for a number of reasons: 1) our studies show that MRP9 and MRP5 play a concerted and compensatory role in spermatogenesis and male reproductive fitness; 2) the combined loss of MRP9 and MRP5 significantly impacts metabolite profiles in the testes, which have never been measured in MRP models prior to this study; 3) the subsequent effects of this perturbation on mitochondrial homeostasis and regulatory pathways of the testes distinctly result in altered retinoic acid levels and abnormal sperm mitochondria, a first for MRPs; and 4) our results show that alterations in heme levels and corresponding EIF2a signaling are correlated with mitochondrial dysfunction and ineffective sperm maturation in the testes, similar to the canonical regulation described in erythroid cells.

Taken together, our studies fill significant gaps in our understanding of MRPs uncovering endogenous functions related to reproduction. Male infertility is a significant problem globally, affecting over 70 million people and accounting for 50% of documented issues in infertile couples [120,235,236]. To our knowledge, mutations or SNP variants of MRPs have not yet been investigated for any correlation to cases of male reproductive dysfunction. Our findings here would suggest that it is entirely possible human patients with infertility issues, typically assayed for and characterized by mitochondrial issues, may actually have hypomorphic mutations in MRP9 and MRP5.

Appendices

APPENDIX I

Appendix I – Guide RNA sequences for targeting mouse MRP9 (*ABCC12*)

GENE NAME: **Abcc12** ACCESSION: **NM_172912**	
MRP9_mouse sgRNA#1:	**5'CCAGCATCATCCACAGGATT 3'**
MRP9_mouse sgRNA#2:	**5'TTGATGTCCGATGAGTCATA 3'**

APPENDIX II

Appendix II – List of primers used for genotyping mice

Primer	Sequence
mMRP5 FWD	CTAGAGTCTAATCCGTATTGG
mMRP5 REV	CCCGCAAATACATTCAAACC
mMRP5-HYG FWD	GCTTTCAGCTTCGATGTAGG
mMRP5-HYG REV	CGTCAGGACATTGTTGGAGC
mMRP9 FWD	GGTCAGCAGCTCCTGTAG
mMRP9 REV	CTTCCTCCAGGACCCTGA

APPENDIX III

Appendix III – siRNA targets for MRP9 knockdown

Dharmacon ON-TARGETplus Non-targeting

Catalog Item
D-001810-10-05
ON-TARGETplus Non-targeting Pool

Target Sequences
UGGUUUACAUGUCGACUAA, UGGUUUACAUGUUGUGUGA, UGGUUUACAUGUUUUCUGA, UGGUUUACAUGUUUUCCUA

Dharmacon ON-TARGETplus Human GAPD

Catalog Item
D-001830-01-05
ON-TARGETplus GAPD Control siRNA (Human)

Target Sequence
GUCAACGGAUUUGGUCGUA

Dharmacon ON-TARGETplus Human ABCC12

ON-TARGETplus SMARTpool siRNA J-007310-11, ABCC12
Target Sequence: ACACAGAUUUGUAGCGUGA
Mol. Wt. 13,415.1 (g/mol) **Ext. Coeff.** 375,580 (L/mol·cm)

ON-TARGETplus SMARTpool siRNA J-007310-12, ABCC12
Target Sequence: GUGAAAGGCUACCGGCAAA
Mol. Wt. 13,445.1 (g/mol) **Ext. Coeff.** 362,675 (L/mol·cm)

ON-TARGETplus SMARTpool siRNA J-007310-13, ABCC12
Target Sequence: AGCAAUGGCUGAAGCGAAU
Mol. Wt. 13,430.1 (g/mol) **Ext. Coeff.** 367,125 (L/mol·cm)

ON-TARGETplus SMARTpool siRNA J-007310-14, ABCC12
Target Sequence: GGACAAGGGCUCACGGAUG
Mol. Wt. 13,475.1 (g/mol) **Ext. Coeff.** 356,000 (L/mol·cm)

APPENDIX IV

Appendix IV – Analysis of significantly altered GO pathways in testes RNAseq by IPA

APPENDIX V

Appendix V – Mitochondrial dysfunction gene list for motif discovery

Symbol	Pvalue	WT/DKO Ratio	DKO Expression	FOLD CHANGE
Mrps24	0.007311	2.212025	0.452074	-2.212025
Star	0.012274	1.807360	0.553293	-1.807360
Uqcr10	0.006368	1.778242	0.562353	-1.778242
Romo1	0.037401	1.720561	0.581206	-1.720561
NDUFA2	0.005986	1.670695	0.598553	-1.670695
Gstp1	0.030942	1.669271	0.599064	-1.669271
Timm10b	0.010231	1.652570	0.605118	-1.652570
Ndufs8	0.012606	1.600958	0.624626	-1.600958
Bloc1s1	0.011444	1.588472	0.629536	-1.588472
Mrpl57	0.006865	1.536930	0.650648	-1.536930
NDUFA1	0.015984	1.486440	0.672748	-1.486440
NDUFB10	0.014255	1.471231	0.679703	-1.471231
Dmpk	0.031338	1.467465	0.681447	-1.467465
Mtch1	0.011514	1.460762	0.684574	-1.460762
Arl2	0.003384	1.453082	0.688192	-1.453082
Tmem11	0.006273	1.446690	0.691233	-1.446690
Etfb	0.030848	1.443276	0.692868	-1.443276
Pfdn2	0.030832	1.442910	0.693044	-1.442910
Dynll2	0.006839	1.441672	0.693639	-1.441672
Mrpl43	0.016129	1.438276	0.695277	-1.438276
Mrpl27	0.034279	1.436233	0.696266	-1.436233
Chpf	0.007432	1.423853	0.702320	-1.423853
Atad3a	0.035732	1.408530	0.709960	-1.408530
Mrps17	0.027552	1.406383	0.711044	-1.406383
Atp5d	0.002747	1.393677	0.717526	-1.393677
Timm13	0.002046	1.393428	0.717655	-1.393428
Pet100	0.008306	1.387266	0.720842	-1.387266
Mrps34	0.004430	1.382183	0.723493	-1.382183
Dynlrb1	0.048524	1.374236	0.727677	-1.374236
Alkbh7	0.004696	1.372552	0.728570	-1.372552
D10Jhu81e	0.030112	1.369891	0.729985	-1.369891
Mrpl10	0.012984	1.360672	0.734931	-1.360672
Ndufa6	0.009791	1.356071	0.737424	-1.356071
Mrps12	0.001163	1.352640	0.739295	-1.352640
Phb	0.006290	1.339526	0.746532	-1.339526
Mrpl15	0.007645	1.329037	0.752424	-1.329037
Clpp	0.037920	1.328515	0.752720	-1.328515
Uqcrq	0.008347	1.320388	0.757353	-1.320388
Pld6	0.015832	1.314555	0.760714	-1.314555
Tomm7	0.010795	1.313724	0.761195	-1.313724
COX4I1	0.008321	1.312695	0.761791	-1.312695
Uqcc3	0.026268	1.311006	0.762773	-1.311006
Polrmt	0.015332	1.310573	0.763025	-1.310573
Timm10	0.023845	1.303774	0.767004	-1.303774
Nsun4	0.007848	1.302410	0.767807	-1.302410
Slc25a10	0.027576	1.299961	0.769254	-1.299961
Cyc1	0.029106	1.299534	0.769507	-1.299534
NDUFS7	0.005940	1.281331	0.780438	-1.281331
NDUFB9	0.021954	1.273253	0.785390	-1.273253
Dync1h1	0.025599	1.270069	0.787359	-1.270069
Atp5i	0.011836	1.269110	0.787954	-1.269110
Sod2	0.004325	1.266667	0.789474	-1.266667
Eral1	0.005083	1.257119	0.795469	-1.257119
Cisd1	0.029881	1.252505	0.798400	-1.252505
Mrpl4	0.008629	1.252408	0.798462	-1.252408
1810043G02Rik	0.006944	1.250794	0.799492	-1.250794
Trp53	0.035607	1.250604	0.799614	-1.250604
Mrpl28	0.016234	1.246020	0.802555	-1.246020
Hsdl1	0.022915	1.245294	0.803023	-1.245294
Tomm40	0.000735	1.244398	0.803602	-1.244398
Sdhc	0.025673	1.242923	0.804555	-1.242923
Apex1	0.006652	1.240433	0.806170	-1.240433
Pnkd	0.031822	1.235833	0.809171	-1.235833
Vat1	0.022305	1.235093	0.809656	-1.235093
Ptpmt1	0.013109	1.230299	0.812811	-1.230299
Wwox	0.037803	1.222736	0.817838	-1.222736
Slirp	0.024981	1.222219	0.818184	-1.222219
Cox5a	0.024062	1.215188	0.822918	-1.215188
Mrps26	0.004465	1.215053	0.823009	-1.215053
COX5B	0.015293	1.213922	0.823776	-1.213922
Slc25a25	0.017146	1.209056	0.827092	-1.209056
Cox6a1	0.048488	1.207983	0.827826	-1.207983
Gadd45gip1	0.000860	1.207160	0.828391	-1.207160
Mrpl53	0.019128	1.206578	0.828790	-1.206578
Dctn1	0.041460	1.198811	0.834160	-1.198811
Fkbp8	0.015853	1.196738	0.835605	-1.196738
Slc25a28	0.029603	1.195754	0.836292	-1.195754
Ndufa9	0.016487	1.192922	0.838278	-1.192922
Actb	0.039253	1.192746	0.838402	-1.192746
Prelid1	0.018998	1.186199	0.843029	-1.186199
Mrpl55	0.003102	1.180960	0.846769	-1.180960
Mul1	0.014442	1.180087	0.847395	-1.180087
Idh3b	0.046233	1.179408	0.847883	-1.179408
Hagh	0.022698	1.174774	0.851228	-1.174774
Gfer	0.042695	1.173201	0.852369	-1.173201
Fh1	0.040449	1.172588	0.852814	-1.172588
Coa6	0.006239	1.166986	0.856908	-1.166986
Ndufs6	0.009105	1.166164	0.857512	-1.166164
Slc35f6	0.034653	1.165897	0.857708	-1.165897
Mpg	0.004640	1.162254	0.860397	-1.162254
Pacs2	0.021823	1.160243	0.861889	-1.160243
Txn2	0.011444	1.158865	0.862913	-1.158865
NDUFB8	0.006869	1.155148	0.865690	-1.155148
Dynll1	0.044696	1.154744	0.865993	-1.154744
Pi4kb	0.046528	1.153946	0.866592	-1.153946
Bad	0.017330	1.153214	0.867142	-1.153214
NDUFA4L2	0.009957	1.152850	0.867415	-1.152850
Park7	0.016380	1.151062	0.868763	-1.151062
Chchd6	0.012215	1.148496	0.870704	-1.148496
Slc25a33	0.007460	1.148184	0.870940	-1.148184
Glyctk	0.031214	1.146067	0.872549	-1.146067
Crat	0.026588	1.140132	0.877092	-1.140132
2410015M20Rik	0.042824	1.137759	0.878921	-1.137759
Stk11	0.035015	1.136760	0.879693	-1.136760
Nt5m	0.014062	1.136714	0.879729	-1.136714
Coa4	0.046681	1.135989	0.880290	-1.135989
Elac2	0.032174	1.135616	0.880579	-1.135616
Atpaf2	0.034650	1.131782	0.883563	-1.131782
Mcat	0.027229	1.129877	0.885052	-1.129877
Ak2	0.004192	1.128570	0.886077	-1.128570
Ndufaf3	0.032340	1.128551	0.886092	-1.128551
Letm1	0.028232	1.121121	0.891964	-1.121121
Tbrg4	0.003951	1.114512	0.897254	-1.114512
ATP5O	0.024665	1.111592	0.899611	-1.111592
Pgs1	0.030770	1.104036	0.905768	-1.104036
Spg7	0.018281	1.092047	0.915712	-1.092047
Mtch2	0.015264	1.082329	0.923934	-1.082329
Mapk10	0.003230	1.081951	0.924256	-1.081951
Ppa2	0.037764	1.081145	0.924945	-1.081145
NDUFV2	0.037911	1.080197	0.925757	-1.080197
Chchd7	0.024313	1.072418	0.932472	-1.072418
Atg4d	0.044079	1.069289	0.935201	-1.069289

Symbol	Pvalue	WT/DKO Ratio	DKO Expression	FOLD CHANGE
2010107E04Rik	0.011523	0.581138	1.720762	1.720762
Cox20	0.042471	0.603869	1.655987	1.655987
Apoo	0.028511	0.654119	1.528775	1.528775
Coq10b	0.015861	0.672936	1.486026	1.486026
Vrk2	0.015305	0.686173	1.457359	1.457359
Fez1	0.023478	0.716864	1.394965	1.394965
Abcg2	0.027597	0.726659	1.376162	1.376162
Pdk3	0.019202	0.728919	1.371894	1.371894
Mrpl47	0.020857	0.739072	1.353048	1.353048
Mrps31	0.019568	0.743902	1.344262	1.344262
Vdac3	0.019720	0.756524	1.321836	1.321836
Ranbp2	0.033326	0.757848	1.319527	1.319527
COX7B2	0.016821	0.759822	1.316098	1.316098
Mtpap	0.017700	0.760382	1.315129	1.315129
Mterf3	0.011514	0.760930	1.314182	1.314182
Acsl5	0.029890	0.761134	1.313829	1.313829
Tfam	0.012518	0.761317	1.313513	1.313513
Mrpl33	0.009913	0.761458	1.313270	1.313270
Cabs1	0.035717	0.762110	1.312146	1.312146
Dld	0.014629	0.762338	1.311754	1.311754
Mrpl32	0.037341	0.771303	1.296507	1.296507
Tomm20l	0.048495	0.771313	1.296491	1.296491
Cycs	0.022821	0.779026	1.283654	1.283654
Mrps18c	0.031776	0.786878	1.270844	1.270844
Sucla2	0.017986	0.790722	1.264668	1.264668
9430016H08Rik	0.028534	0.794057	1.259355	1.259355
Ccdc90b	0.043636	0.794850	1.258099	1.258099
Slc25a31	0.024196	0.796712	1.255158	1.255158
Isca2	0.032880	0.798093	1.252986	1.252986
Mtif2	0.047270	0.798649	1.252115	1.252115
Osgepl1	0.023030	0.804129	1.243582	1.243582
Mpc2	0.018944	0.806231	1.240340	1.240340
Mrpl54	0.011780	0.810775	1.233388	1.233388
Mrpl1	0.016364	0.814430	1.227853	1.227853
Rhot1	0.046659	0.815977	1.225525	1.225525
Slc25a37	0.003204	0.817304	1.223535	1.223535
Actr10	0.019327	0.819625	1.220069	1.220069
Ndufc1	0.022754	0.821787	1.216860	1.216860
Dnaja1	0.022703	0.823324	1.214588	1.214588
Ghitm	0.040918	0.830038	1.204765	1.204765
Acot9	0.032083	0.831763	1.202268	1.202268
Clpx	0.035216	0.832797	1.200772	1.200772
Gk2	0.017916	0.833052	1.200405	1.200405
Cbr4	0.006576	0.834123	1.198865	1.198865
Tdrkh	0.003821	0.835742	1.196541	1.196541
Hadhb	0.025870	0.839687	1.190920	1.190920
Mrpl45	0.039604	0.845137	1.183241	1.183241
Capza1	0.006612	0.847371	1.180121	1.180121
Agtpbp1	0.002504	0.847537	1.179889	1.179889
Lzhgdh	0.040125	0.848375	1.178725	1.178725
Ppp2r2b	0.024667	0.850016	1.176448	1.176448
Sqrdl	0.019417	0.852274	1.173331	1.173331
Tomm22	0.030449	0.858460	1.164876	1.164876
Lias	0.019329	0.862654	1.159213	1.159213
Mrps5	0.009885	0.863777	1.157707	1.157707
Dlat	0.042672	0.864633	1.156560	1.156560
Akap10	0.046565	0.864692	1.156481	1.156481
Adcy10	0.021335	0.866695	1.153808	1.153808
Mrpl48	0.045793	0.868364	1.151590	1.151590
Efhd1	0.007221	0.872922	1.145577	1.145577
Usp8	0.031141	0.873806	1.144419	1.144419
Spata5	0.003151	0.878884	1.137807	1.137807
Mfn1	0.035581	0.879304	1.137263	1.137263
ATP5C1	0.048857	0.879571	1.136918	1.136918
Letm2	0.019099	0.882217	1.133508	1.133508
Rnf144b	0.029618	0.883361	1.132040	1.132040
Uqcrc2	0.013755	0.886973	1.127430	1.127430
Dap3	0.035951	0.889750	1.123911	1.123911
Afg3l1	0.005996	0.894020	1.118543	1.118543
Sord	0.024857	0.900567	1.110412	1.110412
Gatc	0.015670	0.901560	1.109188	1.109188
Dync1li2	0.026768	0.901828	1.108858	1.108858
Pdhb	0.047660	0.908402	1.100834	1.100834
Immt	0.032490	0.912639	1.095723	1.095723
Mief1	0.000359	0.912993	1.095298	1.095298
Hax1	0.030241	0.913864	1.094255	1.094255
Cox16	0.040139	0.914506	1.093487	1.093487
Mrps22	0.034107	0.917752	1.089619	1.089619

Bibliography

1. Sassa, S.: Why heme needs to be degraded to iron, biliverdin IXalpha, and carbon monoxide? *Antioxid Redox Signal* 2004, 6(5):819-24.[PMID:15345141]
2. Reedy, C. J., and Gibney, B. R.: Heme protein assemblies. *Chem Rev* 2004, 104(2):617-49.[PMID:14871137]
3. Kumar, S., and Bandyopadhyay, U.: Free heme toxicity and its detoxification systems in human. *Toxicol Lett* 2005, 157(3):175-88.[PMID:15917143]
4. Severance, S., and Hamza, I.: Trafficking of heme and porphyrins in metazoa. *Chem Rev* 2009, 109(10):4596-616.[PMID:19764719]
5. Hamza, I., and Dailey, H. A.: One ring to rule them all: trafficking of heme and heme synthesis intermediates in the metazoans. *Biochim Biophys Acta* 2012, 1823(9):1617-32.[PMID:22575458]
6. Chiabrando, D., Vinchi, F., Fiorito, V., Mercurio, S., and Tolosano, E.: Heme in pathophysiology: a matter of scavenging, metabolism and trafficking across cell membranes. *Front Pharmacol* 2014, 5:61.[PMID:24782769]
7. Poulos, T. L.: Heme Enzyme Structure and Function. *Chemical Reviews* 2014, 114(7):3919-3962.[PMID:24400737]
8. Reddi, A. R., and Hamza, I.: Heme Mobilization in Animals: A Metallolipid's Journey. *Accounts of Chemical Research* 2016, 49(6):1104-1110
9. Chiabrando, D., Fiorito, V., Petrillo, S., and Tolosano, E.: Unraveling the Role of Heme in Neurodegeneration. *Front Neurosci* 2018, 12:712.[PMID:30356807]
10. Korolnek, T., and Hamza, I.: Like iron in the blood of the people: the requirement for heme trafficking in iron metabolism. *Front Pharmacol* 2014, 5:126.[PMID:24926267]
11. Ponka, P.: Cell biology of heme. *Am J Med Sci* 1999, 318(4):241-56.[PMID:10522552]
12. Tsiftsoglou, A. S., Tsamadou, A. I., and Papadopoulou, L. C.: Heme as key regulator of major mammalian cellular functions: molecular, cellular, and pharmacological aspects. *Pharmacol Ther* 2006, 111(2):327-45.[PMID:16513178]
13. Faller, M., Matsunaga, M., Yin, S., Loo, J. A., and Guo, F.: Heme is involved in microRNA processing. *Nat Struct Mol Biol* 2007, 14(1):23-9.[PMID:17159994]
14. Yin, L., Wu, N., Curtin, J. C., Qatanani, M., Szwergold, N. R., Reid, R. A., Waitt, G. M., Parks, D. J., Pearce, K. H., Wisely, G. B., and Lazar, M. A.: Rev-erbalpha, a heme sensor that coordinates metabolic and circadian pathways. *Science* 2007, 318(5857):1786-9.[PMID:18006707]
15. Mense, S. M., and Zhang, L.: Heme: a versatile signaling molecule controlling the activities of diverse regulators ranging from transcription factors to MAP kinases. *Cell Res* 2006, 16(8):681-92.[PMID:16894358]

16. Reddi, A. R., and Hamza, I.: Heme Mobilization in Animals: A Metallolipid's Journey. *Acc Chem Res* 2016, 49(6):1104-10.[PMID:27254265]
17. Hanna, D. A., Martinez-Guzman, O., and Reddi, A. R.: Heme Gazing: Illuminating Eukaryotic Heme Trafficking, Dynamics, and Signaling with Fluorescent Heme Sensors. *Biochemistry* 2017, 56(13):1815-1823
18. Shimizu, T., Lengalova, A., Martínek, V., and Martínková, M.: Heme: emergent roles of heme in signal transduction, functional regulation and as catalytic centres. *Chem Soc Rev* 2019, 48(24):5624-5657.[PMID:31748766]
19. Donegan, R. K., Moore, C. M., Hanna, D. A., and Reddi, A. R.: Handling heme: The mechanisms underlying the movement of heme within and between cells. *Free Radic Biol Med* 2019, 133:88-100.[PMID:30092350]
20. Zhang, L. (2020) Heme Biology. Heme Biology
21. Pradhan, P., Vijayan, V., Gueler, F., and Immenschuh, S.: Interplay of Heme with Macrophages in Homeostasis and Inflammation. *International Journal of Molecular Sciences* 2020, 21(3):740.[PMID:doi:10.3390/ijms21030740]
22. Woldt, E., Sebti, Y., Solt, L. A., Duhem, C., Lancel, S., Eeckhoute, J., Hesselink, M. K., Paquet, C., Delhaye, S., Shin, Y., Kamenecka, T. M., Schaart, G., Lefebvre, P., Neviere, R., Burris, T. P., Schrauwen, P., Staels, B., and Duez, H.: Rev-erb-alpha modulates skeletal muscle oxidative capacity by regulating mitochondrial biogenesis and autophagy. *Nat Med* 2013, 19(8):1039-46.[PMID:23852339]
23. Wu, N., Yin, L., Hanniman, E. A., Joshi, S., and Lazar, M. A.: Negative feedback maintenance of heme homeostasis by its receptor, Rev-erbalpha. *Genes Dev* 2009, 23(18):2201-9.[PMID:19710360]
24. Matoba, S., Kang, J. G., Patino, W. D., Wragg, A., Boehm, M., Gavrilova, O., Hurley, P. J., Bunz, F., and Hwang, P. M.: p53 regulates mitochondrial respiration. *Science* 2006, 312(5780):1650-3.[PMID:16728594]
25. Dohi, Y., Ikura, T., Hoshikawa, Y., Katoh, Y., Ota, K., Nakanome, A., Muto, A., Omura, S., Ohta, T., Ito, A., Yoshida, M., Noda, T., and Igarashi, K.: Bach1 inhibits oxidative stress-induced cellular senescence by impeding p53 function on chromatin. *Nat Struct Mol Biol* 2008, 15(12):1246-54.[PMID:19011633]
26. Pfeifer, K., Kim, K. S., Kogan, S., and Guarente, L.: Functional dissection and sequence of yeast HAP1 activator. *Cell* 1989, 56(2):291-301.[PMID:2643482]
27. Zhang, L., and Guarente, L.: Heme binds to a short sequence that serves a regulatory function in diverse proteins. *EMBO J* 1995, 14(2):313-20.[PMID:7835342]
28. Igarashi, K., and Sun, J.: The heme-Bach1 pathway in the regulation of oxidative stress response and erythroid differentiation. *Antioxid Redox Signal* 2006, 8(1-2):107-18.[PMID:16487043]
29. Ogawa, K., Sun, J., Taketani, S., Nakajima, O., Nishitani, C., Sassa, S., Hayashi, N., Yamamoto, M., Shibahara, S., Fujita, H., and Igarashi, K.: Heme mediates derepression of Maf recognition element through direct binding to transcription repressor Bach1. *EMBO J* 2001, 20(11):2835-43.[PMID:11387216]

30. Shen, J., Sheng, X., Chang, Z., Wu, Q., Wang, S., Xuan, Z., Li, D., Wu, Y., Shang, Y., Kong, X., Yu, L., Li, L., Ruan, K., Hu, H., Huang, Y., Hui, L., Xie, D., Wang, F., and Hu, R.: Iron metabolism regulates p53 signaling through direct heme-p53 interaction and modulation of p53 localization, stability, and function. *Cell Rep* 2014, 7(1):180-93.[PMID:24685134]
31. Raghuram, S., Stayrook, K. R., Huang, P., Rogers, P. M., Nosie, A. K., McClure, D. B., Burris, L. L., Khorasanizadeh, S., Burris, T. P., and Rastinejad, F.: Identification of heme as the ligand for the orphan nuclear receptors REV-ERBalpha and REV-ERBbeta. *Nat Struct Mol Biol* 2007, 14(12):1207-13.[PMID:18037887]
32. Burton, M. J., Kapetanaki, S. M., Chernova, T., Jamieson, A. G., Dorlet, P., Santolini, J., Moody, P. C., Mitcheson, J. S., Davies, N. W., Schmid, R., Raven, E. L., and Storey, N. M.: A heme-binding domain controls regulation of ATP-dependent potassium channels. *Proc Natl Acad Sci U S A* 2016, 113(14):3785-90.[PMID:27006498]
33. Barr, I., Smith, A. T., Chen, Y., Senturia, R., Burstyn, J. N., and Guo, F.: Ferric, not ferrous, heme activates RNA-binding protein DGCR8 for primary microRNA processing. *Proc Natl Acad Sci U S A* 2012, 109(6):1919-24.[PMID:22308374]
34. Quick-Cleveland, J., Jacob, J. P., Weitz, S. H., Shoffner, G., Senturia, R., and Guo, F.: The DGCR8 RNA-binding heme domain recognizes primary microRNAs by clamping the hairpin. *Cell Rep* 2014, 7(6):1994-2005.[PMID:24910438]
35. Weitz, S. H., Gong, M., Barr, I., Weiss, S., and Guo, F.: Processing of microRNA primary transcripts requires heme in mammalian cells. *Proc Natl Acad Sci U S A* 2014, 111(5):1861-6.[PMID:24449907]
36. Barrientos, A., Zambrano, A., and Tzagoloff, A.: Mss51p and Cox14p jointly regulate mitochondrial Cox1p expression in Saccharomyces cerevisiae. *EMBO J* 2004, 23(17):3472-82.[PMID:15306853]
37. Fontanesi, F., Soto, I. C., Horn, D., and Barrientos, A.: Mss51 and Ssc1 facilitate translational regulation of cytochrome c oxidase biogenesis. *Mol Cell Biol* 2010, 30(1):245-59.[PMID:19858289]
38. Ryter, S. W., and Tyrrell, R. M.: The heme synthesis and degradation pathways: role in oxidant sensitivity: Heme oxygenase has both pro- and antioxidant properties. *Free Radical Biology and Medicine* 2000, 28(2):289-309
39. Ajioka, R. S., Phillips, J. D., and Kushner, J. P.: Biosynthesis of heme in mammals. *Biochimica et Biophysica Acta (BBA) - Molecular Cell Research* 2006, 1763(7):723-736
40. Bonkovsky, H. L., Guo, J. T., Hou, W., Li, T., Narang, T., and Thapar, M.: Porphyrin and heme metabolism and the porphyrias. *Compr Physiol* 2013, 3(1):365-401.[PMID:23720291]
41. Sun, F., Cheng, Y., and Chen, C.: Regulation of heme biosynthesis and transport in metazoa. *Science China Life Sciences* 2015, 58(8):757-764

42. Swenson, S. A., Moore, C. M., Marcero, J. R., Medlock, A. E., Reddi, A. R., and Khalimonchuk, O.: From Synthesis to Utilization: The Ins and Outs of Mitochondrial Heme. *Cells* 2020, 9(3):579
43. Bianchetti, C. M., Yi, L., Ragsdale, S. W., and Phillips, G. N., Jr.: Comparison of apo- and heme-bound crystal structures of a truncated human heme oxygenase-2. *J Biol Chem* 2007, 282(52):37624-31.[PMID:17965015]
44. Schuller, D. J., Wilks, A., Ortiz de Montellano, P. R., and Poulos, T. L.: Crystal structure of human heme oxygenase-1. *Nat Struct Biol* 1999, 6(9):860-7.[PMID:10467099]
45. Unno, M., Matsui, T., and Ikeda-Saito, M.: Crystallographic studies of heme oxygenase complexed with an unstable reaction intermediate, verdoheme. *J Inorg Biochem* 2012, 113:102-9.[PMID:22673156]
46. Ajioka, R. S., Phillips, J. D., and Kushner, J. P.: Biosynthesis of heme in mammals. *Biochim Biophys Acta* 2006, 1763(7):723-36.[PMID:16839620]
47. Hamza, I.: Intracellular Trafficking of Porphyrins. *ACS Chemical Biology* 2006, 1(10):627-629
48. Schultz, I. J., Chen, C., Paw, B. H., and Hamza, I.: Iron and porphyrin trafficking in heme biogenesis. *J Biol Chem* 2010, 285(35):26753-9.[PMID:20522548]
49. Yuan, X., Fleming, M. D., and Hamza, I.: Heme transport and erythropoiesis. *Current Opinion in Chemical Biology* 2013, 17(2):204-211
50. Balla, G., Vercellotti, G. M., Muller-Eberhard, U., Eaton, J., and Jacob, H. S.: Exposure of endothelial cells to free heme potentiates damage mediated by granulocytes and toxic oxygen species. *Lab Invest* 1991, 64(5):648-55.[PMID:2030579]
51. Jeney, V., Balla, J., Yachie, A., Varga, Z., Vercellotti, G. M., Eaton, J. W., and Balla, G.: Pro-oxidant and cytotoxic effects of circulating heme. *Blood* 2002, 100(3):879-887
52. Donegan, R. K., Moore, C. M., Hanna, D. A., and Reddi, A. R.: Handling heme: The mechanisms underlying the movement of heme within and between cells. *Free Radical Biology and Medicine* 2019, 133:88-100
53. Bunn, H. F., and Jandl, J. H.: Exchange of heme among hemoglobins and between hemoglobin and albumin. *J Biol Chem* 1968, 243(3):465-75.[PMID:4966113]
54. Halliwell, B., and Gutteridge, J. M. C.: The antioxidants of human extracellular fluids. *Archives of Biochemistry and Biophysics* 1990, 280(1):1-8
55. Vercellotti, G. M., Balla, G., Balla, J., Nath, K., Eaton, J. W., and Jacob, H. S.: Heme and the vasculature: an oxidative hazard that induces antioxidant defenses in the endothelium. *Artif Cells Blood Substit Immobil Biotechnol* 1994, 22(2):207-13.[PMID:8087243]
56. Kumar, S., and Bandyopadhyay, U.: Free heme toxicity and its detoxification systems in human. *Toxicology Letters* 2005, 157(3):175-188
57. Fibach, E., and Rachmilewitz, E.: The role of oxidative stress in hemolytic anemia. *Curr Mol Med* 2008, 8(7):609-19.[PMID:18991647]
58. Dutra, F. F., Alves, L. S., Rodrigues, D., Fernandez, P. L., De Oliveira, R. B., Golenbock, D. T., Zamboni, D. S., and Bozza, M. T.: Hemolysis-induced

lethality involves inflammasome activation by heme. *Proceedings of the National Academy of Sciences* 2014, 111(39):E4110-E4118
59. Bratosin, D., Mazurier, J., Tissier, J. P., Estaquier, J., Huart, J. J., Ameisen, J. C., Aminoff, D., and Montreuil, J.: Cellular and molecular mechanisms of senescent erythrocyte phagocytosis by macrophages. A review. *Biochimie* 1998, 80(2):173-95.[PMID:9587675]
60. Knutson, M., and Wessling-Resnick, M.: Iron Metabolism in the Reticuloendothelial System. *Critical Reviews in Biochemistry and Molecular Biology* 2003, 38(1):61-88
61. Ganz, T.: Macrophages and Systemic Iron Homeostasis. *Journal of Innate Immunity* 2012, 4(5-6):446-453
62. Klei, T. R. L., Meinderts, S. M., Van Den Berg, T. K., and Van Bruggen, R.: From the Cradle to the Grave: The Role of Macrophages in Erythropoiesis and Erythrophagocytosis. *Frontiers in Immunology* 2017, 8
63. Knutson, M. D., Vafa, M. R., Haile, D. J., and Wessling-Resnick, M.: Iron loading and erythrophagocytosis increase ferroportin 1 (FPN1) expression in J774 macrophages. *Blood* 2003, 102(12):4191-7.[PMID:12907459]
64. Knutson, M. D., Oukka, M., Koss, L. M., Aydemir, F., and Wessling-Resnick, M.: Iron release from macrophages after erythrophagocytosis is up-regulated by ferroportin 1 overexpression and down-regulated by hepcidin. *Proceedings of the National Academy of Sciences* 2005, 102(5):1324-1328
65. Delaby, C., Pilard, N., Hetet, G., Driss, F., Grandchamp, B., Beaumont, C., and Canonne-Hergaux, F.: A physiological model to study iron recycling in macrophages. *Exp Cell Res* 2005, 310(1):43-53.[PMID:16095591]
66. Winter, W. E., Bazydlo, L. A. L., and Harris, N. S.: The Molecular Biology of Human Iron Metabolism. *Laboratory Medicine* 2014, 45(2):92-102
67. Yoshida, T., and Sato, M.: Posttranslational and direct integration of heme oxygenase into microsomes. *Biochem Biophys Res Commun* 1989, 163(2):1086-92.[PMID:2783112]
68. Yanatori, I., Tabuchi, M., Kawai, Y., Yasui, Y., Akagi, R., and Kishi, F.: Heme and non-heme iron transporters in non-polarized and polarized cells. *BMC Cell Biology* 2010, 11(1):39
69. Gottlieb, Y., Truman, M., Cohen, L. A., Leichtmann-Bardoogo, Y., and Meyron-Holtz, E. G.: Endoplasmic reticulum anchored heme-oxygenase 1 faces the cytosol. *Haematologica* 2012, 97(10):1489-1493
70. White, C., Yuan, X., Paul, Bresciani, E., Tamika, Campagna, D., Hall, C., Bishop, K., Monica, Lapierre, A., Diane, Liu, P., Mark, and Hamza, I.: HRG1 Is Essential for Heme Transport from the Phagolysosome of Macrophages during Erythrophagocytosis. *Cell Metabolism* 2013, 17(2):261-270
71. Ponka, P., Sheftel, A. D., English, A. M., Scott Bohle, D., and Garcia-Santos, D.: Do Mammalian Cells Really Need to Export and Import Heme? *Trends in Biochemical Sciences* 2017, 42(5):395-406
72. Rao, A. U., Carta, L. K., Lesuisse, E., and Hamza, I.: Lack of heme synthesis in a free-living eukaryote. *Proceedings of the National Academy of Sciences* 2005, 102(12):4270-4275

73. Chung, J., Chen, C., and Paw, B. H.: Heme Metabolism and Erythropoiesis. *Curr Opin Hematol* 2012, 19(3):156-62.[PMID:22406824]
74. Sinclair, J., and Hamza, I.: Lessons from bloodless worms: heme homeostasis in C. elegans. *Biometals* 2015, 28(3):481-9.[PMID:25724951]
75. Pek, R. H., Yuan, X., Rietzschel, N., Zhang, J., Jackson, L., Nishibori, E., Ribeiro, A., Simmons, W., Jagadeesh, J., Sugimoto, H., Alam, M. Z., Garrett, L., Haldar, M., Ralle, M., Phillips, J. D., Bodine, D. M., and Hamza, I.: Hemozoin produced by mammals confers heme tolerance. *eLife* 2019, 8
76. Chiabrando, D., Mercurio, S., and Tolosano, E.: Heme and erythropoieis: more than a structural role. *Haematologica* 2014, 99(6):973-83.[PMID:24881043]
77. Chiabrando, D., Bertino, F., and Tolosano, E.: Hereditary Ataxia: A Focus on Heme Metabolism and Fe-S Cluster Biogenesis. *Int J Mol Sci* 2020, 21(11).[PMID:32466579]
78. Chambers, I. G., Willoughby, M. M., Hamza, I., and Reddi, A. R.: One ring to bring them all and in the darkness bind them: The trafficking of heme without deliverers. *Biochim Biophys Acta Mol Cell Res* 2021, 1868(1):118881.[PMID:33022276]
79. Rajagopal, A., Rao, A. U., Amigo, J., Tian, M., Upadhyay, S. K., Hall, C., Uhm, S., Mathew, M. K., Fleming, M. D., Paw, B. H., Krause, M., and Hamza, I.: Haem homeostasis is regulated by the conserved and concerted functions of HRG-1 proteins. *Nature* 2008, 453(7198):1127-31.[PMID:18418376]
80. Zhang, J., Chambers, I., Yun, S., Phillips, J., Krause, M., and Hamza, I.: Hrg1 promotes heme-iron recycling during hemolysis in the zebrafish kidney. *PLOS Genetics* 2018, 14(9):e1007665
81. Zhang, J., and Hamza, I.: Zebrafish as a model system to delineate the role of heme and iron metabolism during erythropoiesis. *Molecular Genetics and Metabolism* 2019, 128(3):204-212
82. Korolnek, T., Zhang, J., Beardsley, S., Scheffer, G. L., and Hamza, I.: Control of metazoan heme homeostasis by a conserved multidrug resistance protein. *Cell Metab* 2014, 19(6):1008-19.[PMID:24836561]
83. Yuan, X., Rietzschel, N., Kwon, H., Walter Nuno, A. B., Hanna, D. A., Phillips, J. D., Raven, E. L., Reddi, A. R., and Hamza, I.: Regulation of intracellular heme trafficking revealed by subcellular reporters. *Proc Natl Acad Sci U S A* 2016, 113(35):E5144-52.[PMID:27528661]
84. Jedlitschky, G., Burchell, B., and Keppler, D.: The Multidrug Resistance Protein 5 Functions as an ATP-dependent Export Pump for Cyclic Nucleotides. *Journal of Biological Chemistry* 2000, 275(39):30069-30074
85. Jones, P. M., and George, A. M.: The ABC transporter structure and mechanism: perspectives on recent research. *Cellular and Molecular Life Sciences CMLS* 2004, 61(6):682-699
86. Fath, M. J., and Kolter, R.: ABC transporters: bacterial exporters. *Microbiological Reviews* 1993, 57(4):995-1017
87. Lee, J.-Y., and Rosenbaum, D. M.: Transporters Revealed. *Cell* 2017, 168(6):951-953

88. Kool, M., de Haas, M., Scheffer, G. L., Scheper, R. J., van Eijk, M. J., Juijn, J. A., Baas, F., and Borst, P.: Analysis of expression of cMOAT (MRP2), MRP3, MRP4, and MRP5, homologues of the multidrug resistance-associated protein gene (MRP1), in human cancer cell lines. *Cancer Res* 1997, 57(16):3537-47.[PMID:9270026]
89. McAleer, M. A., Breen, M. A., White, N. L., and Matthews, N.: pABC11 (Also Known as MOAT-C and MRP5), a Member of the ABC Family of Proteins, Has Anion Transporter Activity but Does Not Confer Multidrug Resistance When Overexpressed in Human Embryonic Kidney 293 Cells. *Journal of Biological Chemistry* 1999, 274(33):23541-23548
90. Borst, P., Evers, R., Kool, M., and Wijnholds, J.: A family of drug transporters: the multidrug resistance-associated proteins. *J Natl Cancer Inst* 2000, 92(16):1295-302.[PMID:10944550]
91. Slot, A. J., Molinski, S. V., and Cole, S. P.: Mammalian multidrug-resistance proteins (MRPs). *Essays Biochem* 2011, 50(1):179-207.[PMID:21967058]
92. Cole, S., Bhardwaj, G., Gerlach, J., Mackie, J., Grant, C., Almquist, K., Stewart, A., Kurz, E., Duncan, A., and Deeley, R.: Overexpression of a transporter gene in a multidrug-resistant human lung cancer cell line. *Science* 1992, 258(5088):1650-1654
93. Cole, S. P. C.: Targeting Multidrug Resistance Protein 1 (MRP1, ABCC1): Past, Present, and Future. *Annual Review of Pharmacology and Toxicology* 2014, 54(1):95-117.[PMID:24050699]
94. Saitou, N., and Nei, M.: The neighbor-joining method: a new method for reconstructing phylogenetic trees. *Molecular Biology and Evolution* 1987, 4(4):406-425
95. Zuckerkandl, E., and Pauling, L. (1965) Evolutionary Divergence and Convergence in Proteins. 97-166. Evolving Genes and Proteins. Edited by Bryson, V., and Vogel, H. J., Academic Press
96. Kumar, S., Stecher, G., Li, M., Knyaz, C., and Tamura, K.: MEGA X: Molecular Evolutionary Genetics Analysis across Computing Platforms. *Molecular biology and evolution* 2018, 35(6):1547-1549.[PMID:29722887]
97. Stecher, G., Tamura, K., and Kumar, S.: Molecular Evolutionary Genetics Analysis (MEGA) for macOS. *Mol Biol Evol* 2020, 37(4):1237-1239.[PMID:31904846]
98. Ritter, C. A., Jedlitschky, G., Meyer zu Schwabedissen, H., Grube, M., Kock, K., and Kroemer, H. K.: Cellular export of drugs and signaling molecules by the ATP-binding cassette transporters MRP4 (ABCC4) and MRP5 (ABCC5). *Drug Metab Rev* 2005, 37(1):253-78.[PMID:15747503]
99. Deeley, R. G., Westlake, C., and Cole, S. P.: Transmembrane transport of endo- and xenobiotics by mammalian ATP-binding cassette multidrug resistance proteins. *Physiol Rev* 2006, 86(3):849-99.[PMID:16816140]
100. Wang, L., Johnson, Z. L., Wasserman, M. R., Levring, J., Chen, J., and Liu, S.: Characterization of the kinetic cycle of an ABC transporter by single-molecule and cryo-EM analyses. *eLife* 2020, 9
101. Johnson, Z. L., and Chen, J.: Structural Basis of Substrate Recognition by the Multidrug Resistance Protein MRP1. *Cell* 2017, 168(6):1075-1085.e9

102. Severance, S., Rajagopal, A., Rao, A. U., Cerqueira, G. C., Mitreva, M., El-Sayed, N. M., Krause, M., and Hamza, I.: Genome-Wide Analysis Reveals Novel Genes Essential for Heme Homeostasis in Caenorhabditis elegans. *PLoS Genetics* 2010, 6(7):e1001044
103. Sinclair, J., and Hamza, I.: A Novel Heme-responsive Element Mediates Transcriptional Regulation inCaenorhabditis elegans. *Journal of Biological Chemistry* 2010, 285(50):39536-39543
104. Jedlitschky, G., Burchell, B., and Keppler, D.: The multidrug resistance protein 5 functions as an ATP-dependent export pump for cyclic nucleotides. *J Biol Chem* 2000, 275(39):30069-74.[PMID:10893247]
105. Jansen, R. S., Mahakena, S., de Haas, M., Borst, P., and van de Wetering, K.: ATP-binding Cassette Subfamily C Member 5 (ABCC5) Functions as an Efflux Transporter of Glutamate Conjugates and Analogs. *J Biol Chem* 2015, 290(51):30429-40.[PMID:26515061]
106. Reid, G., Wielinga, P., Zelcer, N., de Haas, M., van Deemter, L., Wijnholds, J., Balzarini, J., and Borst, P.: Characterization of the Transport of Nucleoside Analog Drugs by the Human Multidrug Resistance Proteins MRP4 and MRP5. *Molecular Pharmacology* 2003, 63(5):1094-1103
107. Beardsley, S.: Genetic Suppressors of mrp-5 Lethality in C. elegans. 2016,
108. Hodgkin, J.: Male Phenotypes and Mating Efficiency in CAENORHABDITIS ELEGANS. *Genetics* 1983, 103(1):43-64.[PMID:17246100]
109. Sherlekar, A. L., and Lints, R.: Nematode Tango Milonguero - the C. elegans male's search for the hermaphrodite vulva. *Semin Cell Dev Biol* 2014, 33:34-41.[PMID:24862858]
110. Sarkadi, B., Müller, M., and Holló, Z.: The multidrug transporters—proteins of an ancient immune system. *Immunology Letters* 1996, 54(2):215-219
111. Holland, I. B., and A. Blight, M.: ABC-ATPases, adaptable energy generators fuelling transmembrane movement of a variety of molecules in organisms from bacteria to humans. *Journal of Molecular Biology* 1999, 293(2):381-399
112. Yoshiura, K.-i., Kinoshita, A., Ishida, T., Ninokata, A., Ishikawa, T., Kaname, T., Bannai, M., Tokunaga, K., Sonoda, S., Komaki, R., Ihara, M., Saenko, V. A., Alipov, G. K., Sekine, I., Komatsu, K., Takahashi, H., Nakashima, M., Sosonkina, N., Mapendano, C. K., Ghadami, M., Nomura, M., Liang, D.-S., Miwa, N., Kim, D.-K., Garidkhuu, A., Natsume, N., Ohta, T., Tomita, H., Kaneko, A., Kikuchi, M., Russomando, G., Hirayama, K., Ishibashi, M., Takahashi, A., Saitou, N., Murray, J. C., Saito, S., Nakamura, Y., and Niikawa, N.: A SNP in the ABCC11 gene is the determinant of human earwax type. *Nature Genetics* 2006, 38(3):324-330
113. Toyoda, Y., Sakurai, A., Mitani, Y., Nakashima, M., Yoshiura, K.-i., Nakagawa, H., Sakai, Y., Ota, I., Lezhava, A., Hayashizaki, Y., Niikawa, N., and Ishikawa, T.: Earwax, osmidrosis, and breast cancer: why does one SNP (538G>A) in the human ABC transporter ABCC11 gene determine earwax type? *The FASEB Journal* 2009, 23(6):2001-2013
114. Ono, N., Van der Heijden, I., Scheffer, G. L., Van de Wetering, K., Van Deemter, E., De Haas, M., Boerke, A., Gadella, B. M., De Rooij, D. G., Neefjes, J. J., Groothuis, T. A., Oomen, L., Brocks, L., Ishikawa, T., and

Borst, P.: Multidrug resistance-associated protein 9 (ABCC12) is present in mouse and boar sperm. *Biochem J* 2007, 406(1):31-40.[PMID:17472575]
115. Shimizu, H., Taniguchi, H., Hippo, Y., Hayashizaki, Y., Aburatani, H., and Ishikawa, T.: Characterization of the mouse Abcc12 gene and its transcript encoding an ATP-binding cassette transporter, an orthologue of human ABCC12. *Gene* 2003, 310:17-28
116. Amaral, A., Lourenço, B., Marques, M., and Ramalho-Santos, J.: Mitochondria functionality and sperm quality. *REPRODUCTION* 2013, 146(5):R163-R174
117. Gu, N.-H., Zhao, W.-L., Wang, G.-S., and Sun, F.: Comparative analysis of mammalian sperm ultrastructure reveals relationships between sperm morphology, mitochondrial functions and motility. *Reproductive Biology and Endocrinology* 2019, 17(1):66
118. Lord, T., and Nixon, B.: Metabolic Changes Accompanying Spermatogonial Stem Cell Differentiation. *Dev Cell* 2020, 52(4):399-411.[PMID:32097651]
119. Srivastava, N., and Pande, M.: Mitochondrion: Features, functions and comparative analysis of specific probes in detecting sperm cell damages. *Asian Pacific Journal of Reproduction* 2016, 5(6):445-452
120. Nowicka-Bauer, K., Lepczynski, A., Ozgo, M., Kamieniczna, M., Fraczek, M., Stanski, L., Olszewska, M., Malcher, A., Skrzypczak, W., and Kurpisz, M. K.: Sperm mitochondrial dysfunction and oxidative stress as possible reasons for isolated asthenozoospermia. *J Physiol Pharmacol* 2018, 69(3).[PMID:30149371]
121. Losano, J. D. D. A., Angrimani, D. D. S. R., Ferreira Leite, R., Simões Da Silva, B. D. C., Barnabe, V. H., and Nichi, M.: Spermatic mitochondria: role in oxidative homeostasis, sperm function and possible tools for their assessment. *Zygote* 2018, 26(4):251-260
122. Olson, G. E., and Winfrey, V. P.: Structural organization of surface domains of sperm mitochondria. *Molecular Reproduction and Development* 1992, 33(1):89-98
123. Maneesh, M., and Jayalekshmi, H.: Role of reactive oxygen species and antioxidants on pathophysiology of male reproduction. *Indian journal of clinical biochemistry : IJCB* 2006, 21(2):80-89.[PMID:23105620]
124. Koppers, Adam J., Mitchell, Lisa A., Wang, P., Lin, M., and Aitken, R. J.: Phosphoinositide 3-kinase signalling pathway involvement in a truncated apoptotic cascade associated with motility loss and oxidative DNA damage in human spermatozoa. *Biochemical Journal* 2011, 436(3):687-698
125. Amaral, A., and Ramalho-Santos, J.: Assessment of mitochondrial potential: implications for the correct monitoring of human sperm function. *Int J Androl* 2010, 33(1):e180-6.[PMID:19751363]
126. Alamo, A., De Luca, C., Mongioì, L. M., Barbagallo, F., Cannarella, R., La Vignera, S., Calogero, A. E., and Condorelli, R. A.: Mitochondrial Membrane Potential Predicts 4-Hour Sperm Motility. *Biomedicines* 2020, 8(7):196.[PMID:doi:10.3390/biomedicines8070196]
127. Amaral, A., Paiva, C., Attardo Parrinello, C., Estanyol, J. M., Ballescà, J. L., Ramalho-Santos, J., and Oliva, R.: Identification of proteins involved in

human sperm motility using high-throughput differential proteomics. *J Proteome Res* 2014, 13(12):5670-84.[PMID:25250979]
128. Duarte, A., Poderoso, C., Cooke, M., Soria, G., Cornejo Maciel, F., Gottifredi, V., and Podestá, E. J.: Mitochondrial Fusion Is Essential for Steroid Biosynthesis. *PLOS ONE* 2012, 7(9):e45829
129. Liesa, M., Palacín, M., and Zorzano, A.: Mitochondrial Dynamics in Mammalian Health and Disease. *Physiological Reviews* 2009, 89(3):799-845.[PMID:19584314]
130. Campello, S., and Scorrano, L.: Mitochondrial shape changes: orchestrating cell pathophysiology. *EMBO Rep* 2010, 11(9):678-84.[PMID:20725092]
131. Martin, S. J.: Mitochondrial Fusion: Bax to the Fussure. *Developmental Cell* 2011, 20(2):142-143
132. Lepesheva, G. I., and Usanov, S. A.: Dynamics and functional activity of cytochrome P450scc selectively labeled with fluorescein isothiocyanate. *Biochemistry (Mosc)* 1997, 62(6):648-56.[PMID:9324423]
133. Miller, W. L.: Steroid hormone synthesis in mitochondria. *Molecular and Cellular Endocrinology* 2013, 379(1):62-73
134. Varuzhanyan, G., Rojansky, R., Sweredoski, M. J., Graham, R. L., Hess, S., Ladinsky, M. S., and Chan, D. C.: Mitochondrial fusion is required for spermatogonial differentiation and meiosis. *eLife* 2019, 8
135. Fang, F., Ni, K., Shang, J., Zhang, X., Xiong, C., and Meng, T.: Expression of mitofusin 2 in human sperm and its relationship to sperm motility and cryoprotective potentials. *Exp Biol Med (Maywood)* 2018, 243(12):963-969.[PMID:30058380]
136. Tvrda, E., Peer, R., Sikka, S. C., and Agarwal, A.: Iron and copper in male reproduction: a double-edged sword. *J Assist Reprod Genet* 2015, 32(1):3-16.[PMID:25245929]
137. Yassin, M. A., Soliman, A. T., and Desanctis, V.: Intravenous Iron Replacement Therapy In Eugonadal Males With Iron Deficiency Anemia (IDA): Effects On Pituitary Gonadal Axis and Sperm Parameters. *Blood* 2013, 122(21):967-967
138. Muckenthaler, M. U., Rivella, S., Hentze, M. W., and Galy, B.: A Red Carpet for Iron Metabolism. *Cell* 2017, 168(3):344-361
139. Boral, M. C., Kaul, P., Dey, S. K., and Deb, C.: Effect of experimentally induced anemia on the testicular activity of the toad (Bufo melanostictus). *J Exp Zool* 1974, 188(1):77-87.[PMID:4822551]
140. Paul, B. T., Manz, D. H., Torti, F. M., and Torti, S. V.: Mitochondria and Iron: current questions. *Expert review of hematology* 2017, 10(1):65-79.[PMID:27911100]
141. Lieu, P. T., Heiskala, M., Peterson, P. A., and Yang, Y.: The roles of iron in health and disease. *Mol Aspects Med* 2001, 22(1-2):1-87.[PMID:11207374]
142. Wise, T., Lunstra, D. D., Rohrer, G. A., and Ford, J. J.: Relationships of testicular iron and ferritin concentrations with testicular weight and sperm production in boars. *J Anim Sci* 2003, 81(2):503-11.[PMID:12643495]

143. Johnson, L., Petty, C. S., and Neaves, W. B.: A comparative study of daily sperm production and testicular composition in humans and rats. *Biol Reprod* 1980, 22(5):1233-43.[PMID:7417656]
144. Toebosch, A. M., Kroos, M. J., and Grootegoed, J. A.: Transport of transferrin-bound iron into rat Sertoli cells and spermatids. *Int J Androl* 1987, 10(6):753-64.[PMID:3429053]
145. Stallard, B. J., and Griswold, M. D.: Germ Cell Regulation of Sertoli Cell Transferrin mRNA Levels. *Molecular Endocrinology* 1990, 4(3):393-401
146. Agbaraji, V. O., Scott, R. B., Leto, S., and Kingslow, L. W.: Fertility studies in sickle cell disease: semen analysis in adult male patients. *Int J Fertil* 1988, 33(5):347-52.[PMID:2904423]
147. Hidiroglou, M.: Trace element deficiencies and fertility in ruminants: a review. *J Dairy Sci* 1979, 62(8):1195-206.[PMID:387829]
148. Sahoo, L. K., Kullu, B. K., Patel, S., Patel, N. K., Rout, P., Purohit, P., and Meher, S.: Study of Seminal Fluid Parameters and Fertility of Male Sickle Cell Disease Patients and Potential Impact of Hydroxyurea Treatment. *J Assoc Physicians India* 2017, 65(6):22-25.[PMID:28782309]
149. Nikolaev, A. A., Lutskii, D. L., Nikolaeva, N. N., and Lozhkina, L. V.: [Iron and nonheme iron protein metabolism in ejaculates with varying degrees of fertility]. *Urol Nefrol (Mosk)* 1998, (5):27-31.[PMID:9820043]
150. Metzendorf, C., and Lind, M. I.: Drosophila mitoferrin is essential for male fertility: evidence for a role of mitochondrial iron metabolism during spermatogenesis. 2010, 10(1):68
151. Hales, K. G.: Iron testes: sperm mitochondria as a context for dissecting iron metabolism. *BMC Biology* 2010, 8(1):79
152. Klein, D. M., Wright, S. H., and Cherrington, N. J.: Localization of Multidrug Resistance-Associated Proteins along the Blood-Testis Barrier in Rat, Macaque, and Human Testis. *Drug Metabolism and Disposition* 2014, 42(1):89-93
153. Jung, M., Wells, D., Rusch, J., Ahmad, S., Marchini, J., Myers, S. R., and Conrad, D. F.: Unified single-cell analysis of testis gene regulation and pathology in five mouse strains. *Elife* 2019, 8.[PMID:31237565]
154. Sissung, T. M., Deeken, J., Leibrand, C. R., Price, D. K., Ehrlich, S., Steinberg, S. M., Liewehr, D. J., Dahut, W., and Figg, W. D.: Identification of novel SNPs associated with risk and prognosis in patients with castration-resistant prostate cancer. *Pharmacogenomics* 2016, 17(18):1979-1986
155. Bertollotto, G. M., De Oliveira, M. G., Alexandre, E. C., Calmasini, F. B., Passos, G. R., Antunes, E., and Mónica, F. Z.: Inhibition of Multidrug Resistance Proteins by MK 571 Enhances Bladder, Prostate, and Urethra Relaxation through cAMP or cGMP Accumulation. *Journal of Pharmacology and Experimental Therapeutics* 2018, 367(1):138-146
156. Alexandre, E. C., Cao, N., Mizoguchi, S., Saito, T., Kurobe, M., Gotoh, D., Okorie, M., Igarashi, T., Antunes, E., and Yoshimura, N.: Urethral dysfunction in a rat model of chemically induced prostatic inflammation: potential involvement of the MRP5 pump. *Am J Physiol Renal Physiol* 2020, 318(3):F754-F762.[PMID:32036697]

157. Shi, B., Xu, F.-F., Xiang, C.-P., Jia, R., Yan, C.-H., Ma, S.-Q., Wang, N., Wang, A.-J., and Fan, P.: Effect of sodium butyrate on ABC transporters in lung cancer A549 and colorectal cancer HCT116 cells. *Oncology letters* 2020, 20(5):148-148.[PMID:32934716]
158. Nakagata, N. (2011) Cryopreservation of Mouse Spermatozoa and In Vitro Fertilization. 57-73. Transgenic Mouse Methods and Protocols. Edited by Hofker, M. H., and van Deursen, J., Humana Press, Totowa, NJ
159. Ho, Y., Wigglesworth, K., Eppig, J. J., and Schultz, R. M.: Preimplantation development of mouse embryos in KSOM: Augmentation by amino acids and analysis of gene expression. *Molecular Reproduction and Development* 1995, 41(2):232-238
160. Chen, A. J., Yuan, X., Li, J., Dong, P., Hamza, I., and Cheng, J.-X.: Label-Free Imaging of Heme Dynamics in Living Organisms by Transient Absorption Microscopy. *Analytical Chemistry* 2018, 90(5):3395-3401
161. Zhu, Y., and Cheng, J.-X.: Transient absorption microscopy: Technological innovations and applications in materials science and life science. *The Journal of Chemical Physics* 2020, 152(2):020901
162. Williams, D. A., Rosenblatt, M. F., Beier, D. R., and Cone, R. D.: Generation of murine stromal cell lines supporting hematopoietic stem cell proliferation by use of recombinant retrovirus vectors encoding simian virus 40 large T antigen. *Molecular and Cellular Biology* 1988, 8(9):3864-3871
163. Chong, J., Soufan, O., Li, C., Caraus, I., Li, S., Bourque, G., Wishart, D. S., and Xia, J.: MetaboAnalyst 4.0: towards more transparent and integrative metabolomics analysis. *Nucleic Acids Research* 2018, 46(W1):W486-W494
164. Chong, J., Yamamoto, M., and Xia, J.: MetaboAnalystR 2.0: From Raw Spectra to Biological Insights. *Metabolites* 2019, 9(3):57.[PMID:doi:10.3390/metabo9030057]
165. Chong, J., Wishart, D. S., and Xia, J.: Using MetaboAnalyst 4.0 for Comprehensive and Integrative Metabolomics Data Analysis. *Current Protocols in Bioinformatics* 2019, 68(1):e86
166. Li, S., Park, Y., Duraisingham, S., Strobel, F. H., Khan, N., Soltow, Q. A., Jones, D. P., and Pulendran, B.: Predicting Network Activity from High Throughput Metabolomics. *PLOS Computational Biology* 2013, 9(7):e1003123
167. Jones, J. W., Pierzchalski, K., Yu, J., and Kane, M. A.: Use of fast HPLC multiple reaction monitoring cubed for endogenous retinoic acid quantification in complex matrices. *Anal Chem* 2015, 87(6):3222-30.[PMID:25704261]
168. Kane, M. A., Chen, N., Sparks, S., and Napoli, J. L.: Quantification of endogenous retinoic acid in limited biological samples by LC/MS/MS. *Biochem J* 2005, 388(Pt 1):363-9.[PMID:15628969]
169. Kane, M. A., Folias, A. E., Wang, C., and Napoli, J. L.: Quantitative profiling of endogenous retinoic acid in vivo and in vitro by tandem mass spectrometry. *Anal Chem* 2008, 80(5):1702-8.[PMID:18251521]
170. Kane, M. A., and Napoli, J. L.: Quantification of endogenous retinoids. *Methods Mol Biol* 2010, 652:1-54.[PMID:20552420]

171. Kane, M. A., Folias, A. E., and Napoli, J. L.: HPLC/UV quantitation of retinal, retinol, and retinyl esters in serum and tissues. *Anal Biochem* 2008, 378(1):71-9.[PMID:18410739]
172. Bult, C. J., Blake, J. A., Smith, C. L., Kadin, J. A., and Richardson, J. E.: Mouse Genome Database (MGD) 2019. *Nucleic Acids Res* 2019, 47(D1):D801-d806.[PMID:30407599]
173. Hayamizu, T. F., Mangan, M., Corradi, J. P., Kadin, J. A., and Ringwald, M.: The Adult Mouse Anatomical Dictionary: a tool for annotating and integrating data. *Genome Biol* 2005, 6(3):R29.[PMID:15774030]
174. Smith, C. L., and Eppig, J. T.: The mammalian phenotype ontology: enabling robust annotation and comparative analysis. *Wiley Interdiscip Rev Syst Biol Med* 2009, 1(3):390-399.[PMID:20052305]
175. Smith, J. R., Hayman, G. T., Wang, S. J., Laulederkind, S. J. F., Hoffman, M. J., Kaldunski, M. L., Tutaj, M., Thota, J., Nalabolu, H. S., Ellanki, S. L. R., Tutaj, M. A., De Pons, J. L., Kwitek, A. E., Dwinell, M. R., and Shimoyama, M. E.: The Year of the Rat: The Rat Genome Database at 20: a multi-species knowledgebase and analysis platform. *Nucleic Acids Res* 2020, 48(D1):D731-d742.[PMID:31713623]
176. Wieckowski, M. R., Giorgi, C., Lebiedzinska, M., Duszynski, J., and Pinton, P.: Isolation of mitochondria-associated membranes and mitochondria from animal tissues and cells. *Nature Protocols* 2009, 4(11):1582-1590
177. Chen, J. J., and Zhang, S.: Heme-regulated eIF2alpha kinase in erythropoiesis and hemoglobinopathies. *Blood* 2019, 134(20):1697-1707.[PMID:31554636]
178. Han, A. P., Yu, C., Lu, L., Fujiwara, Y., Browne, C., Chin, G., Fleming, M., Leboulch, P., Orkin, S. H., and Chen, J. J.: Heme-regulated eIF2alpha kinase (HRI) is required for translational regulation and survival of erythroid precursors in iron deficiency. *EMBO J* 2001, 20(23):6909-18.[PMID:11726526]
179. Igarashi, J., Murase, M., Iizuka, A., Pichierri, F., Martinkova, M., and Shimizu, T.: Elucidation of the Heme Binding Site of Heme-regulated Eukaryotic Initiation Factor 2α Kinase and the Role of the Regulatory Motif in Heme Sensing by Spectroscopic and Catalytic Studies of Mutant Proteins. *Journal of Biological Chemistry* 2008, 283(27):18782-18791
180. Suragani, R. N. V. S., Zachariah, R. S., Velazquez, J. G., Liu, S., Sun, C.-W., Townes, T. M., and Chen, J.-J.: Heme-regulated eIF2α kinase activated Atf4 signaling pathway in oxidative stress and erythropoiesis. *Blood* 2012, 119(22):5276-5284
181. Mellor, H., Flowers, K. M., Kimball, S. R., and Jefferson, L. S.: Cloning and characterization of cDNA encoding rat hemin-sensitive initiation factor-2 alpha (eIF-2 alpha) kinase. Evidence for multitissue expression. *Journal of Biological Chemistry* 1994, 269(14):10201-10204
182. Berlanga, J. J., Herrero, S., and de Haro, C.: Characterization of the Hemin-sensitive Eukaryotic Initiation Factor 2α Kinase from Mouse Nonerythroid Cells*. *Journal of Biological Chemistry* 1998, 273(48):32340-32346
183. Page, A. B., Owen, C. R., Kumar, R., Miller, J. M., Rafols, J. A., White, B. C., DeGracia, D. J., and Krause, G. S.: Persistent eIF2alpha(P) is colocalized

with cytoplasmic cytochrome c in vulnerable hippocampal neurons after 4 hours of reperfusion following 10-minute complete brain ischemia. *Acta Neuropathol* 2003, 106(1):8-16.[PMID:12687390]
184. Tsuyama, T., Tsubouchi, A., Usui, T., Imamura, H., and Uemura, T.: Mitochondrial dysfunction induces dendritic loss via eIF2α phosphorylation. *Journal of Cell Biology* 2017, 216(3):815-834
185. Frey, A. G., Palenchar, D. J., Wildemann, J. D., and Philpott, C. C.: A Glutaredoxin.BolA Complex Serves as an Iron-Sulfur Cluster Chaperone for the Cytosolic Cluster Assembly Machinery. *J Biol Chem* 2016, 291(43):22344-22356.[PMID:27519415]
186. Patel, S. J., Frey, A. G., Palenchar, D. J., Achar, S., Bullough, K. Z., Vashisht, A., Wohlschlegel, J. A., and Philpott, C. C.: A PCBP1-BolA2 chaperone complex delivers iron for cytosolic [2Fe-2S] cluster assembly. *Nat Chem Biol* 2019, 15(9):872-881.[PMID:31406370]
187. Zhang, S., Macias-Garcia, A., Ulirsch, J. C., Velazquez, J., Butty, V. L., Levine, S. S., Sankaran, V. G., and Chen, J.-J.: HRI coordinates translation necessary for protein homeostasis and mitochondrial function in erythropoiesis. *eLife* 2019, 8:e46976.[PMID:31033440]
188. Miyagi, Y., Kerr, S., Sugiyama, A., Asai, A., Shibuya, M., Fujimoto, H., and Kuchino, Y.: Abundant expression of translation initiation factor EIF-4E in post-meiotic germ cells of the rat testis. *Lab Invest* 1995, 73(6):890-8.[PMID:8558852]
189. Puttagunta, R., and Di Giovanni, S.: Retinoic acid signaling in axonal regeneration. *Front Mol Neurosci* 2011, 4:59.[PMID:22287943]
190. Marill, J., Idres, N., Capron, C. C., Nguyen, E., and Chabot, G. G.: Retinoic acid metabolism and mechanism of action: a review. *Curr Drug Metab* 2003, 4(1):1-10.[PMID:12570742]
191. Kedishvili, N. Y.: Enzymology of retinoic acid biosynthesis and degradation: Thematic Review Series: Fat-Soluble Vitamins: Vitamin A. *Journal of Lipid Research* 2013, 54(7):1744-1760
192. Cunningham, T. J., and Duester, G.: Mechanisms of retinoic acid signalling and its roles in organ and limb development. *Nature Reviews Molecular Cell Biology* 2015, 16(2):110-123
193. Everts, H. B., and Berdanier, C. D.: Regulation of Mitochondrial Gene Expression by Retinoids. *IUBMB Life (International Union of Biochemistry and Molecular Biology: Life)* 2002, 54(2):45-49
194. Berdanier, C. D., Everts, H. B., Hermoyian, C., and Mathews, C. E.: Role of vitamin A in mitochondrial gene expression. *Diabetes Res Clin Pract* 2001, 54 Suppl 2:S11-27.[PMID:11733105]
195. NOY, N.: Retinoid-binding proteins: mediators of retinoid action. *Biochemical Journal* 2000, 348(3):481-495
196. Napoli, J. L.: Cellular retinoid binding-proteins, CRBP, CRABP, FABP5: Effects on retinoid metabolism, function and related diseases. *Pharmacology & therapeutics* 2017, 173:19-33.[PMID:28132904]
197. Liu, R.-Z., Garcia, E., Glubrecht, D. D., Poon, H. Y., Mackey, J. R., and Godbout, R.: CRABP1 is associated with a poor prognosis in breast cancer:

adding to the complexity of breast cancer cell response to retinoic acid. *Molecular Cancer* 2015, 14(1):129
198. Hogarth, C. A., and Griswold, M. D.: The key role of vitamin A in spermatogenesis. *J Clin Invest* 2010, 120(4):956-62.[PMID:20364093]
199. Amory, J. K., Ostrowski, K. A., Gannon, J. R., Berkseth, K., Stevison, F., Isoherranen, N., Muller, C. H., and Walsh, T.: Isotretinoin administration improves sperm production in men with infertility from oligoasthenozoospermia: a pilot study. *Andrology* 2017, 5(6):1115-1123.[PMID:28980413]
200. Busada, J. T., Chappell, V. A., Niedenberger, B. A., Kaye, E. P., Keiper, B. D., Hogarth, C. A., and Geyer, C. B.: Retinoic acid regulates Kit translation during spermatogonial differentiation in the mouse. 2015, 397(1):140-149
201. Griswold, M. D.: Spermatogenesis: The Commitment to Meiosis. *Physiol Rev* 2016, 96(1):1-17.[PMID:26537427]
202. Peluso-Iltis, C., Osz, J., and Rochel, N. (2020) DNA recognition by retinoic acid nuclear receptors. 235-260. Elsevier
203. Gallone, G., Haerty, W., Disanto, G., Ramagopalan, S. V., Ponting, C. P., and Berlanga-Taylor, A. J.: Identification of genetic variants affecting vitamin D receptor binding and associations with autoimmune disease. *Human molecular genetics* 2017, 26(11):2164-2176.[PMID:28335003]
204. Song, H. W., Anderson, R. A., Bayne, R. A., Gromoll, J., Shimasaki, S., Chang, R. J., Parast, M. M., Laurent, L. C., de Rooij, D. G., Hsieh, T. C., and Wilkinson, M. F.: The RHOX homeobox gene cluster is selectively expressed in human oocytes and male germ cells. *Hum Reprod* 2013, 28(6):1635-46.[PMID:23482336]
205. Borgmann, J., Tüttelmann, F., Dworniczak, B., Röpke, A., Song, H. W., Kliesch, S., Wilkinson, M. F., Laurentino, S., and Gromoll, J.: The human RHOX gene cluster: target genes and functional analysis of gene variants in infertile men. *Hum Mol Genet* 2016, 25(22):4898-4910.[PMID:28171660]
206. Costello, S., Michelangeli, F., Nash, K., Lefievre, L., Morris, J., Machado-Oliveira, G., Barratt, C., Kirkman-Brown, J., and Publicover, S.: Ca2+-stores in sperm: their identities and functions. *Reproduction (Cambridge, England)* 2009, 138(3):425-437.[PMID:19542252]
207. Karna, K. K., Shin, Y. S., Choi, B. R., Kim, H. K., and Park, J. K.: The Role of Endoplasmic Reticulum Stress Response in Male Reproductive Physiology and Pathology: A Review. *The World Journal of Men's Health* 2019, 37
208. Ying, X., Liu, Y., Guo, Q., Qu, F., Guo, W., Zhu, Y., and Ding, Z.: Endoplasmic reticulum protein 29 (ERp29), a protein related to sperm maturation is involved in sperm-oocyte fusion in mouse. *Reproductive biology and endocrinology : RB&E* 2010, 8:10-10.[PMID:20132541]
209. Hofmann, M. C., Hess, R. A., Goldberg, E., and Millán, J. L.: Immortalized germ cells undergo meiosis in vitro. *Proc Natl Acad Sci U S A* 1994, 91(12):5533-7.[PMID:8202522]
210. Hofmann, M. C., Abramian, D., and Millán, J. L.: A haploid and a diploid cell coexist in an in vitro immortalized spermatogenic cell line. *Dev Genet* 1995, 16(2):119-27.[PMID:7736662]

211. Wolkowicz, M. J., Coonrod, S. A., Reddi, P. P., Millan, J. L., Hofmann, M. C., and Herr, J. C.: Refinement of the differentiated phenotype of the spermatogenic cell line GC-2spd(ts). *Biol Reprod* 1996, 55(4):923-32.[PMID:8879510]
212. Mazeyrat, S., Saut, N., Grigoriev, V., Mahadevaiah, S. K., Ojarikre, O. A., Rattigan, Á., Bishop, C., Eicher, E. M., Mitchell, M. J., and Burgoyne, P. S.: A Y-encoded subunit of the translation initiation factor Eif2 is essential for mouse spermatogenesis. *Nature Genetics* 2001, 29(1):49-53
213. de Brito, O. M., and Scorrano, L.: Mitofusin 2 tethers endoplasmic reticulum to mitochondria. *Nature* 2008, 456(7222):605-10.[PMID:19052620]
214. Larrea, D., Pera, M., Gonnelli, A., Quintana–Cabrera, R., Akman, H. O., Guardia-Laguarta, C., Velasco, K. R., Area-Gomez, E., Dal Bello, F., De Stefani, D., Horvath, R., Shy, M. E., Schon, E. A., and Giacomello, M.: MFN2 mutations in Charcot–Marie–Tooth disease alter mitochondria-associated ER membrane function but do not impair bioenergetics. *Human Molecular Genetics* 2019, 28(11):1782-1800
215. Naon, D., Zaninello, M., Giacomello, M., Varanita, T., Grespi, F., Lakshminaranayan, S., Serafini, A., Semenzato, M., Herkenne, S., Hernández-Alvarez, M. I., Zorzano, A., De Stefani, D., Dorn, G. W., and Scorrano, L.: Critical reappraisal confirms that Mitofusin 2 is an endoplasmic reticulum–mitochondria tether. *Proceedings of the National Academy of Sciences* 2016, 113(40):11249-11254
216. Filadi, R., Greotti, E., Turacchio, G., Luini, A., Pozzan, T., and Pizzo, P.: Mitofusin 2 ablation increases endoplasmic reticulum–mitochondria coupling. *Proceedings of the National Academy of Sciences* 2015, 112(17):E2174-E2181
217. Thul, P. J., Åkesson, L., Wiking, M., Mahdessian, D., Geladaki, A., Ait Blal, H., Alm, T., Asplund, A., Björk, L., Breckels, L. M., Bäckström, A., Danielsson, F., Fagerberg, L., Fall, J., Gatto, L., Gnann, C., Hober, S., Hjelmare, M., Johansson, F., Lee, S., Lindskog, C., Mulder, J., Mulvey, C. M., Nilsson, P., Oksvold, P., Rockberg, J., Schutten, R., Schwenk, J. M., Sivertsson, Å., Sjöstedt, E., Skogs, M., Stadler, C., Sullivan, D. P., Tegel, H., Winsnes, C., Zhang, C., Zwahlen, M., Mardinoglu, A., Pontén, F., von Feilitzen, K., Lilley, K. S., Uhlén, M., and Lundberg, E.: A subcellular map of the human proteome. *Science* 2017, 356(6340):eaal3321
218. Uhlén, M., Fagerberg, L., Hallström, B. M., Lindskog, C., Oksvold, P., Mardinoglu, A., Sivertsson, Å., Kampf, C., Sjöstedt, E., Asplund, A., Olsson, I., Edlund, K., Lundberg, E., Navani, S., Szigyarto, C. A.-K., Odeberg, J., Djureinovic, D., Takanen, J. O., Hober, S., Alm, T., Edqvist, P.-H., Berling, H., Tegel, H., Mulder, J., Rockberg, J., Nilsson, P., Schwenk, J. M., Hamsten, M., von Feilitzen, K., Forsberg, M., Persson, L., Johansson, F., Zwahlen, M., von Heijne, G., Nielsen, J., and Pontén, F.: Tissue-based map of the human proteome. *Science* 2015, 347(6220):1260419
219. Weissig, V.: Drug Development for the Therapy of Mitochondrial Diseases. *Trends in Molecular Medicine* 2020, 26(1):40-57

220. Huang, M. L. H., Chiang, S., Kalinowski, D. S., Bae, D.-H., Sahni, S., and Richardson, D. R.: The Role of the Antioxidant Response in Mitochondrial Dysfunction in Degenerative Diseases: Cross-Talk between Antioxidant Defense, Autophagy, and Apoptosis. *Oxidative Medicine and Cellular Longevity* 2019, 2019:6392763
221. Nicolson, G. L.: Mitochondrial Dysfunction and Chronic Disease: Treatment With Natural Supplements. *Integrative medicine (Encinitas, Calif.)* 2014, 13(4):35-43.[PMID:26770107]
222. Mourier, A., Motori, E., Brandt, T., Lagouge, M., Atanassov, I., Galinier, A., Rappl, G., Brodesser, S., Hultenby, K., Dieterich, C., and Larsson, N.-G.: Mitofusin 2 is required to maintain mitochondrial coenzyme Q levels. *The Journal of cell biology* 2015, 208(4):429-442.[PMID:25688136]
223. LeBoeuf, B., Correa, P., Jee, C., and García, L. R.: Caenorhabditis elegans male sensory-motor neurons and dopaminergic support cells couple ejaculation and post-ejaculatory behaviors. *eLife* 2014, 3:e02938.[PMID:24915976]
224. Johnson, Z. L., and Chen, J.: Structural Basis of Substrate Recognition by the Multidrug Resistance Protein MRP1. *Cell* 2017, 168(6):1075-1085 e9.[PMID:28238471]
225. Kelley, L. A., Mezulis, S., Yates, C. M., Wass, M. N., and Sternberg, M. J. E.: The Phyre2 web portal for protein modeling, prediction and analysis. *Nat. Protocols* 2015, 10(6):845-858
226. Kelley, L. A., Mezulis, S., Yates, C. M., Wass, M. N., and Sternberg, M. J. E.: The Phyre2 web portal for protein modeling, prediction and analysis. *Nature Protocols* 2015, 10(6):845-858
227. Frelet, A., and Klein, M.: Insight in eukaryotic ABC transporter function by mutation analysis. *FEBS Lett* 2006, 580(4):1064-84.[PMID:16442101]
228. Karczewski, K. J., et al.: The mutational constraint spectrum quantified from variation in 141,456 humans. *Nature* 2020, 581(7809):434-443
229. Toyoda, Y., Hagiya, Y., Adachi, T., Hoshijima, K., Kuo, M. T., and Ishikawa, T.: MRP class of human ATP binding cassette (ABC) transporters: historical background and new research directions. *Xenobiotica* 2008, 38(7-8):833-62.[PMID:18668432]
230. Zhang, Y. K., Wang, Y. J., Gupta, P., and Chen, Z. S.: Multidrug Resistance Proteins (MRPs) and Cancer Therapy. *AAPS J* 2015, 17(4):802-12.[PMID:25840885]
231. Lorico, A., Rappa, G., Finch, R. A., Yang, D., Flavell, R. A., and Sartorelli, A. C.: Disruption of the murine MRP (multidrug resistance protein) gene leads to increased sensitivity to etoposide (VP-16) and increased levels of glutathione. *Cancer Res* 1997, 57(23):5238-42.[PMID:9393741]
232. Wijnholds, J., Evers, R., van Leusden, M. R., Mol, C. A., Zaman, G. J., Mayer, U., Beijnen, J. H., van der Valk, M., Krimpenfort, P., and Borst, P.: Increased sensitivity to anticancer drugs and decreased inflammatory response in mice lacking the multidrug resistance-associated protein. *Nat Med* 1997, 3(11):1275-9.[PMID:9359705]

233. De Wolf, C. J. F., Yamaguchi, H., Van Der Heijden, I., Wielinga, P. R., Hundscheid, S. L., Ono, N., Scheffer, G. L., De Haas, M., Schuetz, J. D., Wijnholds, J., and Borst, P.: cGMP transport by vesicles from human and mouse erythrocytes. *FEBS Journal* 2007, 274(2):439-450
234. Borst, P., de Wolf, C., and van de Wetering, K.: Multidrug resistance-associated proteins 3, 4, and 5. *Pflugers Arch* 2007, 453(5):661-73.[PMID:16586096]
235. Hwang, K., Walters, R. C., and Lipshultz, L. I.: Contemporary concepts in the evaluation and management of male infertility. *Nat Rev Urol* 2011, 8(2):86-94.[PMID:21243017]
236. Fainberg, J., and Kashanian, J. A.: Recent advances in understanding and managing male infertility. *F1000Res* 2019, 8.[PMID:31143441]